Hepcidin/Ferroportin/HIF-2α Regulation of Iron Metabolism at the Systemic and Cellular Level

by

Andrew J. Schwartz

A dissertation submitted in partial fulfillment
of the requirements for the degree of
Doctor of Philosophy
(Molecular and Integrative Physiology)
in the University of Michigan
2019

Doctoral Committee:

Professor Yatrik M. Shah, Chair
Assistant Professor Costas A. Lyssiotis
Associate Professor Marina Pasca di Magliano
Professor Linda C. Samuelson

Andrew J. Schwartz

andrschw@umich.edu

ORCID iD: 0000-0003-3681-1422

Acknowledgements

The completion of this work can only be explained by the help, guidance, and support from countless people, near and far. I owe many thanks to my mentor, Yatrik Shah. Much of my success in graduate school can be attributed to Yatrik's unending and unwavering dedication to his trainees. I have transformed into a scientist and a thinker under his mentorship, better able now to think through the logical principles necessary for scientific discovery and for living an informed life outside of the lab. From the moment I joined his group, Yatrik was steadfast in his commitment to my academic and professional development. We constantly discussed biological principles, experimental design, and career advice, including on the weekends. Yatrik is unafraid to chase interesting questions and it has been exciting to work over the last five years with someone so passionate about basic science discovery. Yatrik has also spent countless hours over the years teaching me how to convey an effective story through oral presentation and providing feedback about my writing. His commitment to my training and success is something I will never forget. I also want to thank the members of my dissertation committee, Linda Samuelson, Marina Pasca di Magliano, and Costas Lyssiotis for their scientific and career advice over the years.

I also owe tremendous thanks to the many past and present members of Yatrik's lab that I have had the privilege to call colleagues during graduate school. In particular, I'd like to acknowledge the team of scientists that were in the laboratory when I started my dissertation research: Nupur Das, Sadeesh Ramakrishnan, Xiang Xue, Huabing

Zhang, and Danny Triner. Each of these individuals taught me about dedication, perseverance, and patience in science when I was very new to basic research. Special thanks to Nupur, who is the only member of Yatrik's lab present from the start to finish of my dissertation; your friendship and mentorship over the years have defined my graduate school experience and I owe you many thanks. Another special thanks to Danny Triner, a scientific confidant, friend, and only other PhD student in Yatrik's lab during my training for many years. I lastly need to recognize the other students and trainees that have been in the laboratory during my PhD training: Xiaoya Ma, Sammi Devenport, Sumeet Solanki, Cristina Castillo, Joseph Taranto, Hannah Bell, Rashi Singhal, Josh Goyert, Mazen Hasan and Delawrence Sykes. Each of you has helped me get to where I am today.

Many thanks to the Molecular and Integrative Physiology (MIP) family at large, beginning with my graduate program chairs, Sue Moenter and Dan Michele. I feel so fortunate to have had an amazing duo of grad chairs during my training. Your mentorship and commitment have propelled me forward. Thank you to Michele Boggs, who as the graduate program coordinator always helped me behind the scenes, from reserving rooms for committee meetings to helping me navigate the complicated formalities of defending a PhD. Special thanks to MIP alumni Jonathan Gumucio and Matt Taylor; your friendship was instrumental to my success in graduate school.

I want to recognize the lifelong friends I have made through the Program in Biomedical Science (PIBS), particularly Jacob Johnson, Allison Kowalsky, Paloma Garcia, and Owen Funk. We met in a human genetics course our first year in PIBS and quickly found ourselves bonding over pizza and confusing homework debates about 5'

Rapid Amplification of cDNA Ends. This crew has been a constant for me over the last five years, whether we were discussing science or enjoying a family dinner/movie night together. I appreciate each of your friendship and support. I also want to thank Tim NeCamp and Lizz Ultee, two incredible people that I met during graduate school through Rackham's Institute for Social Change. Each of you personify true friendship and I have thoroughly enjoyed your humor, intelligence, and support over the years.

I need to recognize my childhood friends, Danny Lyons, Jonathan Ben-Zev, Bryan Cannon, Andrew Ricci, and John Hermiz. Each of us, somehow, went on to pursue an MD and/or a PhD after undergrad. It has been wonderful to discuss science and enjoy deep conversations and laughter with you all during the years. You have been instrumental to the completion of this work and to my growing up in this world.

Thank you to my parents, Robin and Bob, for your unconditional love, the opportunities you gave me, and your unending support throughout my entire life. I could not have accomplished even half of the things in my life if you two were not my parents. Thank you to my siblings, Adam and Amy. You both have been incredibly supportive and encouraging during graduate school, and throughout my entire life. Thanks for listening to me talk about my science and for being great cheerleaders.

I lastly want to thank my fiancé, Leah. Thank you for being the mature, wise, and supportive partner that you are. Your love and encouragement have reshaped my entire perspective on life, releasing a happiness in me that I didn't know was there. You make every aspect of my life better, from traveling to cooking dinner to going on long walks. It brings me infinite joy to know that I will spend my remaining days with you. I love you.

Table of Contents

List of Figures

List of Tables

Abstract

Iron is a metal micronutrient that is required by all living organisms, from single cell bacteria to complex, multicellular organisms that include humans. Systemic iron handling in mammals requires, i) the liver-derived, endocrine hormone, hepcidin, and ii) the iron/oxygen sensitive intestinal transcription factor, hypoxia-inducible factor (HIF)-2α. The function of hepcidin is to bind to the only mammalian iron exporter, ferroportin, resulting in ferroportin internalization from the plasma membrane, intracellular degradation, and a reduction of iron export into circulation. At the intestinal level, HIF-2α controls iron absorption by regulating the transcription of apical and basolateral iron transporters.

This dissertation focuses on the integration of hepcidin/ferroportin/HIF-2α signaling in iron homeostasis at the systemic and cellular level, in physiological and pathological contexts. The data in this work unveil a hetero-tissue crosstalk mechanism, whereby hepatic hepcidin regulated intestinal HIF-2α during states of systemic iron deficiency, anemia, and iron overload. I show that the hepcidin target, ferroportin, controlled cell-autonomous iron efflux to stabilize and activate HIF-2α by regulating the activity of iron-dependent intestinal prolyl hydroxylase domain enzymes. Pharmacological blockade of HIF-2α using a clinically relevant and highly specific inhibitor successfully treated iron overload in a mouse model of hepcidin-deficiency.

In addition to iron overload, over one billion people worldwide suffer from iron-deficiency anemia (IDA), a state of systemic iron insufficiency that limits the production

red blood cells and leads to tissue hypoxia and intracellular iron stress. Using a novel genetic mouse model of tamoxifen-inducible intestinal ferroportin deletion, I revealed a robust phenotype of progressive IDA that developed in as little as three months. At end-stage IDA, tissue-specific transcriptional stress responses were observed, whereby the heart showed little to no hypoxic and iron stress as compared to other peripheral organs. However, morphometric and echocardiographic analysis revealed massive cardiac hypertrophy and chamber dilation, albeit with increased cardiac output at very low basal heart rates. These data revealed a model of end-stage IDA that can be used in future studies to investigate IDA progression and cell-specific responses to hypoxic and iron stress.

We lastly investigated mechanisms of local iron handling and extra-hepatic hepcidin expression in the context of colorectal cancer (CRC), a disease in which cellular iron metabolism is perturbed to enhance growth and survival. I revealed that epithelial cells in CRC produce an ectopic source of hepcidin that is necessary and sufficient to control CRC tumorigenesis. Hepcidin promoter analysis demonstrated that hypoxia and its downstream transcription factor, HIF-2α, are sufficient to activate the hepcidin promoter in CRC-derived cell lines. These data suggest that HIF-2α induces hepcidin in the tumor epithelium to establish a paracrine/autocrine axis to degrade local ferroportin and sequester iron in colorectal tumors in order to maintain iron-dependent cancer cell metabolism.

Overall, the data presented in this dissertation unveil mechanisms by which systemic iron handling interacts and integrates with local iron handling, providing insight into targeted therapies for iron related disorders and adjuvant strategies for cancers.

Chapter 1

Introduction

1.1 Background

Iron is an essential metal micronutrient that sustains life, from single cell bacteria to multicellular organisms, including humans. Nearly 70% of the iron in humans can be found within the heme of hemoglobin in red blood cells (RBCs), where it functions to deliver molecular oxygen to every tissue and cell in the body. The other 30% is found ubiquitously as intracellular iron, where iron-containing proteins and free labile iron orchestrate energy metabolism, mitochondrial function, and DNA synthesis, among other basic cellular functions. Humans evolved in tremendous iron scarcity and are devoid of a system for iron excretion. Instead, elaborate mechanisms operate to recycle bodily iron. Iron recycling accounts for over 90% of daily iron demand (20 – 25 mg) and occurs mainly from the turnover of iron in hemoglobin in dying RBCs via splenic macrophages of the reticuloendothelial system; the remaining daily iron demand is met through the intestinal absorption of dietary iron (about 1 mg) (1). Duodenal enterocytes of the proximal small intestine mediate the majority of iron absorption, whereby dietary iron is reduced and either stored intracellularly or exported through the basolateral surface into systemic circulation. Once in circulation, the serum iron cargo protein, transferrin, delivers iron to all cells by interacting with its ubiquitous receptor, TfR1 (2).

Despite these robust systems, iron related disorders persist as a tremendous global health concern. Over two million people worldwide suffer from iron deficiency and

over one million are affected by iron-deficiency anemia (IDA) (3). In IDA, iron absorption and mobilization is limited to an extent that restricts the production of RBCs, ultimately leading to decreased transport of systemic oxygen and the development of intracellular iron stress (4). Conversely, diseases of iron overload are among the most common genetic disorders in humans, affecting over one million people in the United States (5). The prevalence of genetic diseases of iron overload can be explained in part by the survival advantage that systemic iron surplus confers during dietary iron insufficiencies and following blood loss (i.e. these diseases were poorly selected against). In addition to canonical iron overload, several hemoglobinopathies affect the population with high penetrance, including sickle cell disease and β-thalassemia, which are characterized by RBC deformities, decreased oxygen transport, and tissue iron accumulation (6).

Iron homeostasis at the systemic level requires multiple organs working in concert to maintain cellular iron concentrations for metabolism and RBC levels for oxygen transport. Advances in the understanding of tissue- and cell-type specific mechanisms of iron metabolism have begun to redefine the ways in which peripheral organs participate in systemic iron homeostasis while also protecting organ function via cell-autonomous mechanisms during states of iron deficiency. This dissertation focusses on the basic mechanisms of iron metabolism at the cellular and systemic level, expanding on previous work and defining new ways to understand iron homeostasis during physiology and in various disease states.

1.2 Hepcidin/ferroportin signaling

The last two decades of research has established that the master regulator of systemic iron homeostasis and metabolism in mammals is hepcidin, a small, endocrine peptide hormone that is mainly synthesized and secreted by the liver. Due to its cystine-rich structure, which is a hallmark of the defensin and protegrin antimicrobial peptide families, hepcidin was initially discovered in human blood ultrafiltrate and urine during a screen for liver-derived secreted proteins involved in host defense (7, 8). In these original investigations, hepcidin exhibited antifungal activity against Candida albicans, Aspergillus fumigatus, and Aspergillus niger and antibacterial activity against Escherichia coli, Staphylococcus aureus, Staphylococcus epidermidis, and group B Streptococcus (7, 8). Hepcidn mRNA (encoded by *Hamp*) was also shown to be responsive to changes in iron concentrations and inflammation (9). Concurrent with these discoveries, the USF2 gene was under investigation for its role in glucose and lipid metabolism when investigators discovered that mice devoid of *Usf2* developed spontaneous iron overload and expressed low levels of the hepcidin transcript (10). However, subsequent work revealed that this original strategy to delete *Usf2* also disrupted the nearby hepcidin gene, whereas mice deficient for *Hamp* but intact for *Usf2* continued to develop iron overload (11). Conversely, overexpression of *Hamp* led to severe iron deficiency and erythrocyte abnormalities, solidifying the essential role for hepcidin in the maintenance of systemic iron concentrations (12).

Despite these advances, it took several more years for the complete molecular mechanism of hepcidin action to become clear. A pivotal study in 2004 uncovered that hepcidin binds to extracellular residues on the mammalian plasma membrane iron exporter, ferroportin, resulting in ferroportin internalization from the membrane,

intracellular degradation, and an increase in intracellular iron concentrations (Figure 1.1) (13). Ferroportin is predominately expressed and regulated in tissues that maintain systemic iron homeostasis, namely, intestine, liver, and macrophages of the reticuloendothelial system (14). Therefore, in the presence of hepcidin, ferroportin is continually internalized from the membrane and iron mobilization into circulation is limited. In the absence of hepcidin, ferroportin is rapidly stabilized and iron is exported into plasma. Liver hepcidin is the central sensor and first responder to changes in systemic iron levels, whereas decreases in systemic iron concentrations reduce *Hamp* expression in order to stabilize ferroportin and mobilize iron. On the other hand, high levels of systemic iron lead to an increase in hepcidin expression, ferroportin internalization and degradation, and a decrease in iron export into circulation.

The molecular mechanisms by which hepcidin/ferroportin signaling responds to changes in systemic iron concentrations begins with a cascade of interactions between plasma membrane proteins in hepatocytes. Serum iron loading onto TfR1 initiates signaling that involves HFE, BMPRI/II, HJV, and TfR2, which results in downstream activation of SMAD and an increase in *Hamp* transcription (15-18). Hepatocyte non-cell-autonomous mechanisms also exist to regulate hepcidin, whereby liver sinusoidal cells and other nonparenchymal cells mainly secrete a source of BMP6, but also BMP2 and BMP7, that are essential for hepatocyte hepcidin expression (19-22). In addition to iron sensing, hepcidin expression is sensitive to a variety of inflammatory stimuli, particularly IL6, which induces *Hamp* via intracellular activation of JAK/STAT3 signaling (23-25). This inflammatory component of hepcidin regulation is a conserved mechanism to limit extracellular iron as a general defense mechanism against infections by withholding iron

from invading pathogens (26). However, prolonged activation of this pathway during chronic diseases and/or states of persistent inflammation engenders profound anemia due to continual ferroportin internalization from the plasma membrane and insufficient iron concentrations being mobilized into circulation, referred to as anemia of chronic disease (27, 28).

The canonical mechanism by which ferroportin is regulated in the context of systemic iron homeostasis is at the posttranslational level following interaction with hepcidin. However, ferroportin transcription and translation is also regulated by intracellular signaling that includes reactive oxygen species, inflammation, and hypoxia (14). For example, the redox-sensitive transcription factor, *Nrf2*, transcriptionally activates ferroportin, whereas inflammatory stimuli such as LPS leads to a decrease in ferroportin mRNA (29). These mechanisms, among others, enable cells to control cell-autonomous iron concentrations by modulating iron export in different physiological and pathological contexts.

The significance of hepcidin/ferroportin signaling is underscored by decades of research to show that mutations that disrupt hepcidin/ferroportin production or function give rise to genetic diseases of iron overload or deficiency in humans. In the context of iron overload, known as hemochromatosis, the direct loss of *HAMP,* or mutations that render ferroportin unresponsive to hepcidin-mediated degradation, cause hemochromatosis in humans (30, 31). This results from unrestricted ferroportin stabilization and chronic, pathological mobilization of iron into circulation. The majority of cases of hemochromatosis in humans result from mutations that affect the complex of iron-sensing, membrane proteins in hepatocytes that control *HAMP* expression. For

example, the prevalence of mutations to *HFE* is between 1:200 – 300 in Caucasians, though patients across the globe also present with mutations to *HJV* and *TfR2* (32-35). Each of these mutations result in varied intensity of the hemochromatosis phenotype. Direct mutations to *HAMP* or *HJV* are characterized by early onset and severe phenotype, historically referred to as juvenile hemochromatosis; a more mild, adult onset hemochromatosis is observed in patients with mutation to *TfR2* (5). Missense mutations on ferroportin that disrupt the hepcidin/ferroportin interaction are referred to as ferroportin disease, which give rise to a pathological phenotype distinct from all other known forms of hemochromatosis because these patients have intact liver hepcidin production (36). Interestingly, these genetic defects do not affect reproduction and confer evolutionary advantages against iron deficiency, offering insight into the prevalence of hemochromatosis in modern human populations. More recently, genetic mutations that give rise to an increase in *HAMP* expression were discovered, namely *TMPRSS6* (37, 38). This gene encodes a negative regulator of hepcidin production; when lost, chronic degradation of ferroportin and a progressive and robust IDA phenotype ensues.

Given that the iron core of RBC hemoglobin is required for efficient oxygen transport, mammals have evolved intricate mechanisms that link iron and oxygen metabolic pathways. Systemic hypoxia triggers erythropoiesis to expand the RBC pool and increase oxygen transport. This is achieved, in part, via the hypoxic activation of erythropoietin (encoded by *Epo*), a kidney-derived glycoprotein hormone that induces RBC production in bone marrow. To facilitate this increase in RBC numbers, a reciprocal increase in systemic iron levels is essential to maintain hemoglobin

production. Liver hepcidin serves as a central mediator of iron and oxygen metabolism because, in addition to the iron and inflammation sensing pathways mentioned above, hepcidin expression is potently repressed by systemic hypoxia. Shortly after the discovery of hepcidin, it was shown in vitro and in vivo that hypoxia decreases the transcription of *Hamp* (39). Furthermore, it was shown in paired human blood samples at sea level and following exposure to high-altitude that serum hepcidin concentrations are rapidly decreased during systemic hypoxia (40).

The mechanisms by which systemic hypoxia mobilizes iron stores via hepcidin repression are complex and involve both erythropoietin-dependent and –independent processes. Early findings found that activation of liver hypoxic machinery indirectly suppresses *Hamp* via induction of *Epo* transcription, using genetic deletion of *Epo* in mice and erythropoietin neutralizing antibodies (41, 42). This phenomenon is explained, in part, by inhibition of the transcription factor C/EBPα downstream of the hepatocyte erythropoietin receptor, resulting in blockade of *Hamp* transcription (43, 44). Moreover, numerous reports demonstrate that erythropoietin-induced erythropoiesis can inhibit hepcidin expression via erythroid-derived molecules. These secreted factors include growth differentiation factor 15 (GDF15), which is induced during erythroblast differentiation (45). However, *Hamp* mRNA was still decreased when primary hepatocytes were treated with GDF15-depleted serum, indicating the presence of other circulating erythroid-derived factors (45). Several years later, TWSG1 was discovered as another erythroid-derived factor that can inhibit hepcidin expression through a mechanism that involves inhibition of BMP/SMAD signaling (46). Most recently, the erythroblast produced erythroferrone (also known as FAM132B) was discovered, which

is stimulated by erythropoietin-mediated activation of JAK2/STAT5 signaling in erythroblasts (47). Mice that are deficient for erythroferrone fail to suppress hepcidin following injections of recombinant erythropoietin or hemorrhage (47). Erythroferrone acts as a natural ligand trap for BMPs in order to dampen downstream activation of SMAD1/5/8 phosphorylation and inhibit hepcidin in contexts of erythropoiesis (48). Future work will need to characterize the relative contribution of these erythroid-derived factors in hepcidin repression during erythropoiesis. Furthermore, the complete molecular mechanism of hepcidin transcriptional inhibition in hepatocytes by erythroid-derived factors remains unclear.

1.3 Intestinal regulation of systemic iron homeostasis

The intestine serves as the gateway of iron entry into the body. In both physiological and pathological contexts, systemic iron abundance is primarily controlled by the absorption of dietary iron. Moreover, hyper- or hypo-activation of intestinal iron uptake gives rise to profound iron overload or deficiency in humans. The vast majority of human iron absorption takes place in the proximal small intestine, referred to as the duodenum. Here, absorptive duodenal enterocytes reduce dietary ferric iron (Fe^{3+}) into ferrous iron (Fe^{2+}) by the apical ferric reductase, duodenal cytochrome b (DcytB) (49, 50). Ferrous iron is then suitable for apical import via divalent metal transporter-1 (DMT1) (51). Once inside the cytoplasm of enterocytes, iron is either, i) stored and bound to the ubiquitous, intracellular iron storage protein, ferritin, or ii) exported out the basolateral surface into systemic circulation via the sole mammalian iron exporter, ferroportin (52). The expression of duodenal DcytB, DMT1, and ferroportin is massively

upregulated during contexts of iron demand, namely systemic iron deficiency and contexts of erythropoietic drive (53-55). Furthermore, these intestinal players also mediate the hyperabsorption of dietary iron that leads to systemic iron accumulation in diseases of iron overload, including hemochromatosis, β-thalassemia, and sickle cell disease (56-58).

The molecular mechanism governing the intestinal iron response was unclear until a series of papers discovered a central role for intestinal hypoxic machinery in iron absorption. Hypoxia, or the decreased oxygen tension of tissues and cells, promotes the canonical activation of hypoxia-inducible transcription factors (HIF)s. HIFs are basic helix-loop-helix-per-arnt-sim (bHLH-PAS) containing transcription factors that consist of a heterodimer of an oxygen-sensitive α subunit (HIF-1α, HIF-2α, and HIF-3α) and a constitutively expressed β subunit (ARNT) (59). HIF-1α is ubiquitously expressed whereas HIF-2α and HIF-3α expression is more tissue restricted (60-62). HIF-α subunits are regulated by post-translational hydroxylation of proline residues by prolyl hydroxylase domain-containing (PHD-containing) enzymes that are enzymatically dependent on oxygen, iron, and 2-oxoglutarate for their function. HIF hydroxylation leads to association with the von-Hippel Lindau (VHL) tumor suppressor/E3 ubiquitin ligase complex, ubiquitin conjugation, and 26s proteasomal degradation. In contexts that limit PHD activity, such as intracellular oxygen or iron depletion, HIFs are stabilized, dimerize with ARNT, and translocate to the nucleus to regulate transcription of target genes.

Given the intimate connection between oxygen and iron metabolism, it was shown that intestinal HIF-2α, but not other HIFs, is critical to regulate genes that encode

for iron import (Figure 1.2) (53, 55, 63). These reports unveiled that HIF-2α is an intracellular oxygen and iron sensor by directly activating DcytB, DMT1, and ferroportin transcription and serving as the master regulator of iron absorption (53, 55, 63). Genetic deletion of HIF-2α in intestinal epithelial cells prevents the induction of DcytB, DMT1, and ferroportin mRNA in mice on a low-iron diet, which leads to profound iron deficiency and eventually anemia (53, 55, 63). The adaptive increase in DcytB, DMT1, and ferroportin that is observed in contexts of increased erythropoiesis is also lost in mice that are deficient for intestinal epithelial HIF-2α (54). The dependence on HIF-2α to maintain systemic iron homeostasis is also seen during pregnancy and the early postnatal period because maternal mice deficient for intestinal epithelial HIF-2α fail to maintain iron concentrations in breast milk, which leads to neonatal anemia and long-term cognitive defects (64). Conversely, overexpression of HIF-2α in intestinal epithelial cells increases the expression of DcytB, DMT1, and ferroportin in mice (53, 65). The fundamental role of intestinal HIF-2α in iron uptake is also seen in pathologies that are characterized by dietary iron hyperabsorption, whereby genetic deletion or pharmacological inhibition of HIF-2α decreases systemic iron accumulation in models of hemochromatosis, β-thalassemia, and sickle cell disease (56-58).

For many years, intestinal HIF-2α stabilization during contexts of systemic iron demand was thought to be triggered by discrete, local environmental cues. PHDs require both oxygen and iron for their function; therefore, context-dependent substrate depletion was assumed to activate intestinal HIF-2α during hypoxia that triggers erythropoiesis (i.e. intestinal oxygen depletion) and systemic iron deficiency (i.e. intestinal iron depletion). However, the work presented in Chapter 2 of this thesis

unveils the complete molecular cues that initiate and maintain intestinal HIF-2α during physiology and in disease by demonstrating direct integration of liver hepcidin and intestinal HIF-2α pathways. It was shown that liver hepcidin restricts intestinal HIF-2α activity. Moreover, as shown in Chapter 2, inducible, genetic deletion of hepcidin exclusively in hepatocytes dramatically stabilizes the intestinal HIF-2α protein and drives the expression of HIF-2α-dependent genes that are necessary and sufficient to increase iron absorption (e.g. *Dcytb, Dmt1,* and *Ferroportin*). Deletion of the hepcidin target, ferroportin, in the intestinal epithelium completely prevents the canonical activation of HIF-2α during contexts of systemic iron deficiency, erythropoiesis, and in IDA. The mechanism by which hepcidin/ferroportin kinetics regulate HIF-2α is via cell-autonomous iron efflux that decreases the activity of iron-dependent PHD enzymes, even in contexts of decreased oxygen availability. Furthermore, pharmacological blockade of HIF-2α using an orally delivered HIF-2α inhibitor decreased systemic iron accumulation in a mouse model of hepcidin-deficiency iron overload. These collective data now suggest a model that the intestine is completely downstream of liver hepcidin. Moreover, intestinal ferroportin stabilization that follows a decrease in hepcidin serves to activate HIF-2α and transcriptionally drive iron absorption during systemic iron demand and in iron overload. Lastly, this Chapter demonstrates that the canonical intestinal HIF-2α response is regulated primarily by intracellular intestinal epithelial iron levels downstream of hepcidin/ferroportin kinetics and not context-dependent depletion of PHD substrates (i.e. oxygen or iron).

In addition to hepcidin and HIF-2α, another mammalian iron-sensing axis exists via iron-regulatory protein (IRP) and iron-response element (IRE) machinery. There are

two IRPs: IRP1 and IRP2. The IRP/IRE system modulates translation via the binding of IRPs with IREs that exist in the 5′- or 3′-UTR of target transcripts involved in cellular iron handling. This interaction can either block translation or increase mRNA stability in order to alter the stability of iron handling proteins. Decreases in intracellular iron availability activate IRPs, whereas increases in iron levels inhibit IRP function (66).

The gene that encodes ferroportin (*SLC40A1*) contains a 5'-UTR IRE that serves to reduce translation and decrease ferroportin protein abundance during contexts of intracellular iron stress (67, 68). However, intestinal cells can express *SLC40A1* mRNA from an alternate promoter that generates a transcript devoid of IREs, thereby enabling ferroportin expression in contexts of intracellular iron deficiency (69). This isoform in the intestine unveils discrepancies between intestinal iron dynamics and iron handling in peripheral organs and cells. Moreover, the short-lived intestinal epithelium (approximately 3-5 days) is capable of depleting local iron stores and increasing import/export in order to spare systemic organs during contexts of iron demand. Conversely, the peripheral response is a more "selfish" feedback loop that decreases *SLC40A1* translation in order to trap existing iron stores during systemic iron stress. The gene that encodes DMT1 (*SLC11A2*) can also be driven by alternate promoters, further suggesting organ and cell-type specific iron handling responses (70).

In addition to mRNAs that encode for direct iron handling proteins, HIF-2α mRNA also contains a 5' UTR IRE that limits translation during intracellular iron depletion (71-74). One of the hypothesized functions of the HIF-2α IRE is to limit HIF-2α-induced *Epo* transcription during states of IDA, when erythropoiesis is futile in the face of severe iron insufficiencies. However, in context with work to show that intracellular iron depletion

induces HIF-2α protein stabilization, more research will need to be done to fully understand the interaction between IRP/IRE systems and other iron sensing machinery axis during systemic iron demand (56).

Despite these many advances in our understanding of intestinal iron biology, many unanswered questions remain. As shown in Chapter 2 of this thesis, using unbiased, high-throughput RNA-Seq that there are subsets of genes in the intestine that are regulated by either liver hepcidin-deficiency or systemic iron deficiency. In combination with data to show that there are nearly 200 uncharacterized HIF-2α-target genes that are activated in the intestine during systemic iron demand, much work remains in order to define the complete biological function of intestinal HIF-2α in systemic iron homeostasis (53). It also remains unclear as to whether a hepcidin/ferroportin/HIF-2α axis functions in cells other than the intestinal epithelium, which would establish a model in which liver hepcidin controls iron-dependent transcriptional programs in peripheral organs. Lastly, the complete mechanism by which ferroportin-mediated iron efflux selectively stabilized HIF-2α over HIF-1α in Chapter 2 remains unknown, but would provide major insight into the intersection of intracellular oxygen and iron sensing pathways.

1.4 Paracrine and autocrine hepcidin/ferroportin dynamics

Since the discovery of hepcidin/ferroportin signaling, this interaction has primarily been thought of as a liver-derived, endocrine system that acts on major ferroportin expressing cells to control systemic iron mobilization (i.e. hepatocytes, intestinal enterocytes, and splenic macrophages). However, recent reports have started to reveal

extra-hepatic, functional sources of hepcidin that act in paracrine and/or autocrine fashions on local ferroportin (75-77). The ferroportin protein had been hypothesized to be expressed at lower levels in tissues that do not maintain systemic iron handling, namely in cardiomyocytes (78). However, it was not until 2015 that a functional characterization of cardiac ferroportin was executed (75). This report demonstrated profound consequences of genetic ferroportin deletion in cardiomyocytes, which results in massive intracellular iron accumulation and decreased survival of mice (75). Furthermore, ferroportin-dependent iron retention gave rise to dilated cardiomyopathy with left ventricular dysfunction (75). Interestingly, this report showed that hepcidin-deficient iron overload gave rise to massive iron deposition in non-cardiomyocytes and did not impact survival to the extent of cardiomyocyte ferroportin deletion (75). This finding shows the critical importance of maintaining cardiomyocyte iron homeostasis, which seems to be protected even in contexts of iron overload.

Following this report, the race was on to understand the complete molecular mechanisms of cardiac ferroportin regulation. In a seminal paper, investigators published the following year that cardiac ferroportin is primarily regulated by a local, cell-autonomous source of hepcidin (76). Embryonic deletion of cardiomyocyte hepcidin in mice leads to intracellular iron depletion, contractile defects, and metabolic alterations that decrease mitochondrial activity, all of which results in massively decreased survival (76). These observations were phenocopied in mice that expressed a form of ferroportin that is resistant to hepcidin interaction, specifically in the heart, and was rescued by exogenous iron supplementation (76). Recent work revealed that a cell-autonomous hepcidin/ferroportin axis exists in cell types other than cardiomyocytes, namely

pulmonary arterial smooth muscle cells (77). Other data suggests that hepcidin/ferroportin dynamics might control iron trafficking across the blood brain-barrier, using co-cultures of human brain microvascular endothelial cells and an astrocytic cell line (79). Hepcidin has also been reported in the human kidney and placenta (80, 81), while ferroportin has been shown to exert a functional role in erythroblasts and mature RBCs (82, 83).

In context with the systemic liver hepcidin/intestinal HIF-2α axis, these peripheral, cell-autonomous iron regulatory networks raise important questions regarding systemic vs. local iron handling and basic principles about hepcidin/ferroportin biology. First, it is essential to establish the mechanisms by which endocrine, paracrine, and autocrine hepcidin/ferroportin signaling interact with each other. It remains unclear whether cardiac ferroportin responds to changes in liver-derived, endocrine hepcidin. Moreover, during states of systemic iron demand, it is unknown if the cardiac ferroportin protein responds to changes in liver hepcidin, or whether a concomitant increase in local, cardiac hepcidin secretion counteracts all action by liver hepcidin. Interestingly, a report on suckling mice unveiled that the intestine expresses a variant of the ferroportin protein that is of smaller molecular weight and is hypo-responsive to hepcidin-mediated degradation (84). However, following weaning, a ferroportin protein of higher molecular weight is expressed in the intestine and normal hepcidin sensitivity is restored (84). These investigators hypothesized that a post-translational modification on ferroportin might support increased iron absorption during the neonatal period to maintain iron levels for development and cognitive function (64). This paradigm raises important questions about structural differences of the ferroportin protein in peripheral tissues

compared to tissues that maintain systemic iron load, as well as their relative hepcidin responsiveness. Furthermore, it remains to be shown whether the hepcidin that is produced in peripheral tissues is identical to liver-derived hepcidin, or if there are structural and functional differences. Lastly, an enticing question remains as to whether peripheral hepcidin and/or ferroportin exert iron-independent functions. Hepcidin was originally discovered as an antimicrobial peptide and it is possible that local accumulation of hepcidin continues to exert this role. Future research will need to carefully answer these questions in detail to provide a more complete picture of the integration between systemic-level and cellular-level iron homeostasis.

1.5 Local iron metabolism in cancer

In addition to physiological, organ-specific mechanisms of iron homeostasis, diseases such as cancer operate unique pathways that modulate cell-autonomous iron handling and local iron metabolism. Mutations and aberrant gene expression networks in cancer are known to drive energy production and metabolite concentrations that afford tumors a growth and survival advantage. Iron is an essential metal micronutrient in cellular processes that are fundamental to cancer cell metabolism and cell proliferation.

A recent pan-cancer analysis of 14 cancer types revealed robust and conserved gene expression signatures that increase intratumoral iron levels and decrease patient survival (85). Furthermore, there is a large body of human epidemiological data that correlates iron levels with cancer risk, particularly in colorectal cancer (CRC). Red meat intake, which is high in heme iron, and mutations to *HFE* that cause iron overload both

associate with an increase risk of CRC (86-88). Interestingly, CRC is the only malignancy that maintains access to two sources of iron acquisition: i) systemic uptake via transferrin, and ii) intestinal lumen uptake. Accordingly, colon tumors massively upregulate apical iron import by overexpressing DMT1 in a HIF-2α-dependent manner (Figure 1.3) (89, 90). Furthermore, mice deficient for HIF-2α in the intestine develop fewer tumors that have lower intratumoral iron stores (89, 90). In addition to hyper-activating the many physiological functions of iron, cancers can use iron in unique ways to directly activate oncogenic STAT3 pathways, WNT signaling, DNA-synthesis, ROS-induced cell damage, and modulate P53 (91-94).

A burgeoning question is in understanding the mechanisms that enable tumors to hold onto and trap large iron stores. Ferroportin is the only mechanism by which mammals can export intracellular iron. Recent data has begun to demonstrate that cancers can activate cell-autonomous hepcidin/ferroportin dynamics to decrease iron efflux and increase intratumoral iron concentrations. Ferroportin protein abundance is reduced in breast cancer cells compared to nonmalignant breast epithelial cells, and breast cancer cells overexpressing ferroportin exhibited significantly reduced growth after orthotopic implantation (95). Several additional reports show that breast cancers can activate their own source of local hepcidin (96, 97). Reports have also demonstrated decreased expression of ferroportin and concomitant increases in ectopic hepcidin expression in prostate cancer (98, 99). Lastly, investigators show increases in hepcidin mRNA and protein in human CRC (90, 99). Future studies will need to expand on these correlative findings and solidify the functional role of cell-autonomous

hepcidin/ferroportin signaling in cancer. A major focus of Chapter 4 of this dissertation was to begin to address this question in the context of CRC.

Another key question is understanding the molecular basis by which cancer cells activate ectopic hepcidin expression. Reports have implicated a range of intratumoral molecules, including BMP4/7, IL6, Wnt, and GDF15, however, none of these findings have been functionally verified in vivo (96, 97, 99). A hallmark of the tumor microenvironment is hypoxia, as tumors outgrow their blood supply and are challenged by increased metabolic demand and inflammation (100). Interestingly, reports have shown that hypoxia can activate cardiac hepcidin mRNA in rats following 24 hour exposure to 6% oxygen (101). The hypoxia activated molecule, HIF-2α, maintains essential roles in both iron metabolism and CRC progression (56, 90). Future work will need to explore the role of intratumoral hypoxia in hepcidin/ferroportin signaling.

In the years to come, it will be advantageous to use cancer as a model system to understand basic mechanisms of local hepcidin/ferroportin dynamics. Given the intimate link between oxygen and iron metabolism, the possibility remains that intracellular hypoxia signaling is a regulator of local iron handling in normal physiology.

1.6 Conclusion and Perspectives

Iron is a metal micronutrient that is fundamental to both cellular metabolism and systemic biological processes that include oxygen transport and detoxification reactions. Whole organism iron homeostasis requires a symphony of organs working together to maintain iron levels. This process is controlled by two integrated players: i) the liver-derived, endocrine hormone, hepcidin, and ii) local intestinal regulation by the

transcription factor, HIF-2α. In addition to this systemic axis, recent work has unveiled complex organ-specific and cell-autonomous mechanisms of local iron handling. These networks include peripheral expression and regulation of hepcidin/ferroportin signaling that are separate from liver/intestine dynamics. Here, organs such as the heart are capable of modulating local iron levels during states of systemic iron deficiency. Furthermore, disease states, such as cancers, sequester massive iron stores and co-opt hepcidin, ferroportin, and HIF-2α to modulate local iron levels for a growth and survival advantage, particularly in colon cancer.

The purpose of this dissertation is to define the molecular mechanisms of iron metabolism in physiology and disease at both the systemic and cellular level. The work presented in this dissertation unveils a hetero-tissue crosstalk mechanism between liver hepcidin/intestinal HIF-2α that controls systemic iron levels in iron deficiency, anemia, and iron overload (Chapter 2). This work also characterizes the kinetics by which IDA progresses and unveils tissue-specific hypoxic and iron stress responses (Chapter 3). Lastly, I identify mechanisms by which colon cancer establishes ectopic hepcidin/ferroportin signaling to trap intracellular iron stores that are necessary for growth and survival of tumors (Chapter 4). Future studies should be directed towards understanding the mechanisms by which systemic iron handling interacts and integrates with local iron handling, which may lead to targeted therapies for iron related disorders and adjuvant strategies for cancers.

References

1. Korolnek T, and Hamza I. Macrophages and iron trafficking at the birth and death of red cells. *Blood.* 2015;125(19):2893-7.
2. Shah YM, and Xie L. Hypoxia-inducible factors link iron homeostasis and erythropoiesis. *Gastroenterology.* 2014;146(3):630-42.
3. McLean E, Cogswell M, Egli I, Wojdyla D, and de Benoist B. Worldwide prevalence of anaemia, WHO Vitamin and Mineral Nutrition Information System, 1993-2005. *Public Health Nutr.* 2009;12(4):444-54.
4. Muckenthaler MU, Rivella S, Hentze MW, and Galy B. A Red Carpet for Iron Metabolism. *Cell.* 2017;168(3):344-61.
5. Pietrangelo A. Genetics, Genetic Testing, and Management of Hemochromatosis: 15 Years Since Hepcidin. *Gastroenterology.* 2015;149(5):1240-51 e4.
6. Thein SL. Genetic Basis and Genetic Modifiers of beta-Thalassemia and Sickle Cell Disease. *Adv Exp Med Biol.* 2017;1013:27-57.
7. Krause A, Neitz S, Magert HJ, Schulz A, Forssmann WG, Schulz-Knappe P, et al. LEAP-1, a novel highly disulfide-bonded human peptide, exhibits antimicrobial activity. *FEBS Lett.* 2000;480(2-3):147-50.
8. Park CH, Valore EV, Waring AJ, and Ganz T. Hepcidin, a urinary antimicrobial peptide synthesized in the liver. *J Biol Chem.* 2001;276(11):7806-10.
9. Pigeon C, Ilyin G, Courselaud B, Leroyer P, Turlin B, Brissot P, et al. A new mouse liver-specific gene, encoding a protein homologous to human antimicrobial peptide hepcidin, is overexpressed during iron overload. *J Biol Chem.* 2001;276(11):7811-9.
10. Nicolas G, Bennoun M, Devaux I, Beaumont C, Grandchamp B, Kahn A, et al. Lack of hepcidin gene expression and severe tissue iron overload in upstream stimulatory factor 2 (USF2) knockout mice. *Proc Natl Acad Sci U S A.* 2001;98(15):8780-5.
11. Lesbordes-Brion JC, Viatte L, Bennoun M, Lou DQ, Ramey G, Houbron C, et al. Targeted disruption of the hepcidin 1 gene results in severe hemochromatosis. *Blood.* 2006;108(4):1402-5.
12. Nicolas G, Bennoun M, Porteu A, Mativet S, Beaumont C, Grandchamp B, et al. Severe iron deficiency anemia in transgenic mice expressing liver hepcidin. *Proc Natl Acad Sci U S A.* 2002;99(7):4596-601.
13. Nemeth E, Tuttle MS, Powelson J, Vaughn MB, Donovan A, Ward DM, et al. Hepcidin regulates cellular iron efflux by binding to ferroportin and inducing its internalization. *Science.* 2004;306(5704):2090-3.
14. Drakesmith H, Nemeth E, and Ganz T. Ironing out Ferroportin. *Cell Metab.* 2015;22(5):777-87.
15. Ahmad KA, Ahmann JR, Migas MC, Waheed A, Britton RS, Bacon BR, et al. Decreased liver hepcidin expression in the Hfe knockout mouse. *Blood Cells Mol Dis.* 2002;29(3):361-6.
16. Feder JN, Penny DM, Irrinki A, Lee VK, Lebron JA, Watson N, et al. The hemochromatosis gene product complexes with the transferrin receptor and

lowers its affinity for ligand binding. *Proc Natl Acad Sci U S A.* 1998;95(4):1472-7.
17. Corradini E, Rozier M, Meynard D, Odhiambo A, Lin HY, Feng Q, et al. Iron regulation of hepcidin despite attenuated Smad1,5,8 signaling in mice without transferrin receptor 2 or Hfe. *Gastroenterology.* 2011;141(5):1907-14.
18. Nai A, Lidonnici MR, Rausa M, Mandelli G, Pagani A, Silvestri L, et al. The second transferrin receptor regulates red blood cell production in mice. *Blood.* 2015;125(7):1170-9.
19. Andriopoulos B, Jr., Corradini E, Xia Y, Faasse SA, Chen S, Grgurevic L, et al. BMP6 is a key endogenous regulator of hepcidin expression and iron metabolism. *Nat Genet.* 2009;41(4):482-7.
20. Meynard D, Kautz L, Darnaud V, Canonne-Hergaux F, Coppin H, and Roth MP. Lack of the bone morphogenetic protein BMP6 induces massive iron overload. *Nat Genet.* 2009;41(4):478-81.
21. Canali S, Wang CY, Zumbrennen-Bullough KB, Bayer A, and Babitt JL. Bone morphogenetic protein 2 controls iron homeostasis in mice independent of Bmp6. *Am J Hematol.* 2017;92(11):1204-13.
22. Pauk M, Grgurevic L, Brkljacic J, Kufner V, Bordukalo-Niksic T, Grabusic K, et al. Exogenous BMP7 corrects plasma iron overload and bone loss in Bmp6-/- mice. *Int Orthop.* 2015;39(1):161-72.
23. Wrighting DM, and Andrews NC. Interleukin-6 induces hepcidin expression through STAT3. *Blood.* 2006;108(9):3204-9.
24. Pietrangelo A, Dierssen U, Valli L, Garuti C, Rump A, Corradini E, et al. STAT3 is required for IL-6-gp130-dependent activation of hepcidin in vivo. *Gastroenterology.* 2007;132(1):294-300.
25. Verga Falzacappa MV, Vujic Spasic M, Kessler R, Stolte J, Hentze MW, and Muckenthaler MU. STAT3 mediates hepatic hepcidin expression and its inflammatory stimulation. *Blood.* 2007;109(1):353-8.
26. Michels K, Nemeth E, Ganz T, and Mehrad B. Hepcidin and Host Defense against Infectious Diseases. *PLoS Pathog.* 2015;11(8):e1004998.
27. Ganz T. Iron and infection. *Int J Hematol.* 2018;107(1):7-15.
28. Hanudel MR, Rappaport M, Gabayan V, Jung G, Salusky IB, Nemeth E, et al. Increased serum hepcidin contributes to the anemia of chronic kidney disease in a murine model. *Haematologica.* 2017;102(3):e85-e8.
29. Harada N, Kanayama M, Maruyama A, Yoshida A, Tazumi K, Hosoya T, et al. Nrf2 regulates ferroportin 1-mediated iron efflux and counteracts lipopolysaccharide-induced ferroportin 1 mRNA suppression in macrophages. *Arch Biochem Biophys.* 2011;508(1):101-9.
30. Roetto A, Papanikolaou G, Politou M, Alberti F, Girelli D, Christakis J, et al. Mutant antimicrobial peptide hepcidin is associated with severe juvenile hemochromatosis. *Nat Genet.* 2003;33(1):21-2.
31. Njajou OT, de Jong G, Berghuis B, Vaessen N, Snijders PJ, Goossens JP, et al. Dominant hemochromatosis due to N144H mutation of SLC11A3: clinical and biological characteristics. *Blood Cells Mol Dis.* 2002;29(3):439-43.

32. Feder JN, Gnirke A, Thomas W, Tsuchihashi Z, Ruddy DA, Basava A, et al. A novel MHC class I-like gene is mutated in patients with hereditary haemochromatosis. *Nat Genet.* 1996;13(4):399-408.
33. Papanikolaou G, Samuels ME, Ludwig EH, MacDonald ML, Franchini PL, Dube MP, et al. Mutations in HFE2 cause iron overload in chromosome 1q-linked juvenile hemochromatosis. *Nat Genet.* 2004;36(1):77-82.
34. Roetto A, Daraio F, Alberti F, Porporato P, Cali A, De Gobbi M, et al. Hemochromatosis due to mutations in transferrin receptor 2. *Blood Cells Mol Dis.* 2002;29(3):465-70.
35. Merryweather-Clarke AT, Pointon JJ, Shearman JD, and Robson KJ. Global prevalence of putative haemochromatosis mutations. *J Med Genet.* 1997;34(4):275-8.
36. Pietrangelo A. Ferroportin disease: pathogenesis, diagnosis and treatment. *Haematologica.* 2017;102(12):1972-84.
37. Silvestri L, Guillem F, Pagani A, Nai A, Oudin C, Silva M, et al. Molecular mechanisms of the defective hepcidin inhibition in TMPRSS6 mutations associated with iron-refractory iron deficiency anemia. *Blood.* 2009;113(22):5605-8.
38. Finberg KE, Heeney MM, Campagna DR, Aydinok Y, Pearson HA, Hartman KR, et al. Mutations in TMPRSS6 cause iron-refractory iron deficiency anemia (IRIDA). *Nat Genet.* 2008;40(5):569-71.
39. Nicolas G, Chauvet C, Viatte L, Danan JL, Bigard X, Devaux I, et al. The gene encoding the iron regulatory peptide hepcidin is regulated by anemia, hypoxia, and inflammation. *J Clin Invest.* 2002;110(7):1037-44.
40. Piperno A, Galimberti S, Mariani R, Pelucchi S, Ravasi G, Lombardi C, et al. Modulation of hepcidin production during hypoxia-induced erythropoiesis in humans in vivo: data from the HIGHCARE project. *Blood.* 2011;117(10):2953-9.
41. Liu Q, Davidoff O, Niss K, and Haase VH. Hypoxia-inducible factor regulates hepcidin via erythropoietin-induced erythropoiesis. *J Clin Invest.* 2012;122(12):4635-44.
42. Mastrogiannaki M, Matak P, Mathieu JR, Delga S, Mayeux P, Vaulont S, et al. Hepatic hypoxia-inducible factor-2 down-regulates hepcidin expression in mice through an erythropoietin-mediated increase in erythropoiesis. *Haematologica.* 2012;97(6):827-34.
43. Pinto JP, Ribeiro S, Pontes H, Thowfeequ S, Tosh D, Carvalho F, et al. Erythropoietin mediates hepcidin expression in hepatocytes through EPOR signaling and regulation of C/EBPalpha. *Blood.* 2008;111(12):5727-33.
44. Anderson ER, Taylor M, Xue X, Martin A, Moons DS, Omary MB, et al. The hypoxia-inducible factor-C/EBPalpha axis controls ethanol-mediated hepcidin repression. *Mol Cell Biol.* 2012;32(19):4068-77.
45. Tanno T, Bhanu NV, Oneal PA, Goh SH, Staker P, Lee YT, et al. High levels of GDF15 in thalassemia suppress expression of the iron regulatory protein hepcidin. *Nat Med.* 2007;13(9):1096-101.
46. Tanno T, Porayette P, Sripichai O, Noh SJ, Byrnes C, Bhupatiraju A, et al. Identification of TWSG1 as a second novel erythroid regulator of hepcidin expression in murine and human cells. *Blood.* 2009;114(1):181-6.

47. Kautz L, Jung G, Valore EV, Rivella S, Nemeth E, and Ganz T. Identification of erythroferrone as an erythroid regulator of iron metabolism. *Nat Genet.* 2014;46(7):678-84.
48. Arezes J, Foy N, McHugh K, Sawant A, Quinkert D, Terraube V, et al. Erythroferrone inhibits the induction of hepcidin by BMP6. *Blood.* 2018;132(14):1473-7.
49. McKie AT, Barrow D, Latunde-Dada GO, Rolfs A, Sager G, Mudaly E, et al. An iron-regulated ferric reductase associated with the absorption of dietary iron. *Science.* 2001;291(5509):1755-9.
50. Mackenzie B, and Garrick MD. Iron Imports. II. Iron uptake at the apical membrane in the intestine. *Am J Physiol Gastrointest Liver Physiol.* 2005;289(6):G981-6.
51. Fleming MD, Trenor CC, 3rd, Su MA, Foernzler D, Beier DR, Dietrich WF, et al. Microcytic anaemia mice have a mutation in Nramp2, a candidate iron transporter gene. *Nat Genet.* 1997;16(4):383-6.
52. Donovan A, Lima CA, Pinkus JL, Pinkus GS, Zon LI, Robine S, et al. The iron exporter ferroportin/Slc40a1 is essential for iron homeostasis. *Cell Metab.* 2005;1(3):191-200.
53. Taylor M, Qu A, Anderson ER, Matsubara T, Martin A, Gonzalez FJ, et al. Hypoxia-inducible factor-2alpha mediates the adaptive increase of intestinal ferroportin during iron deficiency in mice. *Gastroenterology.* 2011;140(7):2044-55.
54. Anderson ER, Xue X, and Shah YM. Intestinal hypoxia-inducible factor-2alpha (HIF-2alpha) is critical for efficient erythropoiesis. *J Biol Chem.* 2011;286(22):19533-40.
55. Shah YM, Matsubara T, Ito S, Yim SH, and Gonzalez FJ. Intestinal hypoxia-inducible transcription factors are essential for iron absorption following iron deficiency. *Cell Metab.* 2009;9(2):152-64.
56. Schwartz AJ, Das NK, Ramakrishnan SK, Jain C, Jurkovic MT, Wu J, et al. Hepatic hepcidin/intestinal HIF-2alpha axis maintains iron absorption during iron deficiency and overload. *J Clin Invest.* 2019;129(1):336-48.
57. Das N, Xie L, Ramakrishnan SK, Campbell A, Rivella S, and Shah YM. Intestine-specific Disruption of Hypoxia-inducible Factor (HIF)-2alpha Improves Anemia in Sickle Cell Disease. *J Biol Chem.* 2015;290(39):23523-7.
58. Anderson ER, Taylor M, Xue X, Ramakrishnan SK, Martin A, Xie L, et al. Intestinal HIF2alpha promotes tissue-iron accumulation in disorders of iron overload with anemia. *Proc Natl Acad Sci U S A.* 2013;110(50):E4922-30.
59. Semenza GL. Hypoxia-inducible factors in physiology and medicine. *Cell.* 2012;148(3):399-408.
60. Wiesener MS, Jurgensen JS, Rosenberger C, Scholze CK, Horstrup JH, Warnecke C, et al. Widespread hypoxia-inducible expression of HIF-2alpha in distinct cell populations of different organs. *FASEB J.* 2003;17(2):271-3.
61. Wiener CM, Booth G, and Semenza GL. In vivo expression of mRNAs encoding hypoxia-inducible factor 1. *Biochem Biophys Res Commun.* 1996;225(2):485-8.

62. Gu YZ, Moran SM, Hogenesch JB, Wartman L, and Bradfield CA. Molecular characterization and chromosomal localization of a third alpha-class hypoxia inducible factor subunit, HIF3alpha. *Gene Expr.* 1998;7(3):205-13.
63. Mastrogiannaki M, Matak P, Keith B, Simon MC, Vaulont S, and Peyssonnaux C. HIF-2alpha, but not HIF-1alpha, promotes iron absorption in mice. *J Clin Invest.* 2009;119(5):1159-66.
64. Ramakrishnan SK, Anderson ER, Martin A, Centofanti B, and Shah YM. Maternal intestinal HIF-2alpha is necessary for sensing iron demands of lactation in mice. *Proc Natl Acad Sci U S A.* 2015;112(28):E3738-47.
65. Solanki S, Devenport SN, Ramakrishnan SK, and Shah YM. Temporal induction of intestinal epithelial hypoxia-inducible factor (HIF)-2alpha is sufficient to drive colitis. *Am J Physiol Gastrointest Liver Physiol.* 2019.
66. Muckenthaler MU, Galy B, and Hentze MW. Systemic iron homeostasis and the iron-responsive element/iron-regulatory protein (IRE/IRP) regulatory network. *Annu Rev Nutr.* 2008;28:197-213.
67. McKie AT, Marciani P, Rolfs A, Brennan K, Wehr K, Barrow D, et al. A novel duodenal iron-regulated transporter, IREG1, implicated in the basolateral transfer of iron to the circulation. *Mol Cell.* 2000;5(2):299-309.
68. Abboud S, and Haile DJ. A novel mammalian iron-regulated protein involved in intracellular iron metabolism. *J Biol Chem.* 2000;275(26):19906-12.
69. Zhang DL, Hughes RM, Ollivierre-Wilson H, Ghosh MC, and Rouault TA. A ferroportin transcript that lacks an iron-responsive element enables duodenal and erythroid precursor cells to evade translational repression. *Cell Metab.* 2009;9(5):461-73.
70. Lee PL, Gelbart T, West C, Halloran C, and Beutler E. The human Nramp2 gene: characterization of the gene structure, alternative splicing, promoter region and polymorphisms. *Blood Cells Mol Dis.* 1998;24(2):199-215.
71. Sanchez M, Galy B, Muckenthaler MU, and Hentze MW. Iron-regulatory proteins limit hypoxia-inducible factor-2alpha expression in iron deficiency. *Nat Struct Mol Biol.* 2007;14(5):420-6.
72. Ghosh MC, Zhang DL, Jeong SY, Kovtunovych G, Ollivierre-Wilson H, Noguchi A, et al. Deletion of iron regulatory protein 1 causes polycythemia and pulmonary hypertension in mice through translational derepression of HIF2alpha. *Cell Metab.* 2013;17(2):271-81.
73. Anderson SA, Nizzi CP, Chang YI, Deck KM, Schmidt PJ, Galy B, et al. The IRP1-HIF-2alpha axis coordinates iron and oxygen sensing with erythropoiesis and iron absorption. *Cell Metab.* 2013;17(2):282-90.
74. Wilkinson N, and Pantopoulos K. IRP1 regulates erythropoiesis and systemic iron homeostasis by controlling HIF2alpha mRNA translation. *Blood.* 2013;122(9):1658-68.
75. Lakhal-Littleton S, Wolna M, Carr CA, Miller JJ, Christian HC, Ball V, et al. Cardiac ferroportin regulates cellular iron homeostasis and is important for cardiac function. *Proc Natl Acad Sci U S A.* 2015;112(10):3164-9.
76. Lakhal-Littleton S, Wolna M, Chung YJ, Christian HC, Heather LC, Brescia M, et al. An essential cell-autonomous role for hepcidin in cardiac iron homeostasis. *Elife.* 2016;5.

77. Lakhal-Littleton S, Crosby A, Frise MC, Mohammad G, Carr CA, Loick PAM, et al. Intracellular iron deficiency in pulmonary arterial smooth muscle cells induces pulmonary arterial hypertension in mice. *Proc Natl Acad Sci U S A.* 2019;116(26):13122-30.
78. Ge XH, Wang Q, Qian ZM, Zhu L, Du F, Yung WH, et al. The iron regulatory hormone hepcidin reduces ferroportin 1 content and iron release in H9C2 cardiomyocytes. *J Nutr Biochem.* 2009;20(11):860-5.
79. McCarthy RC, and Kosman DJ. Glial cell ceruloplasmin and hepcidin differentially regulate iron efflux from brain microvascular endothelial cells. *PLoS One.* 2014;9(2):e89003.
80. Kulaksiz H, Theilig F, Bachmann S, Gehrke SG, Rost D, Janetzko A, et al. The iron-regulatory peptide hormone hepcidin: expression and cellular localization in the mammalian kidney. *J Endocrinol.* 2005;184(2):361-70.
81. Evans P, Cindrova-Davies T, Muttukrishna S, Burton GJ, Porter J, and Jauniaux E. Hepcidin and iron species distribution inside the first-trimester human gestational sac. *Mol Hum Reprod.* 2011;17(4):227-32.
82. Zhang DL, Senecal T, Ghosh MC, Ollivierre-Wilson H, Tu T, and Rouault TA. Hepcidin regulates ferroportin expression and intracellular iron homeostasis of erythroblasts. *Blood.* 2011;118(10):2868-77.
83. Zhang DL, Ghosh MC, Ollivierre H, Li Y, and Rouault TA. Ferroportin deficiency in erythroid cells causes serum iron deficiency and promotes hemolysis due to oxidative stress. *Blood.* 2018;132(19):2078-87.
84. Frazer DM, Wilkins SJ, Darshan D, Mirciov CSG, Dunn LA, and Anderson GJ. Ferroportin Is Essential for Iron Absorption During Suckling, But Is Hyporesponsive to the Regulatory Hormone Hepcidin. *Cell Mol Gastroenterol Hepatol.* 2017;3(3):410-21.
85. Zhang S, Chang W, Wu H, Wang YH, Gong YW, Zhao YL, et al. Pan-cancer analysis of iron metabolic landscape across the Cancer Genome Atlas. *J Cell Physiol.* 2019.
86. Cross AJ, Ferrucci LM, Risch A, Graubard BI, Ward MH, Park Y, et al. A large prospective study of meat consumption and colorectal cancer risk: an investigation of potential mechanisms underlying this association. *Cancer Res.* 2010;70(6):2406-14.
87. Nelson RL. Iron and colorectal cancer risk: human studies. *Nutr Rev.* 2001;59(5):140-8.
88. Osborne NJ, Gurrin LC, Allen KJ, Constantine CC, Delatycki MB, McLaren CE, et al. HFE C282Y homozygotes are at increased risk of breast and colorectal cancer. *Hepatology.* 2010;51(4):1311-8.
89. Xue X, Taylor M, Anderson E, Hao C, Qu A, Greenson JK, et al. Hypoxia-inducible factor-2alpha activation promotes colorectal cancer progression by dysregulating iron homeostasis. *Cancer Res.* 2012;72(9):2285-93.
90. Xue X, Ramakrishnan SK, Weisz K, Triner D, Xie L, Attili D, et al. Iron Uptake via DMT1 Integrates Cell Cycle with JAK-STAT3 Signaling to Promote Colorectal Tumorigenesis. *Cell Metab.* 2016;24(3):447-61.
91. Brookes MJ, Boult J, Roberts K, Cooper BT, Hotchin NA, Matthews G, et al. A role for iron in Wnt signalling. *Oncogene.* 2008;27(7):966-75.

92. Dixon SJ, and Stockwell BR. The role of iron and reactive oxygen species in cell death. *Nat Chem Biol.* 2014;10(1):9-17.
93. Le NT, and Richardson DR. The role of iron in cell cycle progression and the proliferation of neoplastic cells. *Biochim Biophys Acta.* 2002;1603(1):31-46.
94. Shen J, Sheng X, Chang Z, Wu Q, Wang S, Xuan Z, et al. Iron metabolism regulates p53 signaling through direct heme-p53 interaction and modulation of p53 localization, stability, and function. *Cell Rep.* 2014;7(1):180-93.
95. Pinnix ZK, Miller LD, Wang W, D'Agostino R, Jr., Kute T, Willingham MC, et al. Ferroportin and iron regulation in breast cancer progression and prognosis. *Sci Transl Med.* 2010;2(43):43ra56.
96. Blanchette-Farra N, Kita D, Konstorum A, Tesfay L, Lemler D, Hegde P, et al. Contribution of three-dimensional architecture and tumor-associated fibroblasts to hepcidin regulation in breast cancer. *Oncogene.* 2018;37(29):4013-32.
97. Zhang S, Chen Y, Guo W, Yuan L, Zhang D, Xu Y, et al. Disordered hepcidin-ferroportin signaling promotes breast cancer growth. *Cell Signal.* 2014;26(11):2539-50.
98. Xue D, Zhou CX, Shi YB, Lu H, and He XZ. Decreased expression of ferroportin in prostate cancer. *Oncol Lett.* 2015;10(2):913-6.
99. Tesfay L, Clausen KA, Kim JW, Hegde P, Wang X, Miller LD, et al. Hepcidin regulation in prostate and its disruption in prostate cancer. *Cancer Res.* 2015;75(11):2254-63.
100. Triner D, and Shah YM. Hypoxia-inducible factors: a central link between inflammation and cancer. *J Clin Invest.* 2016;126(10):3689-98.
101. Merle U, Fein E, Gehrke SG, Stremmel W, and Kulaksiz H. The iron regulatory peptide hepcidin is expressed in the heart and regulated by hypoxia and inflammation. *Endocrinology.* 2007;148(6):2663-8.

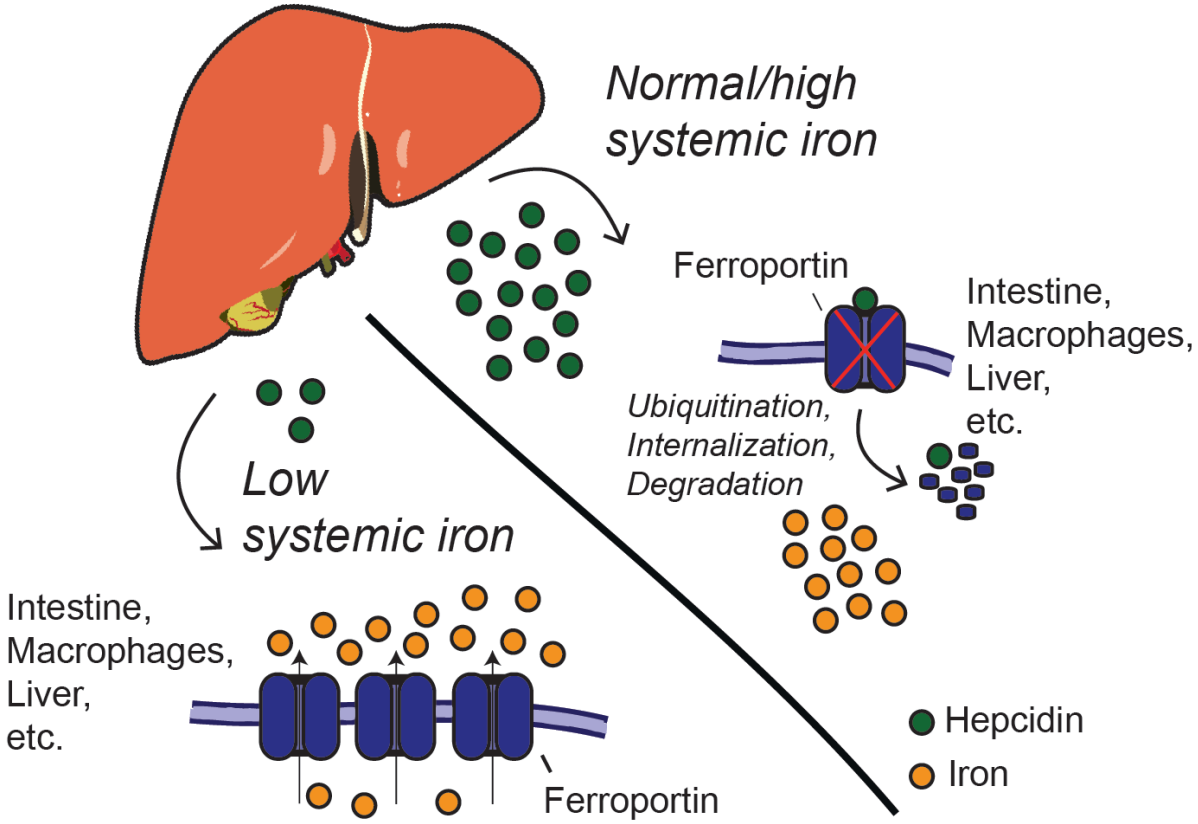

Figure 1.1. Hepcidin-mediated ferroportin degradation. During states of normal/high systemic iron, hepcidin is secreted by the liver into circulation in high quantities. Hepcidin binds to the iron exporter and its only molecular target, ferroportin. This interaction leads to rapid ubiquitination, internalization, and intracellular degradation of ferroportin, all of which limits iron export into circulation. However, under states of low systemic iron, or systemic iron demand, hepcidin production and release from the liver is potently repressed. This leads to downstream stabilization of ferroportin and increased iron mobilization from stores into circulation. Ferroportin is predominately expressed on tissues that regulate systemic iron handling, namely intestine, macrophages, and liver.

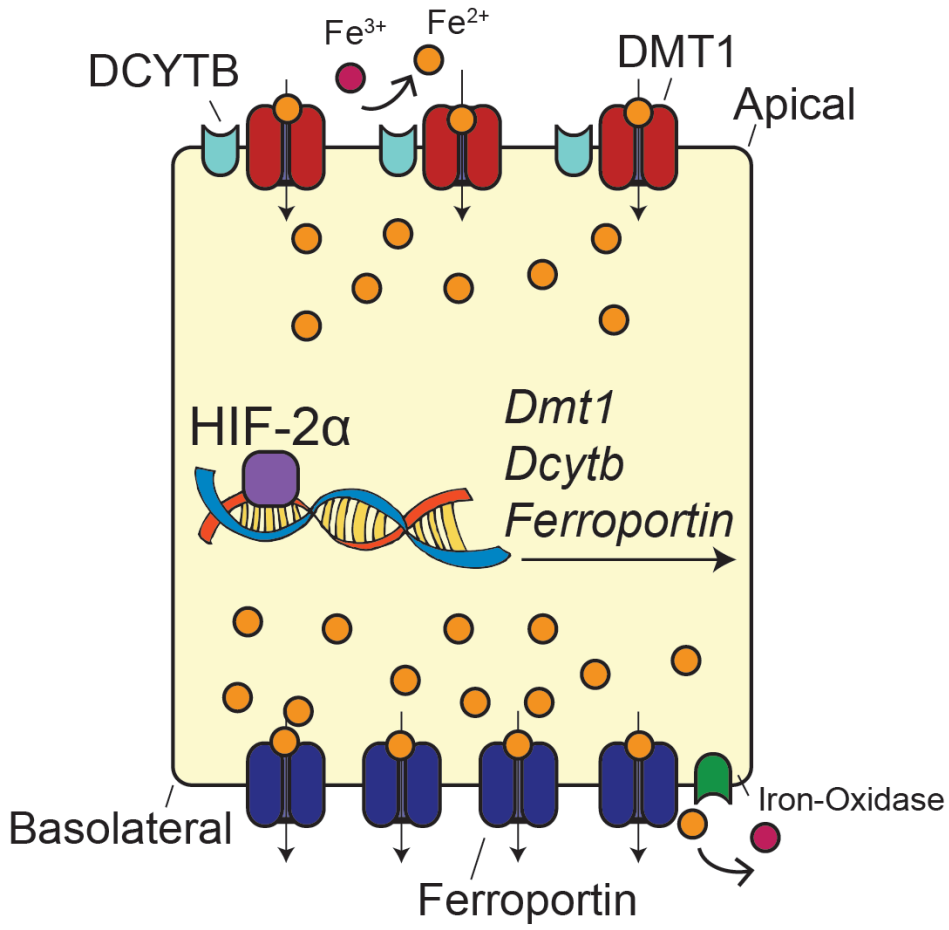

Figure 1.2. HIF-2α is necessary and sufficient to control intestinal iron absorption by transcriptionally regulating apical iron import and basolateral iron export. Absorptive duodenal enterocytes reduce dietary ferric iron (Fe^{3+}) into ferrous iron (Fe^{2+}) by the apical ferric reductase, duodenal cytochrome b (DcytB). Ferrous iron is then suitable for apical import via divalent metal transporter-1 (DMT1). Once inside the cytoplasm of enterocytes, iron is either, i) stored, or ii) exported out the basolateral surface into systemic circulation via the sole mammalian iron exporter, ferroportin. Once iron is exported via ferroportin, it becomes oxidized back to ferric iron and is circulated throughout the body. HIF-2α an intestinal iron sensor that transcriptionally upregulates *Dmt1*, *Dcytb*, and *Ferroportin* during states of systemic iron demand.

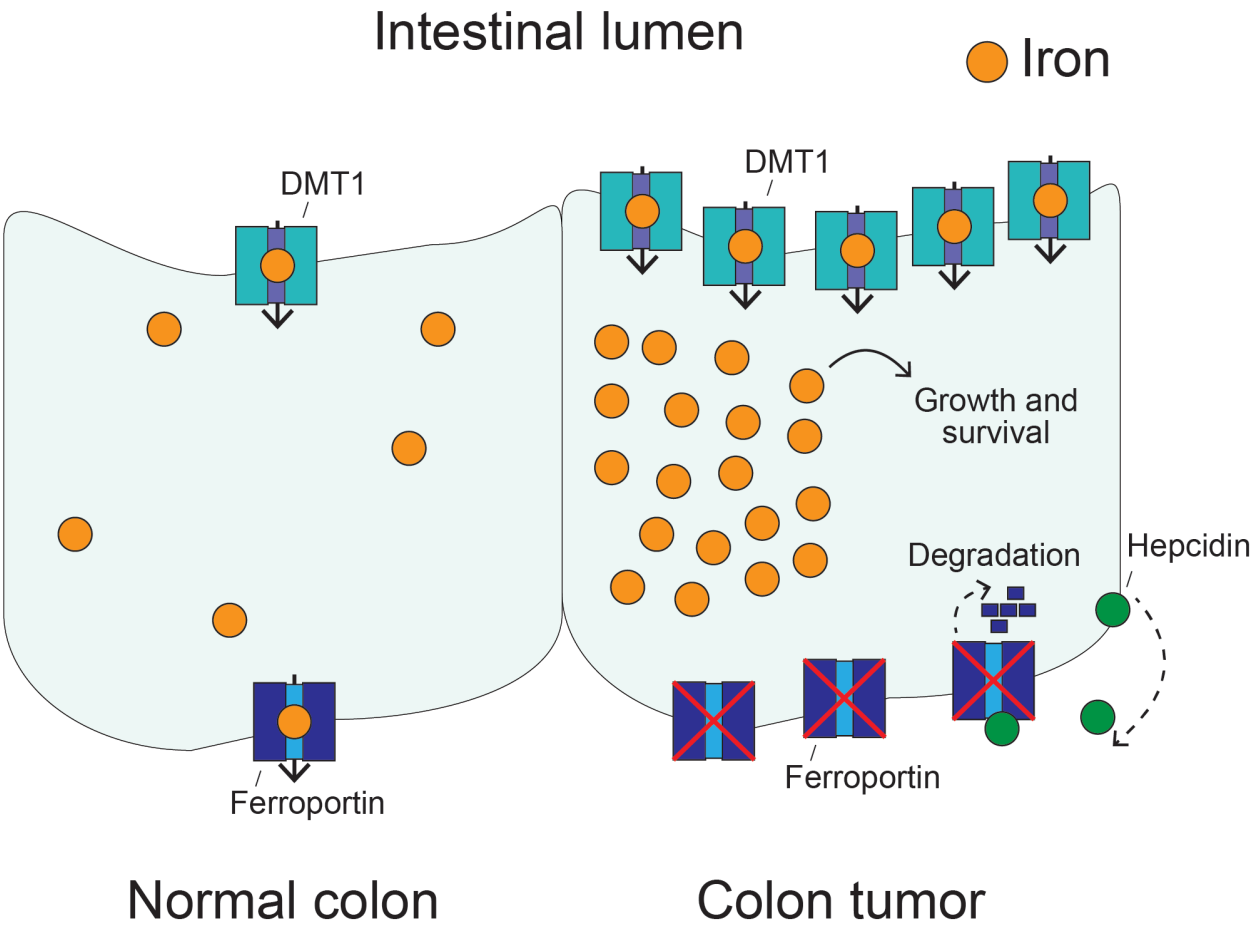

Figure 1.3. Colon tumors perturb local iron handling to trap intracellular iron and increase growth and survival. Compared to the normal adjacent colon, colon tumors massively upregulate the apical iron importer, DMT1, and downregulate the basolateral iron exporter, ferroportin. This leads to iron sequestration that is essential for colon tumor growth and survival. Recent data suggests that cancers, including colorectal cancer, can produce an ectopic source of hepcidin that acts in a paracrine/autocrine manner to downregulate the ferroportin protein in tumors.

Chapter 2[1]

Hepatic Hepcidin/Intestinal HIF-2α Axis Maintains Iron Absorption During Iron Deficiency and Overload

Abstract

Iron-related disorders are among the most prevalent diseases worldwide. Systemic iron homeostasis requires hepcidin, a liver-derived hormone that controls iron mobilization through its molecular target ferroportin (FPN), the only known mammalian iron exporter. This pathway is perturbed in diseases that cause iron overload. Additionally, intestinal HIF-2α is essential for the local absorptive response to systemic iron deficiency and iron overload. Our data demonstrate a hetero-tissue crosstalk mechanism, whereby hepatic hepcidin regulated intestinal HIF-2α in iron deficiency, anemia, and iron overload. I show that FPN controlled cell-autonomous iron efflux to stabilize and activate HIF-2α by regulating the activity of iron-dependent intestinal prolyl hydroxylase domain enzymes. Pharmacological blockade of HIF-2α using a clinically relevant and highly specific inhibitor successfully treated iron overload in a mouse model. These findings demonstrate a molecular link between hepatic hepcidin and intestinal HIF-2α that controls physiological iron uptake and drives iron hyperabsorption during iron overload.

[1] This chapter represents a published manuscript: Schwartz AJ, Das NK, Ramakrishnan SK, Jain C, Jurkovic MT, Wu J, Nemeth E, Lakhal-Littleton S, Colacino JA, Shah YM. Hepatic Hepcidin/Intestinal HIF-2α Axis Maintains Iron Absorption During Iron Deficiency and Overload, *Journal of Clinical Investigation*, *2019*

Introduction

More than 1 billion people worldwide are affected by iron overload, iron deficiency, and states of malnutrition that perturb iron homeostasis (1). Diseases of iron overload are among the most common genetic disorders in humans (2). The morbidity and mortality of patients with genetic iron overload are a result of the pathological hyperabsorption of dietary iron, which leads to systemic iron accumulation and iron-induced oxidant damage (3). The master regulator of systemic iron metabolism in mammals is hepcidin, a highly conserved peptide hormone that is predominately synthesized and secreted by the liver. The function of hepcidin is to bind to the only mammalian iron exporter, ferroportin (FPN), resulting in FPN occlusion, internalization from the plasma membrane, and intracellular degradation (4). In states of normal systemic iron and oxygen levels, hepcidin is abundantly produced, FPN is degraded, and iron mobilization into the plasma is limited. Conversely, during iron demand or systemic hypoxia, hepcidin production is repressed to enable FPN stabilization and iron mobilization into the circulation (5). FPN is predominately expressed and regulated in tissues that maintain systemic iron homeostasis, namely, intestine, liver, and macrophages of the reticuloendothelial system (6). Hepcidin-FPN interaction is the essential mechanism by which physiological iron homeostasis is maintained. Genetic mutations that disrupt the hepcidin/FPN axis give rise to all known forms of iron overload in mammals, referred to as hereditary hemochromatosis (2, 3, 5, 6). These data have fueled much research over the past decade on the molecular mechanisms that regulate hepatic hepcidin production in order to gain insight into how systemic iron homeostasis is maintained.

In addition to hepcidin, local intestinal regulation of iron handling plays an essential role in the maintenance of systemic iron homeostasis. HIF-2α is also sensitive to cellular iron and oxygen levels as the master intestinal transcriptional regulator of apical and basolateral iron transporters and is essential for maintaining postnatal systemic iron levels (7, 8). HIF-2α is necessary and sufficient to mediate the adaptive increase in iron absorption during both systemic iron deficiency and erythropoietic demand under systemic hypoxia through direct transcriptional activation of the iron absorptive machinery (9–11). HIF-2α also controls the hyperabsorption of dietary iron that leads to systemic iron accumulation in diseases of iron overload, such as β-thalassemia and sickle cell disease (12–14). However, the precise molecular cues that initiate and maintain intestinal HIF-2α during normal physiology and in disease are poorly understood. Moreover, it is unclear whether there is a concerted molecular integration of the systemic hepcidin pathway to local intestinal HIF-2α signaling in the regulation of iron homeostasis.

This study establishes that intestinal HIF-2α signaling is regulated by hepatic hepcidin dynamics. Through temporal in vivo and in vitro models of hepcidin and FPN modulation, this work demonstrates that the hepatic hepcidin and intestinal HIF-2α crosstalk is essential during iron overload, systemic iron deficiency, and anemia. Through unbiased whole-genome RNA-Seq analysis, I demonstrated that the canonical HIF-2α transcriptional response in the intestine is mediated by hepatic hepcidin. Mechanistically, the hepcidin/FPN axis controls HIF-2α in a cell-autonomous fashion by limiting the activity of iron-dependent prolyl hydroxylase domain (PHD) enzymes. A pharmacological inhibitor of HIF-2α that is in clinical phase II trials for clear-cell renal

cell carcinoma (NCT03108066; ClinicalTrials.gov) demonstrated reversal of iron overload in a mouse model.

Methods

Animals

For temporal, hepatocyte-specific disruption of hepcidin, mice floxed for *Hamp1* (*Hamp*$^{fl/fl}$) on a C57BL/6J background were crossed with C57BL/6J mice harboring CreERT2 recombinase under the control of the serum albumin promoter (*Alb*^{CreERT2}) to generate *Alb*^{CreERT2};*Hamp*$^{fl/fl}$ mice. *Vil*^{CreERT2};*Fpn*$^{fl/fl}$ and *Vil*^{CreERT2};*Dmt1*$^{fl/fl}$ mice are on a 129S4/SvJae background. Wild-type littermates were used as controls for all animal studies (*Hamp*$^{fl/fl}$, *Fpn*$^{fl/fl}$, and *Dmt1*$^{fl/fl}$), and analysis began on mice that were between 2 and 2.5 months of age for each of the respective experiments. Mice were injected i.p. with tamoxifen (Sigma-Aldrich) at a dose of 100 mg/kg body weight for 3 consecutive days to ensure Cre-mediated recombination. Phz (Sigma-Aldrich) was administered via i.p. injection at a dose of 60 mg/kg body weight, as described previously (9). PT2385 (MedChemExpress) was prepared and administered daily via oral gavage at a dose of 20 mg/kg body weight, as described previously (45). All mice were fed ad libitum and maintained under a 12-hour light/12-hour dark cycle. All mice were fed either a standard chow diet (Research Diets) or a purified AIN-93G iron-replete (350 ppm) or low- iron (<5 ppm) diet (Dyets). All mice were housed in the Unit for Laboratory Animal Management (ULAM) at the University of Michigan.

Cell culture

Stable doxycycline-inducible human FPN^{GFP} HEK293 cells were generated previously (20). To generate stable doxycycline-inducible human FPN^{GFP} IEC-6 cells, IEC-6 cells were purchased from the American Type Culture Collection (ATCC). pLenti

rtTA3 (Addgene) and pLVX-Tight-Puro hFpnGFP plasmids (20) were prepared into lentivirus by the University of Michigan Vector Core, co-infected into IEC-6 cells, and selected with 10 μg/ml blasticidin and 1 μg/ml puromycin. Cells were maintained at 37°C in 5% CO2 and 21% O2. Cells were cultured in DMEM supplemented with 10% FBS and 1% antibiotic/antimycotic. NCOA4-knockout cells were generated with the lentiCRISPR v2 construct (Addgene) using 2 unique sgRNAs against NCOA4 (NCOA4 sg1 and NCOA4 sg2, respectively) (Table 2.1). Briefly, oligonucleotides were subcloned into the lentiCRISPRv2 backbone. Empty vector, NCOA4 sg1, and NCOA4 sg2 constructs were prepared into lentivirus by the University of Michigan Vector Core. FPN^{GFP} cells were infected at a MOI of 10 and selected with 1 μg/ml puromycin. Knockout cells were verified by sequencing. The PHD enzyme activity luciferase reporter was previously described (46). Briefly, FPN^{GFP} cells were infected at 10 MOI overnight and treated the next day with 250 ng/ml doxycycline, 100 μM FG4592 (Selleckchem), 200 μM ferric ammonium citrate (FAC) (Sigma-Aldrich), and/or 1 mg/ml human recombinant hepcidin (Bachem) or 200 μM DFO (Sigma-Aldrich). The HIF-2α IRE luciferase construct was generated previously (24).

Hematological and iron analysis

The Unit for Laboratory Animal Medicine Pathology Core at The University of Michigan performed the complete blood count analysis. Non-heme iron was quantified as described previously (12).

Quantitative reverse transcription PCR

mRNA was measured by quantitative reverse transcription PCR (qPCR) (Life Technologies, Thermo Fisher Scientific). The primers used are listed in Table 2.1. Quantification cycle (Cq) values were normalized to β-actin and expressed as the fold change.

Whole-genome RNA-Seq and analysis

RNA-Seq libraries were prepared using the TruSeq RNA Library Prep Kit v2 (Illumina) according to the manufacturer's recommended protocol. The libraries were sequenced using single-end, 50-cycle reads on a HiSeq 2500 sequencer (Illumina) at the University of Michigan's DNA Sequencing Core Facility. RNA-Seq analysis was performed as described previously (18). Briefly, quality control of raw FastQ files was performed using FastQC, version 0.11.5. FastQ files were mapped to the mouse genome (mm10) using STAR-2.5.3.a with the options "outFilterMultimapNmax 10" and "sjdb- Score 2." Gene expression levels were quantified using the Subread featureCounts (version 1.5.2) package. Differential expression testing was conducted with the Bioconductor package edgeR, version 3.16.5, using glmLRT. To reduce the dispersion of the data set due to lowly expressed genes, genes with a mean aligned read count of less than 5 across all samples were excluded from the analysis. Genes with an FDR of less than 0.01 or 0.1 were considered differentially expressed, to yield high- and low-stringency approaches. The sequencing data are publicly available through ArrayExpress (accession number E-MTAB-7329).

Western blot analysis

Whole-cell, nuclear, and membrane lysates were prepared as described previously (10, 47). In brief, lysates were separated by SDS-PAGE, transferred onto nitrocellulose membranes, and probed overnight at 4°C with antibodies against FPN (MTP11-A, Alpha Diagnostic International [ADI]), DMT1 (NRAMP21-A, ADI), DCYTB (DCYTB-11A, ADI), and TFR1 (13-6800, Invitrogen, Thermo Fisher Scientific) for mouse tissue lysates; FPN (NBP1-21502, Novus), FTH1 (3998S, Cell Signaling Technology), GAPDH (sc-47724, Santa Cruz Biotechnology), GFP (sc-996, Santa Cruz Biotechnology), lamin A/C (3A6-4C11, Active Motif), HIF-2α (BL-95-1A2, Bethyl), and HIF- 1α (179483, Abcam) for human lysates; and actin (60008-1, Proteintech) for mouse tissue and rat cell lysates.

ELISA

High-binding polystyrene microtiter plates were coated with the protein lysates overnight. The plates were then washed in 1×PBS with 0.1% Tween-20 (PBST), blocked with 5% BSA, and incubated with primary antibodies against HIF-2α (AF2997, Novus) and HIF- 1α (179483, Abcam). Next, the plates were washed in PBST, incubated with the appropriate HRP-conjugated secondary antibodies, developed, and read at 450 nm in a plate reader.

Luciferase assay

Cells were lysed in reporter lysis buffer (Promega), and firefly luciferase activity was measured as described previously (48).

Statistics

Results are expressed as the mean ± SEM. Significance between 2 groups was tested using a 2-tailed, unpaired *t* test. Significance among multiple groups was tested using a 1-way or 2-way ANOVA followed by Tukey's post hoc test for multiple comparisons. A *P* value of less than 0.05 was considered statistically significant. GraphPad Prism 7.0 was used to conduct the statistical analyses.

Study approval

All animal procedures were approved by the IACUC of the University of Michigan.

Results

Inducible deletion of hepatic hepcidin leads to the activation of intestinal HIF-2α and rapid iron accumulation

To understand the molecular connection between hepatic hepcidin and intestinal HIF-2α, mice that express a tamoxifen-inducible CreERT2 fusion protein under the control of the serum albumin promoter (*Alb*) were crossed with hepcidin 1–floxed (*Hamp*-floxed) mice ($Alb^{CreERT2};Hamp^{fl/fl}$), giving rise upon tamoxifen administration to mice null for hepatic hepcidin ($Hamp^{\Delta Liv}$) (Figure 2.1A). This inducible model allows for temporal, in vivo study of hepcidin action on HIF-2α, without the confounding effects that arise in later stages of hepcidin deficiency iron overload, namely, the accumulation of ROS (15). Moreover, hepatocyte-specific deletion of hepcidin leaves intact the sources of hepcidin that exist outside of the liver, such as in the heart, where cell-autonomous regulation of cardiac iron homeostasis has recently been shown to exist (16). In this model, the hepcidin transcript *Hamp* was significantly decreased in livers as early as 2 weeks after tamoxifen treatment (Figure 2.1B). Interestingly, liver expression of the serum iron uptake receptor transferrin receptor (*Tfrc*) was significantly decreased at 4 weeks, while the FPN transcript (*Fpn*) was increased at 2 weeks (Figure S2.1A). Prussian blue staining revealed progressive liver iron overload. Liver iron accumulation at 2 weeks was minimal, but I detected a time-dependent increase at 4 and 12 weeks. Histological analysis revealed minimal morphological differences across all time points (Figure 2.1C). An iron assay revealed a significant increase in serum iron as soon as within 2 weeks, with no further increase at 4 or 12 weeks, suggesting that serum iron is rapidly saturated following disruption to hepcidin (Figure 2.1D). A major complication for

patients with hemochromatosis is cardiac dysfunction (17). I found that Prussian blue staining did not detect heart iron accumulation at 2 or 4 weeks following hepcidin deletion but observed significant iron accumulation and disruptions in cellularity and tissue architecture by 12 weeks (Figure S2.1B). I observed similar tissue iron loading in the heart and pancreas (Figure 2.1, E and F, and Figure S2.1B). In order to assess the regulation of intestinal HIF-2α by hepatic hepcidin prior to confounding effects that are associated with iron overload, I performed immunohistochemical analysis on duodenal sections 2 weeks after tamoxifen treatment. I detected a robust increase in HIF-2α protein expression (Figure 2.1G). Consistent with these data, I also observed activation of iron-absorptive, HIF-2α–specific target genes and proteins duodenal cytochrome b (*Dcytb*, also known as *Cybrd1*), divalent metal transporter 1 (*Dmt1*, also known as *Slc11a2*), *Fpn*, and *Ankrd37*, as well as the expression of duodenal *Tfrc*, an indicator of low cellular iron status (Figure 2.1, H and I) (10). I detected no change in the expression of HIF-1α target genes (Figure S2.1C) or HIF-2α inflammatory target genes (Figure 2.1D) (18, 19). Furthermore, I observed no change in HIF-2α–regulated transcripts in the kidneys or spleen, while *Tfrc* expression was decreased in both organs, suggesting that the hepcidin/HIF-2α axis was specific to the intestine (Figure S2.2, A and B). These data indicate that changes to hepcidin regulate HIF-2α stability and activity in physiology and disease.

FPN is necessary for the activation of intestinal HIF-2α during systemic iron deficiency

To address the molecular mechanism by which hepatic hepcidin regulates intestinal HIF-2α, I investigated the intestinal iron exporter and only target of hepcidin, FPN, in a context of systemic iron demand. *Fpn*-floxed mice were bred with mice that express a tamoxifen-inducible CreERT2 fusion protein under the control of the villin (*Vil*) promoter ($Vil^{CreERT2}$;$Fpn^{fl/fl}$), giving rise upon tamoxifen administration to mice null for FPN in the intestinal epithelium ($Fpn^{\Delta IE}$). $Fpn^{fl/fl}$ and *VilCreERT2* $Fpn^{fl/fl}$ mice were placed on a 350-ppm (iron-replete) diet or on a diet of less than 5-ppm iron (low-iron) for 1 week, injected with tamoxifen on 3 consecutive days, and sacrificed after an additional week on the respective diets (Figure 2.2A). This model mimics hepcidin excess at the intestinal level and leads to iron retention in intestinal epithelial cells, despite a state of systemic iron demand (Figure 2.2B). Duodenal *Fpn* was significantly decreased following tamoxifen treatment (Figure 2.2C), and duodenal iron retention was detected by Western blotting for the intracellular iron storage protein ferritin (FTH1) (Figure 2.2D). I found that hepcidin (*Hamp*) transcript levels were significantly decreased in mice on the low-iron diet and in $Fpn^{\Delta IE}$ mice (Figure 2.2E). This time point did not induce anemia, as RBC numbers, hemoglobin (HB) counts, hematocrit (HCT) levels, mean corpuscular hemoglobin (MCH) levels, and mean corpuscular volume (MCV) were all unchanged across the cohorts (Figure 2.2F and Figure S2.3A). As complete blood count parameters were unaffected, this model dissociated the enterocyte cellular response to iron deficiency from hypoxia. As expected, I found that duodenal HIF-2α was stabilized and that HIF-2α–specific iron- absorptive genes were increased in $Fpn^{fl/fl}$ mice on a low-iron diet. These responses were abrogated in $Fpn^{\Delta IE}$ mice (Figure 2.2, G and H). I also observed no changes in the expression of HIF-1α target genes or HIF-2α

inflammatory target genes (Figure S2.3, B and C). These data demonstrate that the intestinal HIF-2α response to systemic iron demand occurs downstream of the hepcidin/FPN axis.

FPN is essential for the intestinal HIF-2α response to erythropoietic demand

Intestinal HIF-2α is critical for the adaptive increase in iron absorption that enables efficient erythropoiesis (9, 10). This increase in erythropoiesus has been postulated to be regulated by changes in intestinal epithelial oxygen levels. I used a phenylhydrazine (Phz) hemolytic anemia model, which stimulates massive erythropoiesis. $Fpn^{fl/fl}$ and $Vil^{CreERT2}$;$Fpn^{fl/fl}$ mice were injected with tamoxifen and allowed to recover for 1 week. Two consecutive injections of either vehicle or Phz were administered, and the mice were sacrificed 48 hours later (Figure 2.3A). I found that the erythropoietin (*Epo*) transcript levels were significantly elevated in the kidneys of Phz-treated mice, indicating a state of erythropoietic drive and systemic hypoxia (Figure 2.3B). Hepcidin (*Hamp*) transcript levels were significantly decreased in the Phz-treated mice and vehicle-treated $Fpn^{\Delta IE}$ mice (Figure 2.3C). I found that duodenal ferritin abundance was decreased following Phz treatment in $Fpn^{fl/fl}$ mice, indicating the mobilization of intestinal iron, while this response was blunted in $Fpn^{\Delta IE}$ mice (Figure 2.3D). Interestingly, and consistent with the low-iron response, the activation of intestinal HIF-2α and HIF-2α–specific iron-absorptive genes during stress erythropoiesis was completely dependent on intact intestinal FPN (Figure 2.3, E and F). I also detected no change in the expression of HIF-1α target genes or HIF-2α inflammatory target

genes (Figure S2.4, A and B). These data demonstrate that the hepcidin/FPN axis is essential for the response of intestinal HIF-2α to low systemic oxygen levels.

Intestinal epithelial iron regulates the HIF-2α response to changes in systemic iron and oxygen

To clearly demonstrate that enterocyte iron flux was the major mechanism by which the hepcidin/FPN axis regulated HIF-2α, I sought to modulate luminal versus enterocyte iron levels. To modulate luminal enterocyte levels, *Dmt1*-floxed mice were bred with mice that express a tamoxifen-inducible Cre^{ERT2} fusion protein under the control of the villin (*Vil*) promoter ($Vil^{CreERT2}$;$Dmt1^{fl/fl}$), giving rise upon tamoxifen administration to mice null for DMT1 in the intestinal epithelium ($Dmt1^{\Delta IE}$). Enterocyte iron levels were modulated using $Fpn^{\Delta IE}$ animals, as explained above. Long-term disruption of DMT1 or FPN gave rise to a state of systemic iron deficiency anemia, with differences seen only in the compartment of iron trapping (i.e., luminal vs. enterocytic iron retention) (Figure 2.4A). $Vil^{CreERT2}$;$Fpn^{fl/fl}$, $Vil^{CreERT2}$;$DMT1^{fl/fl}$, and their littermate controls were assessed 3 months after tamoxifen treatment. I found that *Fpn* and *Dmt1* transcripts levels were significantly decreased in $Fpn^{\Delta IE}$ and $Dmt1^{\Delta IE}$ mice, respectively (Figure 2.4B). *Fpn* transcript levels were significantly elevated in $Dmt1^{\Delta IE}$ mice, while I detected no change in *Dmt1* transcript levels in $Fpn^{\Delta IE}$ mice. As expected, the hepcidin (*Hamp*) transcript was potently repressed in the $Fpn^{\Delta IE}$ and $DMT1^{\Delta IE}$ cohorts as compared with the $Fpn^{fl/fl}$ and $Dmt1^{fl/fl}$ mice, respectively (Figure 2.4C). Furthermore, I detected decreased RBC numbers, HB counts, HCT levels, MCH, and MCV in the $Fpn^{\Delta IE}$ and $Dmt1^{\Delta IE}$ mice compared with their littermate controls, which indicated a state

of systemic iron deficiency anemia (Figure 2.4D and Figure S2.5A). Duodenal ferritin abundance was decreased in *Dmt1*$^{\Delta IE}$ mice, with the opposite response observed in *Fpn*$^{\Delta IE}$ mice (Figure S2.5B). Immunohistochemical analysis revealed significant stabilization of the HIF-2α protein in *Dmt1*$^{\Delta IE}$ mice, with no change in these protein levels in *Fpn*$^{\Delta IE}$ mice (Figure 2.4E). Moreover, expression levels of the HIF-2α–specific iron genes *Dcytb* and *Ankrd37* were significantly elevated in *Dmt1*$^{\Delta IE}$ mice, but not in *Fpn*$^{\Delta IE}$ mice (Figure 2.4F). I found that *Tfrc* expression was unchanged in *Fpn*$^{\Delta IE}$ mice and significantly increased in *Dmt1*$^{\Delta IE}$ mice compared with expression levels in their littermate controls (Figure 2.4F). These data convincingly show that intestinal epithelial iron levels regulate HIF-2α during systemic iron and oxygen deficiency and during iron deficiency anemia.

The intestinal transcriptome during systemic iron demand matches the intestinal response to hepcidin deficiency

The data thus far suggested that the entire intestinal HIF-2α response to systemic iron and erythropoietic demand was controlled by hepatic hepcidin. However, the outputs for these experiments relied on the measurement of canonical HIF-2α target genes involved in intestinal iron handling. I used an unbiased, high-throughput RNA-Seq approach to compare the duodenal transcriptome during systemic iron demand with that of hepcidin deficiency iron overload. *Hamp*$^{fl/fl}$ and *Alb*^{CreERT2};*Hamp*$^{fl/fl}$ mice were placed on iron-replete and low-iron diets and sacrificed 2 weeks after tamoxifen treatment (Figure 2.5A). Hepcidin transcript levels were significantly decreased in *Hamp*$^{fl/fl}$ mice on a low-iron diet and in both *Hamp*$^{\Delta Liv}$ cohorts (Figure 2.5B). To assess

the most significantly changed transcripts when comparing genotype and diet interactions, samples were clustered hierarchically in an unsupervised manner on the basis of the expression of genes that were differentially expressed between conditions at a high-stringency FDR of less than 0.01. I found that the iron-replete *Hamp*$^{fl/fl}$ samples clustered separately from the iron-replete *Hamp*$^{\Delta Liv}$, low-iron *Hamp*$^{fl/fl}$, and low-iron *Hamp*$^{\Delta Liv}$ samples (Figure 2.5C). This demonstrated in an unbiased fashion that the intestinal transcriptomes during systemic iron demand and iron overload were statistically similar to one another, because the 9 treatment samples did not segregate into discrete experimental clusters. I then generated a heatmap, plotting scaled gene expression of the same differentially expressed genes to assess the identity of the genes used for unsupervised hierarchical clustering (Figure 2.5D). Importantly, I identified the canonical HIF-2α iron–regulated genes (i.e., *Slc11a2*, *Cybrd1*, and *Ankrd37*). In order to identify novel transcripts in the RNA-Seq data set, I performed a lower-stringency differential expression analysis (FDR < 0.1). Using this approach, I identified genes that were exclusively regulated by iron deficiency (e.g., *Nos2*, *Ccl20*, and *Serpine1*) and hepcidin deficiency (e.g., *Wdr72*, *A4gn7*, and *Gkn3*), as well as novel target genes regulated in both contexts (e.g., *Mir7082*, *Slc34a2*, and *Itpr1*) (Figure 2.5E). Collectively, these data demonstrate that the most robustly changed intestinal transcripts during systemic iron demand resemble those in primary hepcidin deficiency iron overload.

FPN activates HIF-2α in a cell-autonomous manner that is dependent on intracellular iron efflux

To interrogate the molecular mechanism of HIF-2α stabilization downstream of the hepcidin/FPN axis, I used an in vitro system that models the cellular response to low levels of systemic hepcidin. Most cell lines express very low levels of the FPN protein, and some cell lines appear to be resistant to hepcidin-mediated FPN degradation (10). I assessed hepcidin-sensitive, doxycycline-inducible human FPN^{GFP} HEK293 cells, as described previously (20). Upon doxycycline treatment, I detected robust FPN^{GFP} expression by Western blot analysis (Figure 2.6A). This mimicked a cellular environment of low systemic hepcidin, comparable to that in the intestine, as the fold induction of FPN protein in the FPN^{GFP} HEK293 cells was similar to that observed in duodenums of $Hamp^{\Delta Liv}$ mice (Figure S2.6, A and B). To determine whether the regulation of HIF-2α by hepcidin-FPN is cell autonomous, I treated FPN^{GFP} cells with doxycycline for 24 hours and generated cytosolic and nuclear fractions. For a positive control, I also treated cells with FG4592, a 2-oxoglutarate analog and chemical inhibitor of the PHD-containing enzymes that regulate HIF. I found that HIF-2α was robustly stabilized in the nucleus of FPN^{GFP} cells (Figure 2.6B). Importantly, HIF-2α protein was stabilized to the same extent as that seen with FG4592 treatment, suggesting maximal activation. The HIF-2α response was blunted by iron loading with ferric ammonium citrate (FAC) and recombinant hepcidin treatment, indicating that the activity of HIF-2α in FPN^{GFP} cells was dependent on intracellular iron concentration, downstream of hepcidin-mediated FPN degradation (Figure 2.6C). Together, these data demonstrate cell-autonomous activation of HIF-2α by iron efflux. This mechanism shows some differences as compared with HIF activation by intracellular iron chelation using compounds such as deferoxamine (DFO), which disrupts mitochondrial function and

results in significant cell death (Figure S2.6C) (21–23). The protein stability of HIF-2α is regulated by PHD enzymes. I found that PHD enzymes were downstream of hepcidin-FPN in the regulation of HIF-2α, as FG4592 restored the HIF-2α response in FPN^{GFP} cells following FAC or recombinant hepcidin treatment (Figure 2.6D). PHD enzymes require both iron and oxygen for their function. In order to address whether PHD enzyme activity was decreased following FPN stabilization, an adenovirus-based reporter construct to measure PHD enzyme activity was generat- ed by fusing luciferase to a canonical PHD hydroxylation domain (PHD reporter) (Figure 6E). I detected a significant increase in luciferase activity in FPNGFP cells following doxycycline treatment, and this increase was similar to that seen with chemical inhibition of PHD enzymes by FG4592 treatment (Figure 6F). This response was rescued by loading with FAC and by treatment with recombinant hepcidin. These data demonstrated that stabilization of FPN in the context of low hepatic hepcidin leads to cellular iron efflux, decreased PHD enzyme activity, and, ultimately, cell-autonomous stabilization of HIF-2α. PHD enzymes regulate both HIF-2α and HIF-1α. However, HIF-1α protein was stabilized submaximally following FPN overexpression compared with treatment with FG4592, suggesting selectivity of the hepcidin/FPN axis for HIF-2α over HIF-1α (Figure S2.6D). HIF-2α contains a 5′-UTR iron-responsive element (IRE) that is responsible for translational inhibition during decreases in intracellular iron (24). Using a HIF- 2α IRE luciferase construct, I demonstrated HIF-2α inhibition following FPN overexpression via doxycycline, with DFO and FAC as controls, suggesting a negative feedback mechanism on FPN-mediated activation of HIF-2α (Figure S2.6E). There are 2 major pools of intracellular iron: (a) labile “free” iron, and (b) iron bound by the intracellular iron

storage protein ferritin. The mobilization of ferritin-bound iron requires the lysosomal degradation of ferritin via the rate-limiting cargo protein nuclear receptor coactivator 4 (NCOA4) (25, 26). To address which pool of iron is limited for PHD enzymes by FPN, 2 unique NCOA4-KO cell lines were generated and sequence verified in FPN^{GFP} cells. FPN overexpression led to ferritin degradation in an NCOA4-dependent manner (Figure 2.6G). However, NCOA4 deletion did not prevent the decreased PHD enzyme activity following FPN overexpression (Figure S2.6F). While doxycycline-inducible FPN^{GFP} HEK293 cells have been widely used to study hepcidin-FPN dynamics (20, 27, 28), I sought to interrogate the hepcidin/FPN/HIF-2α axis in an intestinal epithelial cell line. IEC-6 cells are a normal rat small intestinal cell line, and a doxycycline-inducible human FPN^{GFP} IEC-6 cell line was generated. FPN^{GFP} IEC-6 cells showed FPN stabilization after doxycycline treatment to a degree similar to that observed in duodenums of *Hamp*$^{\Delta Liv}$ mice (Figure S2.6B). Moreover, I found that FPN^{GFP} IEC-6 cells were highly sensitive to hepcidin (Figure 2.6H). Several HIF-2α antibodies that were tested did not detect a specific HIF-2α band by Western blot analysis of rat lysates (data not shown). I used an ELISA approach with a HIF-2α antibody that could detect native recombinant HIF-2α. I observed robust HIF-2α stabilization following FPN overexpression via doxycycline treatment and found that co-treatment with doxycycline and hepcidin completely rescued this response, with DFO serving as a positive control (Figure 2.6I). Similar to what was observed in vivo, I detected no increase in HIF-1α following FPN overexpression in the IEC-6 FPN^{GFP} cells, while DFO treatment significantly increased HIF-1α expression, further indicating a difference in the mechanism of action of iron efflux through FPN and iron chelation by DFO (Figure S2.6G). The mechanism of HIF-

2α activation by FPN overexpression in IEC-6 cells was the same as in HEK293 cells, as PHD enzyme activity was decreased by FPN overexpression in an iron- and hepcidin-dependent manner (Figure 2.6J). Collectively, these data demonstrate that in the absence of hepcidin, stabilization of membrane FPN regulates HIF-2α in a cell-autonomous manner by depleting the cellular labile iron pool and limiting the activity of PHD enzymes.

Inhibition of HIF-2α with PT2385 decreases systemic iron accumulation in hepcidin-deficient iron overload

Current therapeutic approaches for patients with iron overload rely on iron chelators and phlebotomy, which lead to significant off-target effects and cause fatigue. I sought to determine whether the hepatic hepcidin/intestinal HIF-2α axis can be therapeutically targeted to treat iron overload. The HIF-2α–specific inhibitor PT2385 was recently developed (29). PT2385 binds to HIF-2α and prevents its heterodimerization with aryl hydrocarbon receptor nuclear translocator (ARNT), thus preventing the transcriptional activity of HIF-2α (29). PT2385 is currently in a phase II clinical trial for the treatment of clear-cell renal cell carcinoma (NCT03108066; ClinicalTrials.gov). *Hamp*$^{fl/fl}$ and *Alb*^{CreERT2};*Hamp*$^{fl/fl}$ mice were injected with tamoxifen, and 2 weeks later, the *Hamp*$^{\Delta Liv}$ mice were orally gavaged with vehicle or PT2385 daily for 2 weeks (Figure 2.7A). I observed no change in body weight during the treatment period (Figure S7A). The hepcidin transcript levels were decreased in both *Hamp*$^{\Delta Liv}$ cohorts (Figure 2.7B). Decreased intestinal iron absorption in mice with a genetic disruption of intestinal HIF-2α leads to anemia (10). Thus, I sought to determine whether prolonged treatment with

PT2385 would lead to systemic anemia. I found that kidney *Epo* transcript levels were decreased in vehicle-treated *Hamp*$^{\Delta Liv}$ mice, while this decrease was abrogated in PT2385-treated *HampΔ*^{Liv} mice (Figure 2.7B). I noted a significant expansion of RBC numbers and increased HB and HCT in vehicle-treated *Hamp*$^{\Delta Liv}$ mice, and these increases were rescued in the PT2385 cohort (Figure 2.7C). MCV and MCH levels were unchanged among all groups (Figure S2.7B). Membrane stabilization of the HIF-2α iron absorptive targets FPN, DMT1, and DCYTB was elevated in the *Hamp*$^{\Delta Liv}$ mice but was completely absent in the PT2385-treated *Hamp*$^{\Delta Liv}$ mice (Figure 2.7D). Prussian blue staining for iron in the liver was decreased in the PT2385-treated *Hamp*$^{\Delta Liv}$ mice compared with that seen in the vehicle-treated mice (Figure 2.7E). Additionally, quantitative iron assays revealed significant decreases in serum, liver, and pancreatic iron content, with a trend toward a decrease of iron in the heart in PT2385-treated *Hamp*$^{\Delta Liv}$ mice (Figure 2.7F). These data show that HIF-2α is a potential pharmacological target downstream of the hepcidin/FPN axis in patients with iron overload (Figure 2.7G).

Discussion

Systemic iron homeostasis requires multiple organs working in concert to maintain cellular iron concentrations for metabolism and RBC levels for systemic oxygen transport. Research over the past decade has shown that this system is centrally regulated by the liver-derived hormone hepcidin and requires intestinal iron absorption for the maintenance of postnatal systemic iron levels. However, a complete biological link between the liver and intestine during iron deficiency and in diseases of iron overload has remained unclear. The present work demonstrates that the liver controls the intestine through a hepatic hepcidin/intestinal HIF- 2α axis that regulates physiological iron uptake during systemic iron deficiency and drives pathological iron absorption during iron overload caused by hepcidin deficiency. Paradoxically, using unbiased, high-throughput RNA-Seq, I show that the intestinal response to systemic iron deficiency and hepcidin deficiency– mediated iron overload is largely the same. The physiological repression of hepcidin during iron demand and the perturbation of hepcidin during genetic iron overload directly trigger iron efflux through intestinal FPN to limit the activity of iron-dependent PHD enzymes. This stabilizes intestinal HIF-2α to activate genes that are necessary and sufficient for intestinal iron absorption. Interestingly, HIF-2α activation downstream of hepcidin was intestine specific, as HIF-2α–dependent transcript levels were unchanged in the kidney and the spleen following hepatic hepcidin deletion. Potential explanations include the presence of intestine-specific coactivators and/or genetic suppressors and enhancers. Consistent with data showing that HIF-2α is necessary for the adaptive increase in intestinal FPN during iron deficiency (10), the present data suggest a feed-forward loop, whereby intestinal FPN

stabilization following a decrease in hepcidin activates HIF-2α to maintain FPN transcript levels during systemic iron demand and in iron overload. Although the hepcidin/FPN/HIF-2α axis is the major trigger for the intestinal transcriptional response following iron demand, the discovery of smaller subsets of genes that are either regulated by systemic iron deficiency or hepcidin deficiency indicates differences in the intestinal response to a decrease in dietary iron compared with iron hyperabsorption during iron overload. A recent report indicated that the HIF response can be modulated by microbiota-derived short-chain fatty acids, which could partly explain the difference between luminal and systemic cues to the intestine (30). More work needs to be done to understand the regulation of this small subset of genes.

Previous studies showed a critical role for HIF-2α in the hyperabsorption of iron in primary and secondary hemochromatosis (12–14). However, the field has relied largely on germline knock- out strategies to study hepcidin disruption, which gives rise to iron loading that begins during embryonic development and can cause ROS that are known inducers of HIF. Furthermore, full-body hepcidin deficiency disrupts sources of hepcidin outside of the liver that have recently been shown to establish a cell-autonomous mechanism of local iron regulation, particularly in the heart, an organ critical for systemic oxygen transport (31). The use of our inducible model of hepatic hepcidin deletion has characterized, for the first time to our knowledge, the kinetics by which iron overload progresses. There are data to show that iron overload is toxic to RBC survival at later stages of hemoglobinopathies (12, 32), while our data demonstrate that there is a significant expansion of the RBC pool in early stages of iron overload, which occurs in a HIF-2α–dependent manner as PT2385 treatment rescues

this response. Recent work has revealed erythroid-derived factors that regulate hepcidin to facilitate erythropoiesis (33–35). The present data conversely suggest that hepcidin restricts the RBC pool, potentially by limiting intestinal iron absorption or through the direct regulation of signaling downstream of FPN- mediated cellular iron efflux in other organs and cell types. Future studies will need to determine the mechanism by which this RBC expansion occurs and whether it is a physiologically relevant process of iron storage during early iron overload.

The dioxygenase superfamily of PHD enzymes regulate the protein stability of both HIF-2α and HIF-1α. However, our laboratory, among others, has demonstrated that intestinal HIF-2α, but not HIF-1α, is stabilized, transcriptionally active, and necessary and sufficient for iron absorption during systemic iron demand (7, 8). Recent reports have demonstrated that certain PHD isoforms, namely PHD3, show selectivity for HIF-2α over HIF-1α (36). Furthermore, small intestinal HIF-2α is more sensitive to pharmacological inhibition of all PHD isoforms than is HIF-1α (37). This selectivity could explain the differential activation of small intestinal HIF-2α over HIF-1α downstream of hepcidin/FPN/PHDs. Future work will need to establish the Km value of intestinal PHD enzymes for iron to determine whether iron efflux through FPN limits the activity of a HIF-2α–specific PHD.

In addition to hepcidin and HIF-2α, another mammalian iron-sensing axis exists via iron-regulatory protein (IRP) and IRE machinery. This system modulates translation via the binding of IRPs with IREs that exist in the 5′- or 3′-UTR of target transcripts involved in cellular iron handling. Duodenal enterocytes produce a FPN transcript that evades IRP-mediated repression in settings of low intracellular iron by lacking an IRE

(38). This variant might function alongside HIF-2α–mediated transcriptional upregulation of *Fpn* to maintain FPN protein levels following intestinal iron efflux. Interestingly, IRP1 is activated following decreases in intracellular iron to negatively regulate HIF-2α translation via action on an IRE in the 5′-UTR of the HIF-2α mRNA, which was shown both in vitro (24) and in vivo (39–41). Recently, this pathway was shown to be pharmacologically targeted to treat HIF-2α–induced polycythemia (42). I also observed repression of the HIF-2α IRE in our in vitro model following FPNGFP stabilization. Taken together, these data show that the hepcidin/FPN/PHD axis may control HIF-2α during systemic iron deficiency and that IRP1-mediated repression of HIF-2α translation may limit the level of activation. More work will need to be done to fully understand the interaction between the IRP and IRE systems and the hepcidin/FPN/PHD/HIF-2α axis during systemic iron demand.

Iron chelators have been shown for decades to regulate HIF, although these molecules dramatically disrupt mitochondrial function and can strip iron from iron-containing proteins. To our knowledge, these data are the first to show that cell-autonomous, biologically relevant iron efflux regulates intestinal HIF-2α–mediated iron absorption in vivo, in contexts of both systemic iron deficiency and low systemic oxygen. The present work shows that the FPN-mediated efflux of iron is a cell-autonomous trigger to stabilize HIF-2α. Moreover, this finding demonstrates in vivo that a liver-derived endocrine signal plays an essential role in the activity of intestinal enzymes that regulate HIF-2α. Numerous reports have recently begun to characterize the function of FPN in organs that do not play a role in maintaining systemic iron homeostasis (16, 43, 44). It will therefore be vital to determine whether FPN- mediated iron efflux directly

regulates iron-dependent proteins and downstream signaling pathways in other cell types, either triggered by changes to hepatic hepcidin or other factors.

Patients with iron overload currently rely on iron chelators and/or phlebotomy to decrease systemic iron levels. However, these therapies often result in suboptimal patient adherence, because iron chelators have off-target effects and chronic phlebotomy can cause fatigue. A selective inhibitor of HIF-2α, PT2385, has recently been developed and is currently in phase II clinical trials for patients with clear-cell renal cell carcinoma (NCT03108066; ClinicalTrials.gov). Here, I sought to address whether oral administration of PT2385 could be used to blunt intestinal iron absorption for the treatment of iron overload. Our data demonstrated that within as little as 2 weeks of PT2385 treatment, systemic iron levels were decreased in mice with established iron overload. This finding provides an exciting impetus for the use of PT2385 in the treatment of human diseases of iron overload, many of which are characterized by dysfunction of the hepcidin/ FPN axis and intestinal iron hyperabsorption.

In conclusion, our work demonstrates that systemic iron deficiency and hepcidin deficiency–mediated iron overload activate the same hepatic hepcidin/intestinal HIF-2α axis. Moreover, I show that cellular iron efflux through the hepcidin target FPN regulates the activity of iron-dependent enzymes and directly activates HIF-2α. Finally, these data suggest that a therapeutic agent currently in development for humans should be repurposed for the treatment of patients with iron overload.

References

1. McLean E, Cogswell M, Egli I, Wojdyla D, and de Benoist B. Worldwide prevalence of anaemia, WHO Vitamin and Mineral Nutrition Information System, 1993-2005. *Public Health Nutr.* 2009;12(4):444-54.
2. Brissot P, Pietrangelo A, Adams PC, de Graaff B, McLaren CE, and Loreal O. Haemochromatosis. *Nat Rev Dis Primers.* 2018;4:18016.
3. Pietrangelo A. Genetics, Genetic Testing, and Management of Hemochromatosis: 15 Years Since Hepcidin. *Gastroenterology.* 2015;149(5):1240-51 e4.
4. Nemeth E, Tuttle MS, Powelson J, Vaughn MB, Donovan A, Ward DM, et al. Hepcidin regulates cellular iron efflux by binding to ferroportin and inducing its internalization. *Science.* 2004;306(5704):2090-3.
5. Ganz T, and Nemeth E. Hepcidin and iron homeostasis. *Biochim Biophys Acta.* 2012;1823(9):1434-43.
6. Drakesmith H, Nemeth E, and Ganz T. Ironing out Ferroportin. *Cell Metab.* 2015;22(5):777-87.
7. Mastrogiannaki M, Matak P, Keith B, Simon MC, Vaulont S, and Peyssonnaux C. HIF-2alpha, but not HIF-1alpha, promotes iron absorption in mice. *J Clin Invest.* 2009;119(5):1159-66.
8. Shah YM, Matsubara T, Ito S, Yim SH, and Gonzalez FJ. Intestinal hypoxia-inducible transcription factors are essential for iron absorption following iron deficiency. *Cell Metab.* 2009;9(2):152-64.
9. Anderson ER, Xue X, and Shah YM. Intestinal hypoxia-inducible factor-2alpha (HIF-2alpha) is critical for efficient erythropoiesis. *J Biol Chem.* 2011;286(22):19533-40.
10. Taylor M, Qu A, Anderson ER, Matsubara T, Martin A, Gonzalez FJ, et al. Hypoxia-inducible factor-2alpha mediates the adaptive increase of intestinal ferroportin during iron deficiency in mice. *Gastroenterology.* 2011;140(7):2044-55.
11. Ramakrishnan SK, Anderson ER, Martin A, Centofanti B, and Shah YM. Maternal intestinal HIF-2alpha is necessary for sensing iron demands of lactation in mice. *Proc Natl Acad Sci U S A.* 2015;112(28):E3738-47.
12. Das N, Xie L, Ramakrishnan SK, Campbell A, Rivella S, and Shah YM. Intestine-specific Disruption of Hypoxia-inducible Factor (HIF)-2alpha Improves Anemia in Sickle Cell Disease. *J Biol Chem.* 2015;290(39):23523-7.
13. Anderson ER, Taylor M, Xue X, Ramakrishnan SK, Martin A, Xie L, et al. Intestinal HIF2alpha promotes tissue-iron accumulation in disorders of iron overload with anemia. *Proc Natl Acad Sci U S A.* 2013;110(50):E4922-30.
14. Mastrogiannaki M, Matak P, Delga S, Deschemin JC, Vaulont S, and Peyssonnaux C. Deletion of HIF-2alpha in the enterocytes decreases the severity of tissue iron loading in hepcidin knockout mice. *Blood.* 2012;119(2):587-90.
15. Berdoukas V, Coates TD, and Cabantchik ZI. Iron and oxidative stress in cardiomyopathy in thalassemia. *Free Radic Biol Med.* 2015;88(Pt A):3-9.

16. Lakhal-Littleton S, Wolna M, Carr CA, Miller JJ, Christian HC, Ball V, et al. Cardiac ferroportin regulates cellular iron homeostasis and is important for cardiac function. *Proc Natl Acad Sci U S A.* 2015;112(10):3164-9.
17. Derchi G, Formisano F, Balocco M, Galanello R, Bina P, Dessi C, et al. Clinical management of cardiovascular complications in patients with thalassaemia major: a large observational multicenter study. *Eur J Echocardiogr.* 2011;12(3):242-6.
18. Triner D, Xue X, Schwartz AJ, Jung I, Colacino JA, and Shah YM. Epithelial Hypoxia-Inducible Factor 2alpha Facilitates the Progression of Colon Tumors through Recruiting Neutrophils. *Mol Cell Biol.* 2017;37(5).
19. Xue X, Ramakrishnan SK, and Shah YM. Activation of HIF-1alpha does not increase intestinal tumorigenesis. *Am J Physiol Gastrointest Liver Physiol.* 2014;307(2):G187-95.
20. Qiao B, Sugianto P, Fung E, Del-Castillo-Rueda A, Moran-Jimenez MJ, Ganz T, et al. Hepcidin-induced endocytosis of ferroportin is dependent on ferroportin ubiquitination. *Cell Metab.* 2012;15(6):918-24.
21. Yoon YS, Yoon DS, Lim IK, Yoon SH, Chung HY, Rojo M, et al. Formation of elongated giant mitochondria in DFO-induced cellular senescence: involvement of enhanced fusion process through modulation of Fis1. *J Cell Physiol.* 2006;209(2):468-80.
22. Yoon YS, Cho H, Lee JH, and Yoon G. Mitochondrial dysfunction via disruption of complex II activity during iron chelation-induced senescence-like growth arrest of Chang cells. *Ann N Y Acad Sci.* 2004;1011:123-32.
23. Chandel NS, McClintock DS, Feliciano CE, Wood TM, Melendez JA, Rodriguez AM, et al. Reactive oxygen species generated at mitochondrial complex III stabilize hypoxia-inducible factor-1alpha during hypoxia: a mechanism of O2 sensing. *J Biol Chem.* 2000;275(33):25130-8.
24. Sanchez M, Galy B, Muckenthaler MU, and Hentze MW. Iron-regulatory proteins limit hypoxia-inducible factor-2alpha expression in iron deficiency. *Nat Struct Mol Biol.* 2007;14(5):420-6.
25. Mancias JD, Pontano Vaites L, Nissim S, Biancur DE, Kim AJ, Wang X, et al. Ferritinophagy via NCOA4 is required for erythropoiesis and is regulated by iron dependent HERC2-mediated proteolysis. *Elife.* 2015;4.
26. Mancias JD, Wang X, Gygi SP, Harper JW, and Kimmelman AC. Quantitative proteomics identifies NCOA4 as the cargo receptor mediating ferritinophagy. *Nature.* 2014;509(7498):105-9.
27. Ross SL, Tran L, Winters A, Lee KJ, Plewa C, Foltz I, et al. Molecular mechanism of hepcidin-mediated ferroportin internalization requires ferroportin lysines, not tyrosines or JAK-STAT. *Cell Metab.* 2012;15(6):905-17.
28. Deshpande CN, Ruwe TA, Shawki A, Xin V, Vieth KR, Valore EV, et al. Calcium is an essential cofactor for metal efflux by the ferroportin transporter family. *Nat Commun.* 2018;9(1):3075.
29. Wallace EM, Rizzi JP, Han G, Wehn PM, Cao Z, Du X, et al. A Small-Molecule Antagonist of HIF2alpha Is Efficacious in Preclinical Models of Renal Cell Carcinoma. *Cancer Res.* 2016;76(18):5491-500.

30. Kelly CJ, Zheng L, Campbell EL, Saeedi B, Scholz CC, Bayless AJ, et al. Crosstalk between Microbiota-Derived Short-Chain Fatty Acids and Intestinal Epithelial HIF Augments Tissue Barrier Function. *Cell Host Microbe.* 2015;17(5):662-71.
31. Lakhal-Littleton S, Wolna M, Chung YJ, Christian HC, Heather LC, Brescia M, et al. An essential cell-autonomous role for hepcidin in cardiac iron homeostasis. *Elife.* 2016;5.
32. Guo S, Casu C, Gardenghi S, Booten S, Aghajan M, Peralta R, et al. Reducing TMPRSS6 ameliorates hemochromatosis and beta-thalassemia in mice. *J Clin Invest.* 2013;123(4):1531-41.
33. Kautz L, Jung G, Valore EV, Rivella S, Nemeth E, and Ganz T. Identification of erythroferrone as an erythroid regulator of iron metabolism. *Nat Genet.* 2014;46(7):678-84.
34. Tanno T, Bhanu NV, Oneal PA, Goh SH, Staker P, Lee YT, et al. High levels of GDF15 in thalassemia suppress expression of the iron regulatory protein hepcidin. *Nat Med.* 2007;13(9):1096-101.
35. Tanno T, Porayette P, Sripichai O, Noh SJ, Byrnes C, Bhupatiraju A, et al. Identification of TWSG1 as a second novel erythroid regulator of hepcidin expression in murine and human cells. *Blood.* 2009;114(1):181-6.
36. Taniguchi CM, Finger EC, Krieg AJ, Wu C, Diep AN, LaGory EL, et al. Cross-talk between hypoxia and insulin signaling through Phd3 regulates hepatic glucose and lipid metabolism and ameliorates diabetes. *Nat Med.* 2013;19(10):1325-30.
37. Taniguchi CM, Miao YR, Diep AN, Wu C, Rankin EB, Atwood TF, et al. PHD inhibition mitigates and protects against radiation-induced gastrointestinal toxicity via HIF2. *Sci Transl Med.* 2014;6(236):236ra64.
38. Zhang DL, Hughes RM, Ollivierre-Wilson H, Ghosh MC, and Rouault TA. A ferroportin transcript that lacks an iron-responsive element enables duodenal and erythroid precursor cells to evade translational repression. *Cell Metab.* 2009;9(5):461-73.
39. Anderson SA, Nizzi CP, Chang YI, Deck KM, Schmidt PJ, Galy B, et al. The IRP1-HIF-2alpha axis coordinates iron and oxygen sensing with erythropoiesis and iron absorption. *Cell Metab.* 2013;17(2):282-90.
40. Ghosh MC, Zhang DL, Jeong SY, Kovtunovych G, Ollivierre-Wilson H, Noguchi A, et al. Deletion of iron regulatory protein 1 causes polycythemia and pulmonary hypertension in mice through translational derepression of HIF2alpha. *Cell Metab.* 2013;17(2):271-81.
41. Wilkinson N, and Pantopoulos K. IRP1 regulates erythropoiesis and systemic iron homeostasis by controlling HIF2alpha mRNA translation. *Blood.* 2013;122(9):1658-68.
42. Ghosh MC, Zhang DL, Ollivierre H, Eckhaus MA, and Rouault TA. Translational repression of HIF2alpha expression in mice with Chuvash polycythemia reverses polycythemia. *J Clin Invest.* 2018;128(4):1317-25.
43. Britton L, Jaskowski LA, Bridle K, Secondes E, Wallace D, Santrampurwala N, et al. Ferroportin Expression in Adipocytes Does Not Contribute to Iron Homeostasis or Metabolic Responses to a High Calorie Diet. *Cell Mol Gastroenterol Hepatol.* 2018;5(3):319-31.

44. Wu LJ, Leenders AG, Cooperman S, Meyron-Holtz E, Smith S, Land W, et al. Expression of the iron transporter ferroportin in synaptic vesicles and the blood-brain barrier. *Brain Res.* 2004;1001(1-2):108-17.
45. Xie C, Yagai T, Luo Y, Liang X, Chen T, Wang Q, et al. Activation of intestinal hypoxia-inducible factor 2alpha during obesity contributes to hepatic steatosis. *Nat Med.* 2017;23(11):1298-308.
46. Kim DI, Liao J, Emont MP, Park MJ, Jun H, Ramakrishnan SK, et al. An OLTAM system for analysis of brown/beige fat thermogenic activity. *Int J Obes (Lond).* 2018.
47. Ramakrishnan SK, Zhang H, Takahashi S, Centofanti B, Periyasamy S, Weisz K, et al. HIF2alpha Is an Essential Molecular Brake for Postprandial Hepatic Glucagon Response Independent of Insulin Signaling. *Cell Metab.* 2016;23(3):505-16.
48. Xue X, Ramakrishnan SK, Weisz K, Triner D, Xie L, Attili D, et al. Iron Uptake via DMT1 Integrates Cell Cycle with JAK-STAT3 Signaling to Promote Colorectal Tumorigenesis. *Cell Metab.* 2016;24(3):447-61.

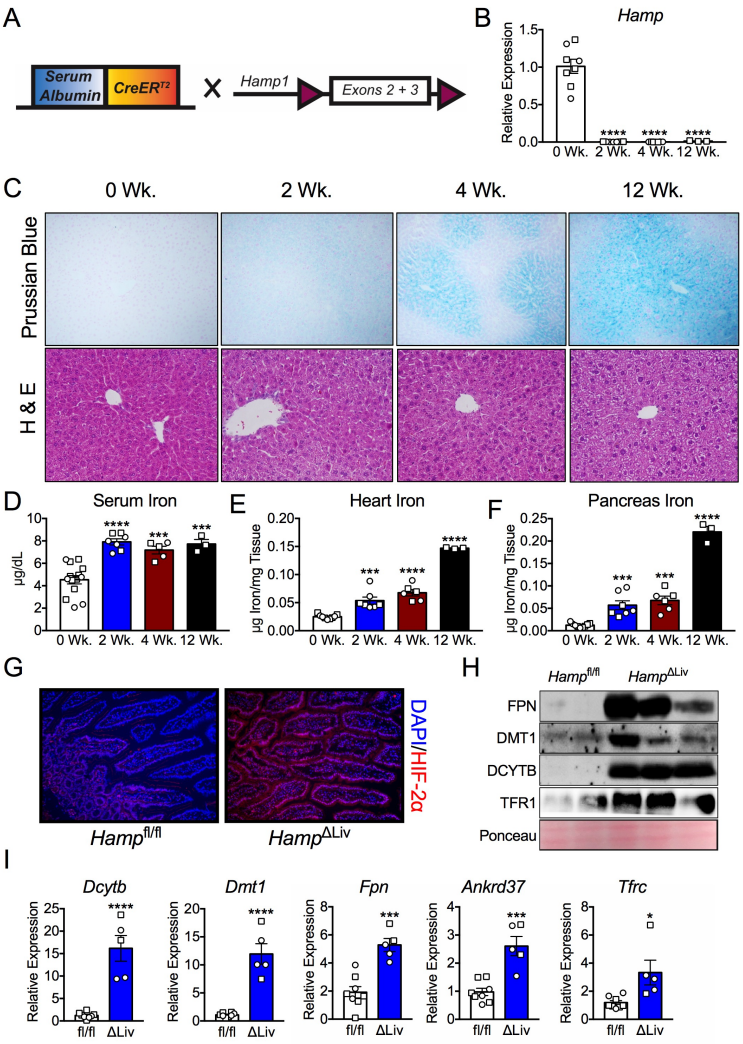

Figure 2.1. Temporal disruption of hepatic hepcidin activates intestinal HIF-2α and leads to rapid iron accumulation. (A) Schematic representation of mice with temporal disruption of hepatocyte hepcidin. (B) qPCR analysis of hepatic hepcidin (*Hamp*) transcript expression levels (n = 3–8 per group). (C) Representative Prussian blue iron staining and H&E staining of liver tissue from $Hamp^{\Delta Liv}$ mice. Original magnification, ×20 (n = 3 per group). (D–F) Serum (D), heart (E), and pancreatic iron content (F) (n = 3–14 per group). (G) Representative HIF-2α staining of duodenal sections 2 weeks after tamoxifen injection into $Hamp^{fl/fl}$ and $Hamp^{\Delta Liv}$ mice. Original magnification, ×20 (n = 3 per group). (H) Western blot analysis of FPN, DMT1, DCYTB, and TFR1 expression in duodenal membrane fractions (n = 2–3 per group). (I) qPCR analysis of duodenal HIF-2α–specific and iron-handling transcripts 2 weeks after tamoxifen injection into $Hamp^{fl/fl}$ and $Hamp^{\Delta Liv}$ mice (n = 5–8 per group). Data represent the mean ± SEM. Male samples are designated as squares, and female samples are designated as circles. Significance was determined by 1-way ANOVA with Tukey's post hoc test (B and D–F) or 2-tailed, unpaired t test (I). $^*P < 0.05$, $^{***}P < 0.001$, and $^{****}P < 0.0001$ versus the $Hamp^{fl/fl}$ group.

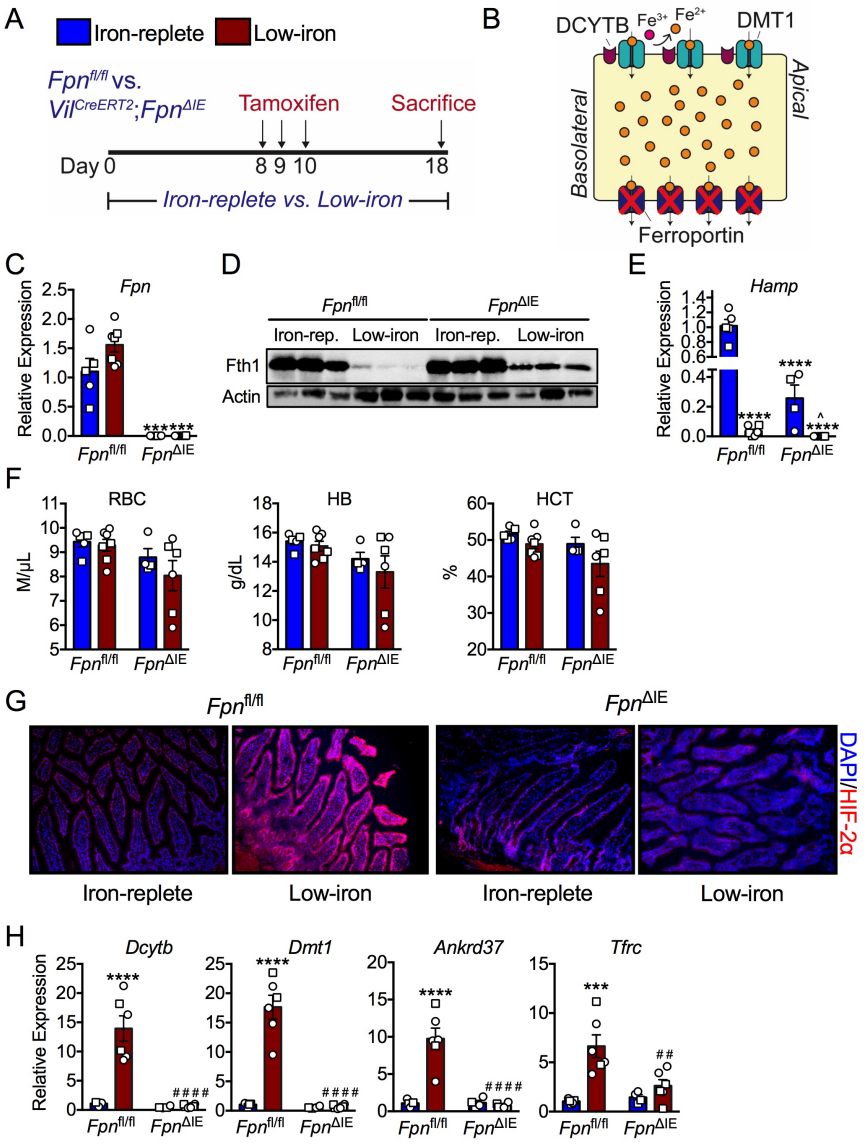

Figure 2.2. Intestinal epithelial FPN is necessary for the activation of intestinal HIF-2α during systemic iron deficiency. (A and B) Schematic representation of the experimental design (A) and of intestinal epithelial iron retention following FPN deletion (B). (C) qPCR analysis of duodenal *Fpn* transcript levels (n = 4–7 per group). (D) Western blot analysis of duodenal FTH1 (n = 3 per group). (E) qPCR analysis of *Hamp* transcript levels (n = 4–7 per group). (F) Analysis of RBC, HB, and HCT (n = 4–7 per group). (G) Representative HIF-2α staining in duodenal sections. Original magnification, ×20 (n = 3 per group). (H) qPCR analysis of HIF-2α–specific and iron-handling transcripts in duodenal samples (n = 4–6 per group). Male samples are designated as squares, and female samples are designated as circles. Data represent the mean ± SEM. Statistical significance was determined by 2-way ANOVA with Tukey's post hoc test. ***P < 0.001 and ****P < 0.0001 versus iron-replete $Fpn^{fl/fl}$; ##P < 0.01 and ####P < 0.0001 versus low-iron $Fpn^{fl/fl}$; †P < 0.05 versus iron-replete $Fpn^{\Delta IE}$.

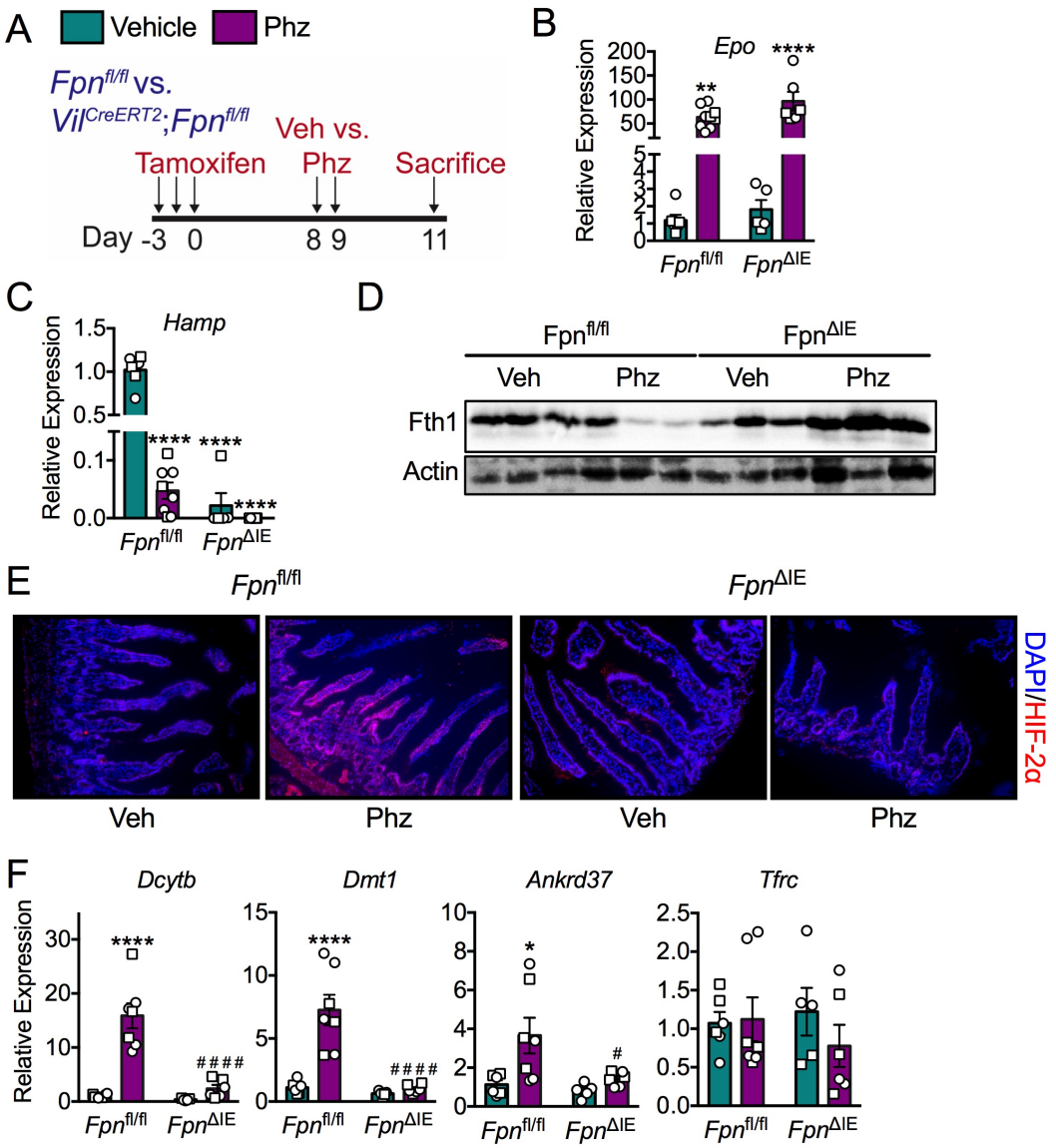

Figure 2.3. Deletion of intestinal epithelial FPN blocks the intestinal HIF-2α response to erythropoietic demand. (A) Experimental design for Phz-induced hemolytic anemia model. (B and C) qPCR analysis of kidney *Epo* (B) and liver *Hamp* (C) transcript levels (n = 5–9 per group). (D) Western blot analysis of duodenal FTH1 (n = 3 per group). (E) Representative HIF-2α staining of duodenal sections. Original magnification, ×20 (n = 3 per group). (F) qPCR analysis of HIF-2α–specific and iron-handling transcripts in duodenal samples (n = 5–7 per group). Male samples are designated as squares, and female samples are designated as circles. Data represent the mean ± SEM. Statistical significance was determined by 2-way ANOVA with Tukey's post hoc test. *P < 0.05, **P < 0.01, and ****P < 0.0001 versus vehicle $Fpn^{fl/fl}$; #P < 0.05 and ####P < 0.0001 versus vehicle $Fpn^{fl/fl}$.

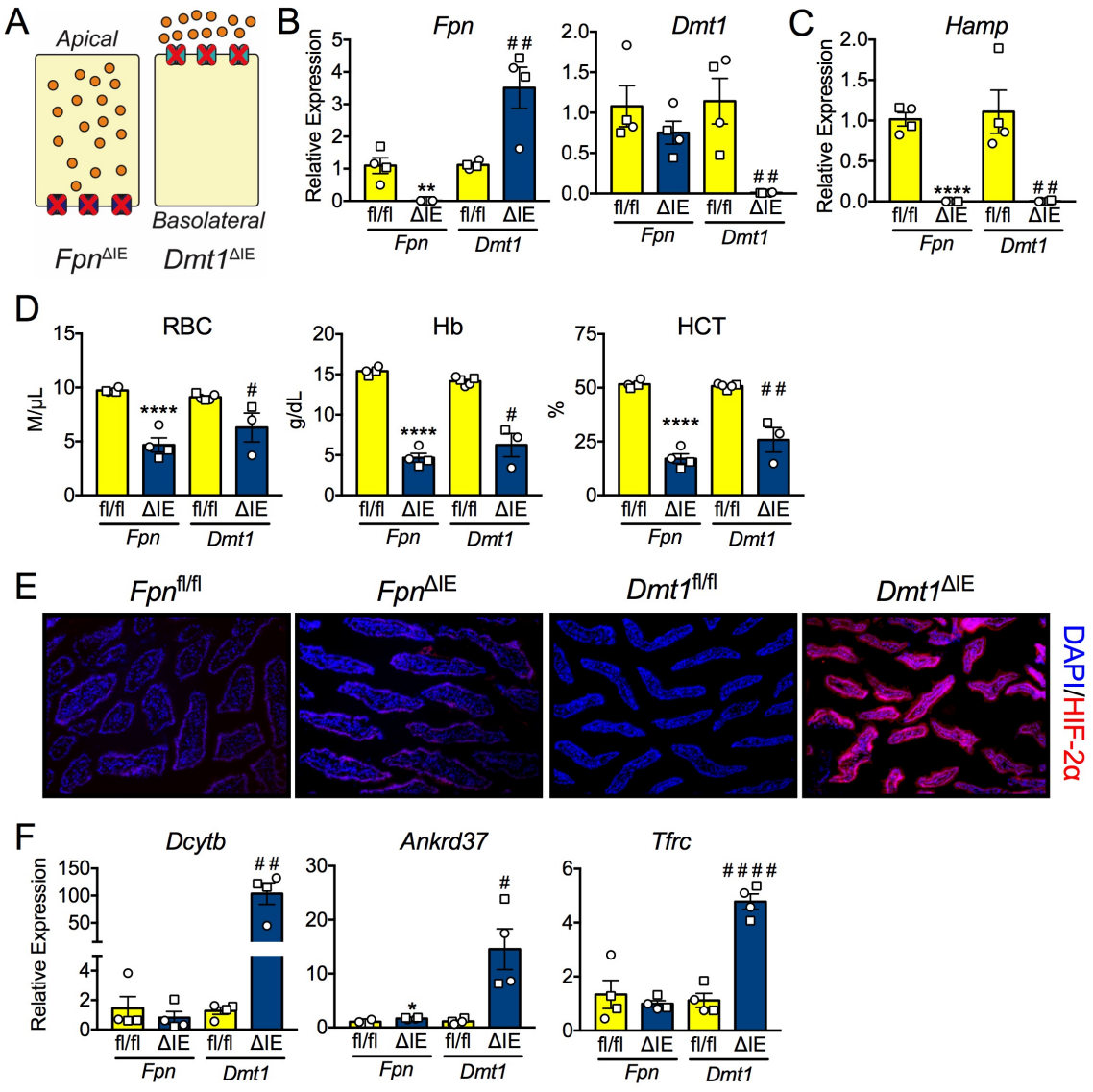

Figure 2.4. The intestinal HIF-2α response to changes in systemic iron and oxygen is driven by epithelial iron levels. (A) Schematic of 3-month, inducible iron trapping in animals lacking intestinal epithelial FPN (*Fpn*$^{\Delta IE}$) or DMT1 (*Dmt1*$^{\Delta IE}$). (B) qPCR analysis of *Fpn* and *Dmt1* transcript levels (*n* = 4 per group). (C) qPCR analysis of hepatic *Hamp* transcript expression levels (*n* = 4 per group). (D) Analysis of RBC, HB, and HCT (*n* = 3–5 per group). (E) Representative HIF-2α staining of duodenal sections. Original magnification, ×20 (*n* = 3 per group). (F) qPCR analysis of HIF-2α–specific and iron-handling transcripts in duodenal samples (*n* = 4 per group). Male samples are designated as squares, and female samples are designated as circles. Data represent the mean ± SEM. Statistical significance was determined by 2-tailed, unpaired *t* test. **P* < 0.05, ***P* < 0.01, and *****P* < 0.0001 compared between *Fpn*$^{fl/fl}$ and *Fpn*$^{\Delta IE}$ cohorts; #*P* < 0.05, ##*P* < 0.01, and ####*P* < 0.0001 compared between *Dmt1*$^{fl/fl}$ and *Dmt1*$^{\Delta IE}$ cohorts.

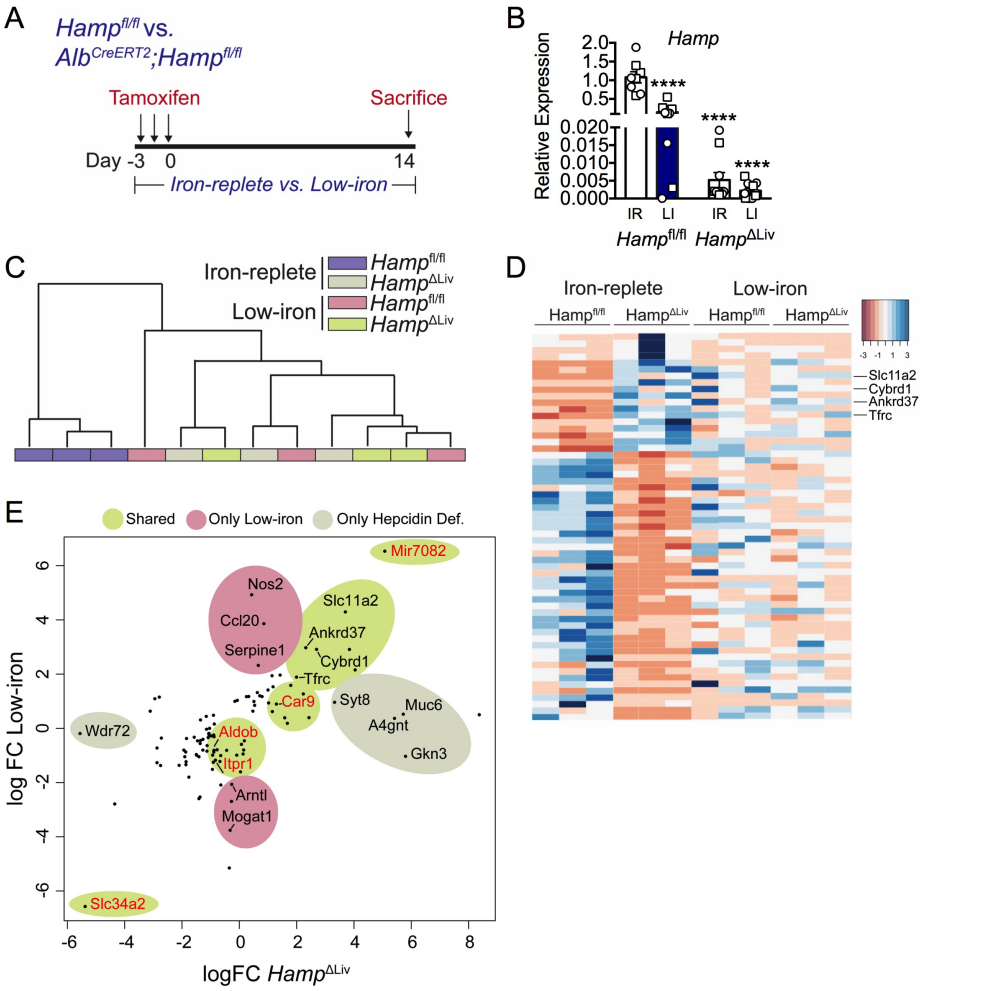

Figure 2.5. The intestinal transcriptome during systemic iron deficiency resembles that of hepcidin deficiency–mediated iron overload. (A) Experimental design for the samples used in whole-genome RNA-Seq. (B) qPCR analysis of liver *Hamp* transcript levels in mice on an iron-replete (IR) or low-iron (LI) diet (n = 8–9 per group). (C) Dendrogram comparing genotype-diet interactions following unsupervised hierarchical clustering of genes differentially expressed at a high-stringency FDR of less than 0.01 (n = 3 per group). (D) Heatmap of genes used for unsupervised hierarchical clustering (n = 3 per group). (E) Lower-stringency differential expression analysis at a FDR of less than 0.1 to uncover transcripts in the RNA-Seq data set unique to iron deficiency and hepcidin deficiency. Genes highlighted in red are novel intestinal transcripts regulated by both low iron and hepcidin deficiency (n = 3 per group). Male samples are designated as squares, and female samples are designated as circles. FC, fold change. Data represent the mean ± SEM. Statistical significance was determined by 2-way ANOVA with Tukey's post hoc test. ****P < 0.0001 versus iron-replete *Hamp*$^{fl/fl}$.

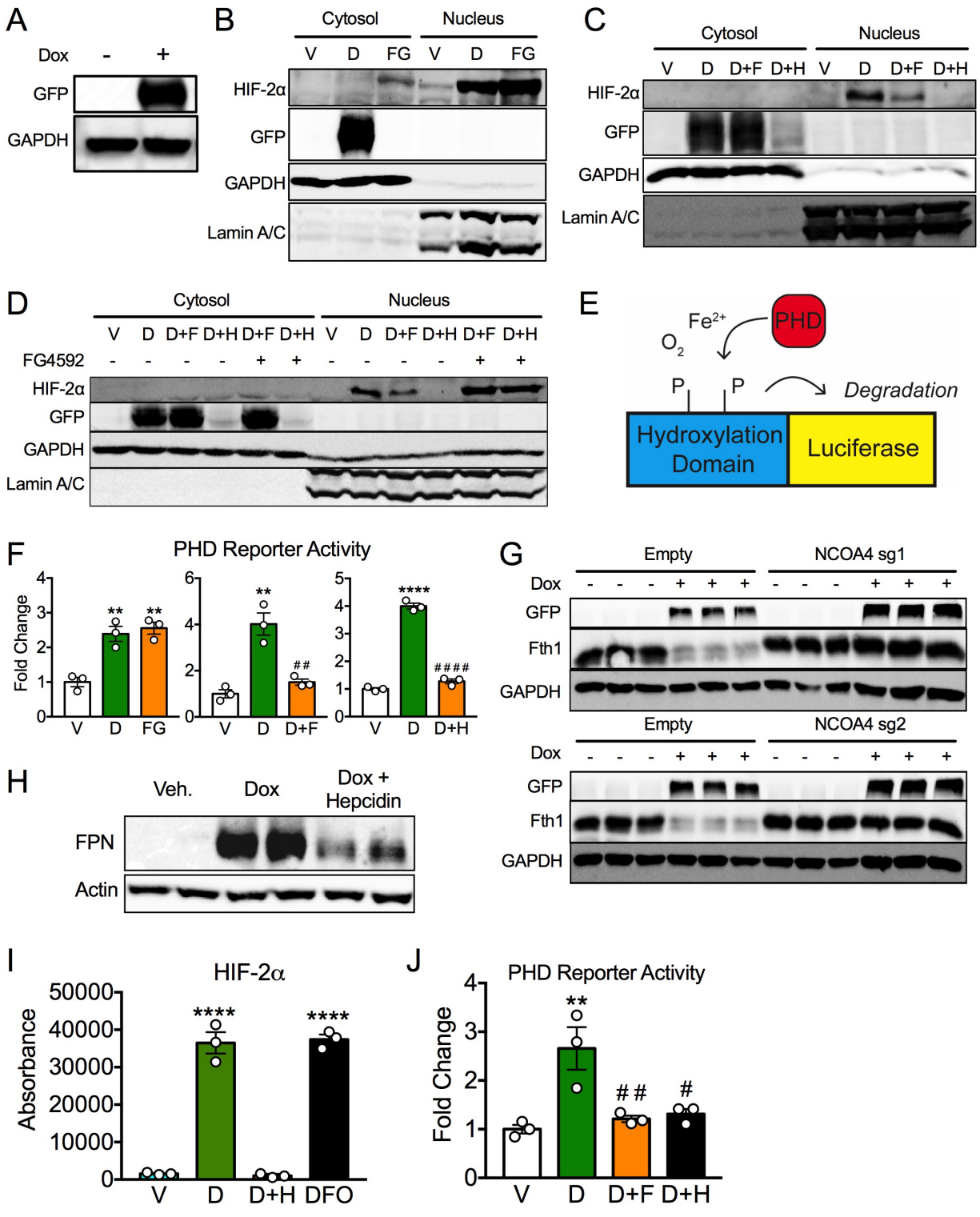
A
Dox - +
GFP
GAPDH
B
Cytosol
Nucleus
V D FG V D FG
HIF-2α
GFP
GAPDH
Lamin A/C
C
Cytosol
Nucleus
V D D+F D+H V D D+F D+H
HIF-2α
GFP
GAPDH
Lamin A/C
D
Cytosol
Nucleus
V D D+F D+H D+F D+H V D D+F D+H D+F D+H
FG4592 - - - - + + - - - - + +
HIF-2α
GFP
GAPDH
Lamin A/C
E
Fe2+
O2
PHD
P P
Degradation
Hydroxylation Domain
Luciferase
F
PHD Reporter Activity
Fold Change
V D FG
V D D+F
V D D+H
G
Empty
NCOA4 sg1
Dox - - - + + + - - - + + +
GFP
Fth1
GAPDH
Empty
NCOA4 sg2
Dox - - - + + + - - - + + +
GFP
Fth1
GAPDH
H
Veh.
Dox
Dox + Hepcidin
FPN
Actin
I
HIF-2α
Absorbance
V D D+H DFO
J
PHD Reporter Activity
Fold Change
V D D+F D+H

Figure 2.6. FPN activates HIF-2α in a cell-autonomous manner that is dependent on efflux of the cellular labile iron pool. (A) Western blot analysis of FPNGFP HEK293 cells following a 24-hour doxycycline treatment. (B) Western blot analysis of cytosolic and nuclear fractions of FPNGFP HEK293 cells treated with vehicle (V), 250 ng/ml doxycycline (D), or 100 μM FG4592 (FG) for 24 hours. (C and D) Western blot analysis of cytosolic and nuclear fractions of FPNGFP HEK293 cells treated with vehicle (V), doxycycline (D), doxycycline and 200 μM FAC (D+F), or doxycycline and 1 mg/ml hepcidin (D+H) for 24 hours (C). Separate doxycycline plus FAC and doxycycline plus hepcidin conditions were also cotreated with FG4592 for 24 hours, as indicated (D). (E) Schematic of the luciferase-based PHD enzyme activity reporter. (F) Fold change of luciferase activity in FPNGFP HEK293 cells infected with the PHD reporter and treated with vehicle, doxycycline, FG4592, FAC and doxycycline, or doxycycline and hepcidin for 24 hours. (G) Western blot analysis of FPNGFP HEK293 cells stable for empty lentiCRISPRv2 (Empty) or unique NCOA4 short guide RNAs (NCOA4 sg1 and NCOA4 sg2). Cells were treated with FAC for 24 hours and then with doxycycline for 24 hours. (H) Western blot analysis of FPNGFP IEC-6 cells treated with vehicle, doxycycline, or doxycycline and hepcidin for 24 hours. (I) ELISA of lysates from FPNGFP IEC-6 cells treated with vehicle, doxycycline, doxycycline and hepcidin, or DFO for 24 hours. (J) Fold change of luciferase activity in FPNGFP IEC-6 cells infected with the PHD reporter and treated with vehicle, doxycycline, FAC and doxycycline, or doxycycline and hepcidin for 24 hours. All cell culture experiments were repeated at least 3 times. Data represent the mean ± SEM. Statistical significance was determined by 1-way ANOVA with Tukey's post hoc test. $^{**}P < 0.01$ and $^{****}P < 0.0001$ versus vehicle; $\#P < 0.05$, $\#\#P < 0.01$, and $\#\#\#\#P < 0.0001$ versus doxycycline.

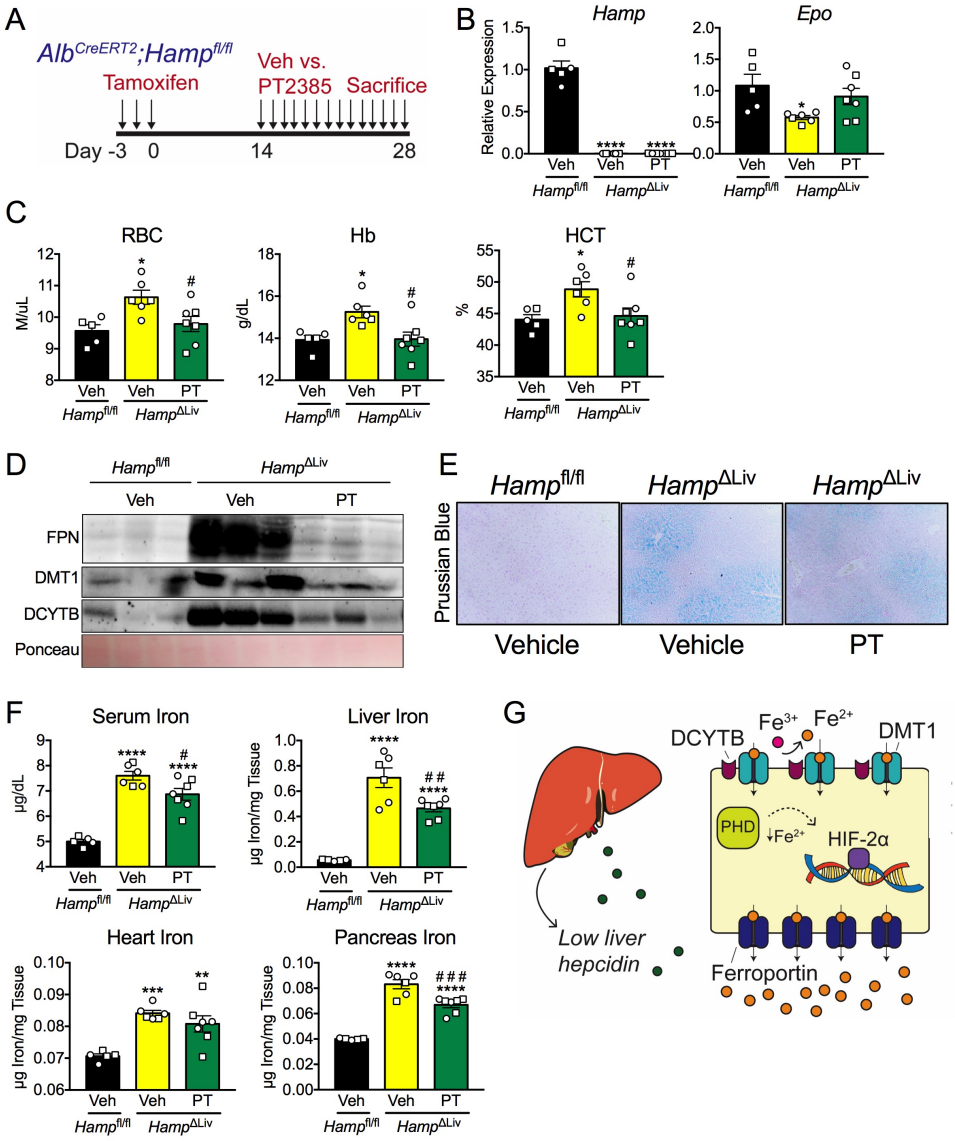

Figure 2.7. Inhibition of HIF-2α using PT2385 reverses iron accumulation in multiple tissues in hepcidin-deficient hemochromatosis. (A) Experimental design for oral gavage of vehicle or PT2385 in *Hamp*$^{\Delta Liv}$ mice. (B) qPCR analysis of hepatic *Hamp* and kidney *Epo* transcript levels (n = 5–7 per group). (C) Analysis of RBC, HB, and HCT (n = 5–7 per group). (D) Western blot analysis of FPN, DMT1, and DCYTB in duodenal membrane fractions (n = 3 per group). (E) Representative Prussian blue staining for iron in liver tissues. Original magnification, ×20 (n = 3 per group). (F) Serum, liver, heart, and pancreatic iron content (n = 5–7 per group). (G) Schematic representation of hepatic hepcidin/intestinal HIF-2α axis. Male samples are designated as squares, and female samples are designated as circles. Data represent the mean ± SEM. Statistical significance was determined by 1-way ANOVA with Tukey's post hoc test. *P < 0.05, **P < 0.01, ***P < 0.001, and ****P < 0.0001 versus vehicle *Hamp*$^{fl/fl}$; #P < 0.05, ##P < 0.01, and ###P < 0.001 versus vehicle *Hamp*$^{\Delta Liv}$. PT, PT2385; Veh, vehicle.

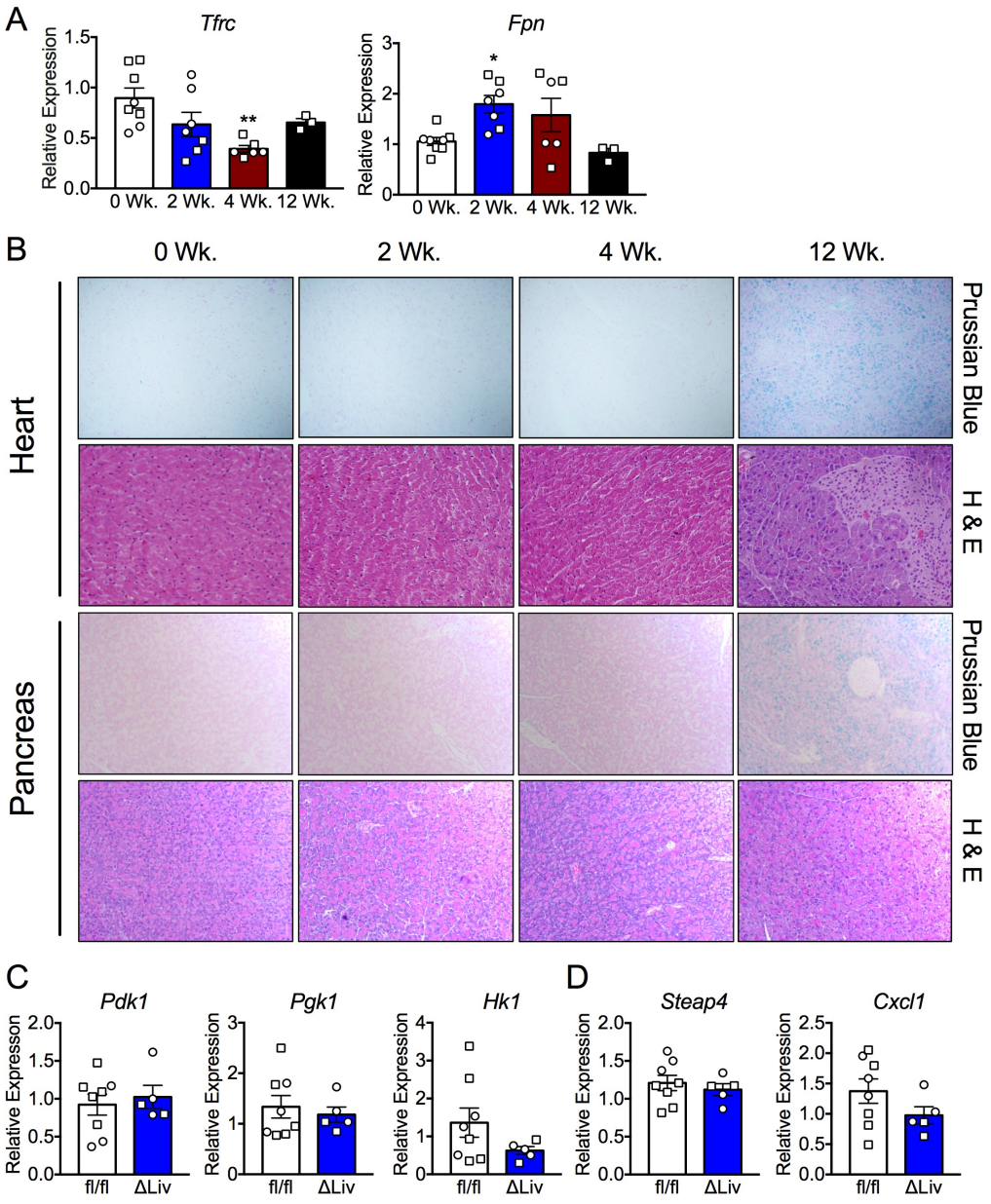

Figure S2.1. Temporal deletion of liver hepcidin alters iron homeostasis and does not affect intestinal HIF-1a target genes or HIF-2a inflammatory targets. (A) qPCR analysis of transferrin receptor (Tfrc) and ferroportin (Fpn) in livers of *Hamp*$^{\Delta Liv}$ mice (n = 3 to 8 per group). (B) Representative Prussian blue iron stain and H&E analysis of hearts and pancreata from *Hamp*$^{\Delta Liv}$ mice. Images, 20x (n = 3 per group). (C) qPCR analysis for HIF-1aspecific transcripts in duodenal samples two-weeks after tamoxifen injection in *Hamp*$^{fl/fl}$ and *Hamp*$^{\Delta Liv}$ mice (n = 5 to 8 per group). (D) qPCR analysis for HIF-2a-specific inflammatory transcripts in duodenal samples two-weeks after tamoxifen injection in *Hamp*$^{fl/fl}$ and *Hamp*$^{\Delta Liv}$ mice (n = 5 to 8 per group). Male samples are designated as squares and female samples are designated as circles. Mean ± SEM are plotted. Significance determined using either one-way ANOVA with Tukey's post hoc (A) or 2-tailed unpaired t test (C and D). *p < 0.05; **p < 0.01 compared to *Hamp*$^{fl/fl}$ group.

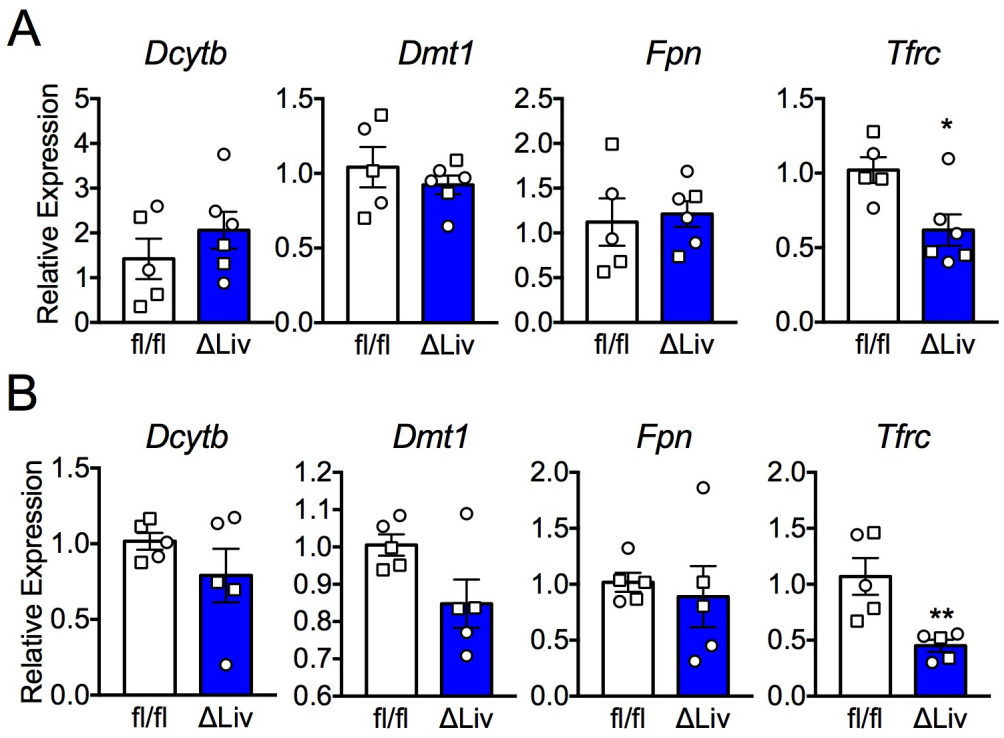

Figure S2.2. Inducible deletion of liver hepcidin does not affect HIF-2α-specific genes in the kidney and spleen. (A and B) qPCR analysis for HIF-2α-specific and iron handling genes in kidney (A) and spleen (B) samples of *Hamp*$^{fl/fl}$ and *Hamp*$^{\Delta Liv}$ mice. Male samples are designated as squares and female samples are designated as circles. Mean ± SEM are plotted. Significance determined using 2-tailed unpaired t test. *p < 0.05; **p < 0.01 compared to *Hamp*$^{fl/fl}$ group.

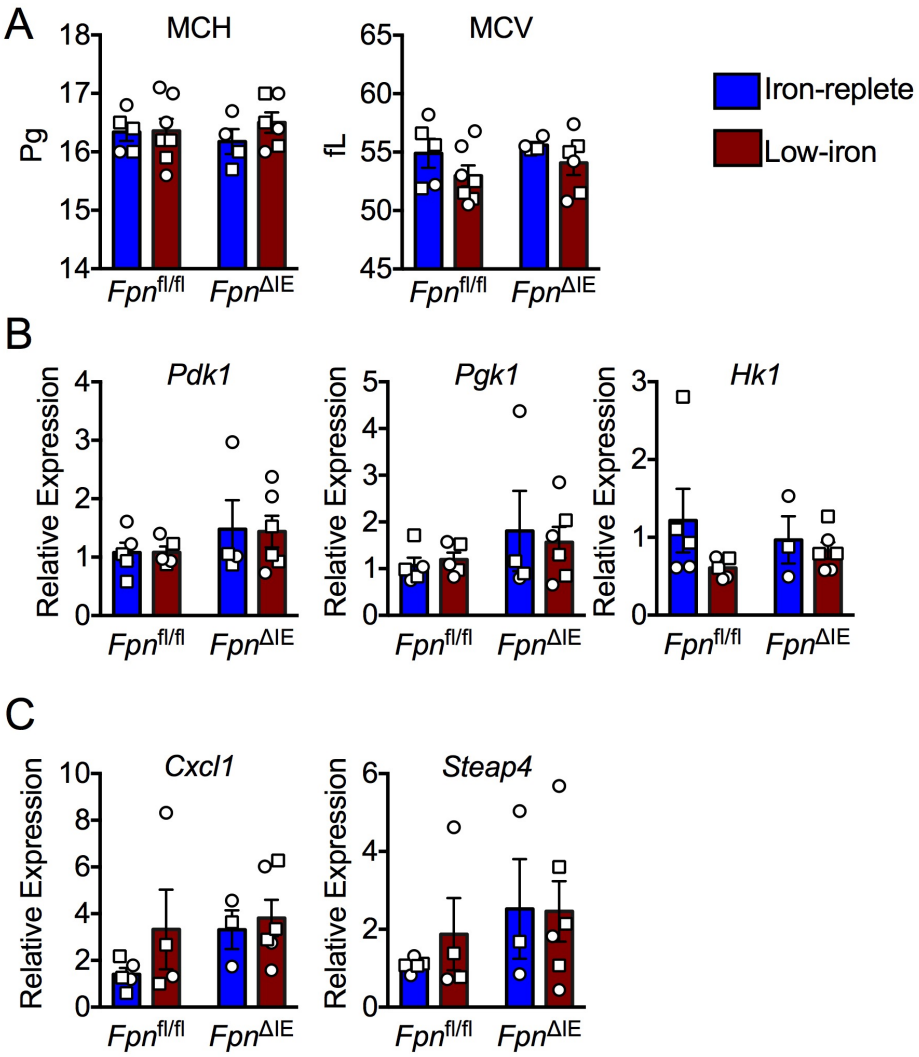

Figure S2.3. The response of intestinal epithelial FPN to systemic iron deficiency does not activate intestinal HIF-1α or HIF-2α inflammatory targets. (A) Analysis of mean corpuscular hemoglobin (MCH) and mean corpuscular volume (MCV). (B) qPCR analysis for HIF-1α-specific transcripts in duodenal samples. (C) qPCR analysis for HIF-2α-specific inflammatory transcripts in duodenal samples. Male samples are designated as squares and female samples are designated as circles. Mean ± SEM are plotted. Significance determined using two-way ANOVA with Tukey's post hoc.

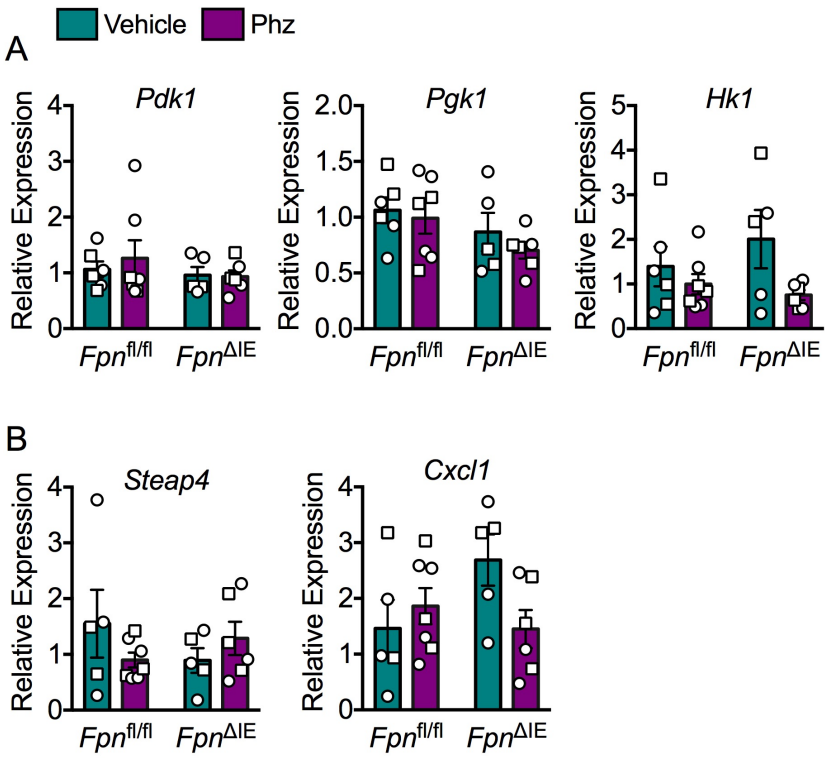

Figure S2.4. Intestinal epithelial FPN does not mediate activation of intestinal HIF-1α or HIF-2α inflammatory targets in response to systemic erythropoietic demand. (A) qPCR analysis for HIF-1α-specific transcripts in duodenal samples. (B) qPCR analysis for HIF-2α-specific inflammatory transcripts in duodenal samples. Male samples are designated as squares and female samples are designated as circles. Mean ± SEM are plotted. Significance determined using two-way ANOVA with Tukey's post hoc.

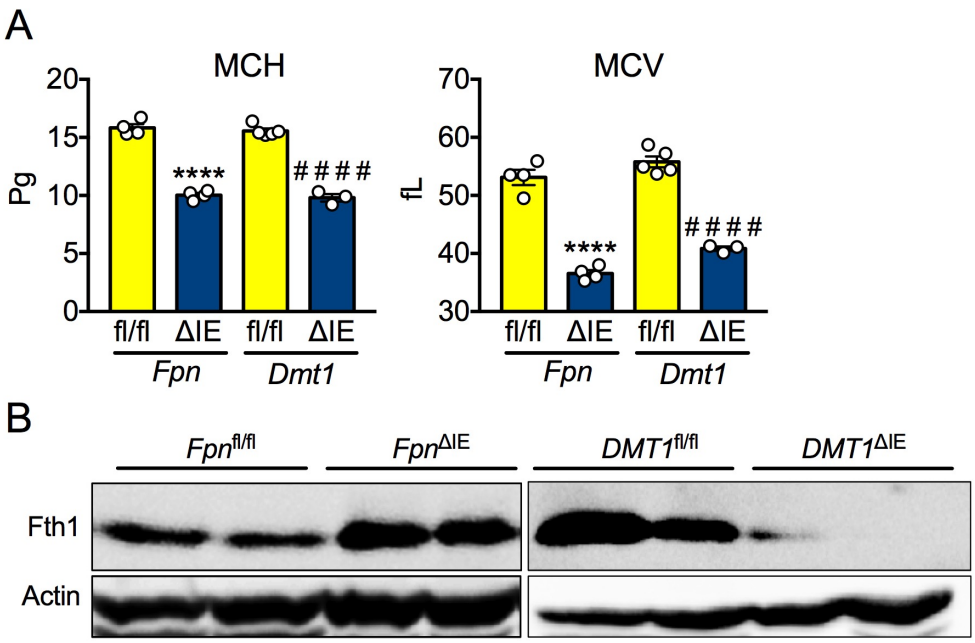

Figure S2.5. Temporal deletion of FPN and DMT1 for three months both lead to iron-deficiency, microcytic and hypochromic anemia with differences in intestinal iron mobilization. (A) Analysis of mean corpuscular hemoglobin (MCH) and mean corpuscular volume (MCV). (B) Western blot analysis for duodenal ferritin (Fth1) in *Fpn*$^{fl/fl}$, *Fpn*$^{\Delta IE}$, *Dmt1*$^{fl/fl}$, and *Dmt1*$^{\Delta IE}$ mice. Male samples are designated as squares and female samples are designated as circles. Mean ± SEM are plotted. Significance determined using 2-tailed unpaired t test. ****p < 0.0001 compared between *Fpn*$^{fl/fl}$ and *Fpn*$^{\Delta IE}$ cohorts. ####p < 0.0001 compared between *Dmt1*$^{fl/fl}$ and *Dmt1*$^{\Delta IE}$ cohorts.

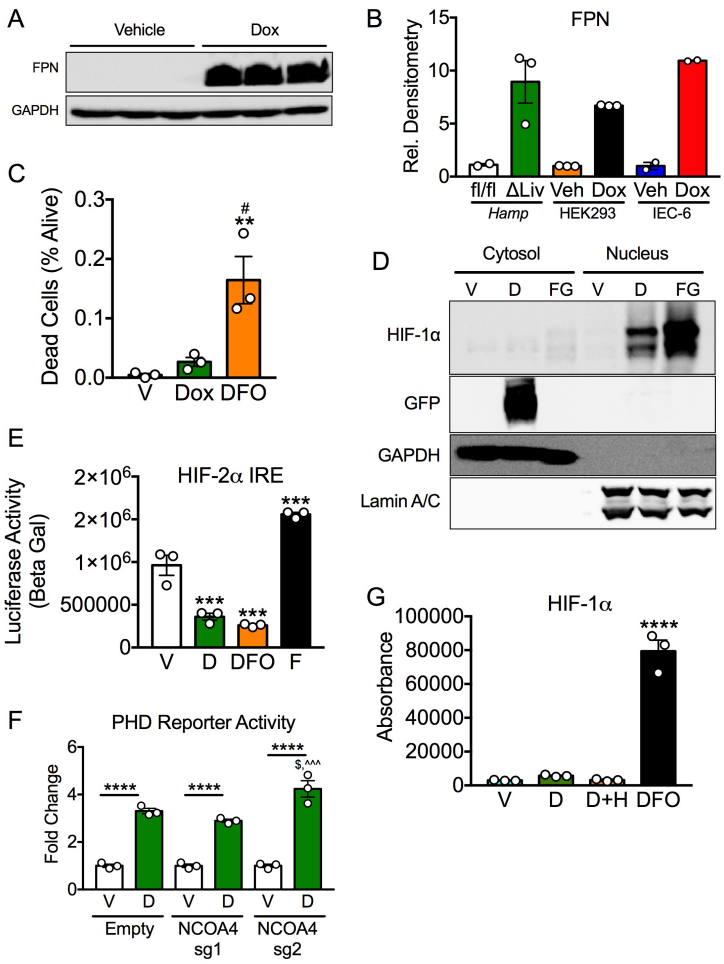

Figure S2.6. Iron efflux through FPN is physiologically relevant and selective for HIF-2α. (A) Western blot analysis for FPN in FPN^{GFP} HEK293 cells treated with vehicle or 250 ng/mL doxycycline for 24-hours. (B) Relative densitometry to calculate fold induction of FPN protein in in vivo and in vitro models using data from Figure 1H, Figure 6I, and Supplemental Figure 6A. (C) Quantitation of dead cells using trypan blue following treatment of FPN^{GFP} HEK293 cells with doxycycline or 200 μM deferoxamine (DFO) for 48-hours. (D) Western blot analysis in cytosolic and nuclear fractions of FPN^{GFP} HEK293 cells treated with vehicle (V), doxycycline (D), or 100 μM FG4592 (FG) for 24-hours. (E) Relative luciferase activity in FPN^{GFP} HEK293 following treatment with vehicle (V), doxycycline (D), DFO, or 200 μM ferric ammonium citrate (FAC) (F). Fold change in luciferase activity in Empty, NCOA4 sg1, and NCOA4 sg2 FPN^{GFP} HEK293 cells infected with the PHD reporter and treated with doxycycline for 24-hours (G) ELISA in lysates from FPN^{GFP} IEC-6 cells treated with vehicle (V), doxycycline (D), doxycycline and 1mg/mL hepcidin (D+H), or DFO for 24-hours. Mean ± SEM are plotted. Significance determined using one-way (C, E, G) or two-way (F) ANOVA with Tukey's post hoc. **p < 0.01; ***p < 0.001; ****p < 0.0001 compared to vehicle. #p < 0.05 compared to doxycycline. $p <0.05 compared to Empty doxycycline. ^^^p<0.001 compared to NCOA4 sg1 doxycycline.

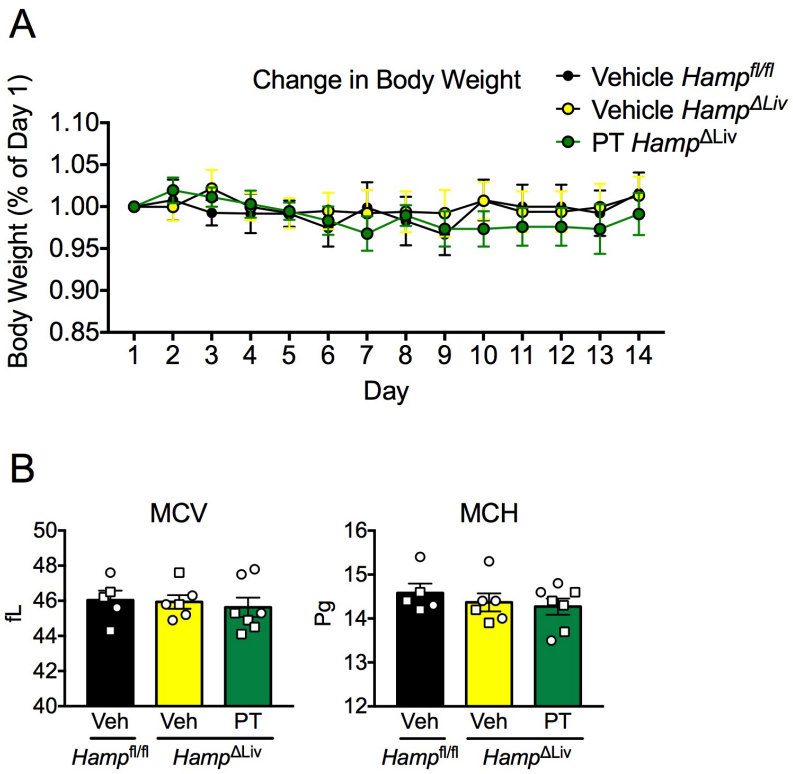

Figure S2.7. Administration of PT2385 does not affect body weight or red blood cell size. (A) Body weight measurements of mice during two-week administration of either vehicle or PT2385. (B) Analysis of mean corpuscular volume (MCV) and mean corpuscular hemoglobin (MCH). Male samples are designated as squares and female samples are designated as circles. Mean ± SEM are plotted. Significance determined using one-way ANOVA with Tukey's post hoc.

Table 2.1. Chapter 2 qPCR and cloning primers.

Gene	*Primer Sequence*
Hamp1 F	CTATCTCCATCAACAGATGAGACAGA
Hamp1 R	AACAGATACCACACTGGGAA
Dcytb F	CATCCTCGCCATCATCTC
Dcytb R	GGCATTGCCTCCATTTAGCTG
DMT1 F	TTGGCAATCATTGGTTCTGA
DMT1 R	CTTCCGCAAGCCATATTTGT
Ferroportin F	ATGGGAACTGTGGCCTTCAC
Ferroportin R	TCCAGGCATGAATACGGAGA
Ankrd37 F	CGGCCTTGCGTGCTTT
Ankrd37 R	TGGTTGAGGTCAGCACCTGTT
Transferrin Receptor F	CAGTCCAGCTGGCAAAGATT
Transferrin Receptor R	GTCCAGTGTGGGAACAGGTC
PDK1 F	TTACTCAGTGGAACACCGCC
PDK1 R	GTTTATCCCCCGATTCAGGT
PGK1 F	CAAATTTGATGAGAATGCCAAGACT
PGK1 R	TTCTTGCTGCTCTCAGTACCACA
HK1 F	GAATTTCATCAGAGAGCCGC
HK1 R	GCGAGGACAGGCTGTAGATG
STEAP4 F	GGAAACTCATCTGCATGTGCT
STEAP4 R	CTAGAAGGCAGAGCCCACC
CXCL1 F	TCTCCGTTACTTGGGGACAC
CXCL1 R	CCACACTCAAGAATGGTCGC
Erythropoietin F	CATCTGCGACAGTCGAGTTCTG
Erythropoietin R	CACAACCCATCGTGACATTTTC

Short Guide RNA for CRISPR/Cas9	
Human NCOA4 sg1	CAGTTGCATAAGCCGTCACC
Human NCOA4 sg2	GTCTTAGAAGCCGTGAGGTA

Chapter 3[2]

A Genetic Mouse Model of Severe Iron-Deficiency Anemia Reveals Tissue-Specific Transcriptional Stress Responses and Cardiac Remodeling

Abstract

Iron is a micronutrient fundamental for life. Iron homeostasis in mammals requires sustained postnatal intestinal iron absorption that maintains intracellular iron concentrations for central and systemic metabolism, as well as for erythropoiesis and oxygen transport. More than one billion people worldwide suffer from iron-deficiency anemia (IDA), a state of systemic iron insufficiency that limits the production of red blood cells (RBCs) and leads to tissue hypoxia and intracellular iron stress. Despite this tremendous public health concern, there are very few genetic models of IDA are available to study its progression. Here, I developed and characterized a novel, genetic mouse model of IDA. I found that tamoxifen-inducible deletion of the mammalian iron exporter, ferroportin (Fpn), exclusively in intestinal epithelial cells leads to loss of intestinal iron absorption. Ferroportin ablation yielded a robust phenotype of progressive IDA that develops in as little as three months following disruption of intestinal iron absorption. I noted that at end-stage IDA, tissue-specific transcriptional stress

[2] This chapter represents a published manuscript: Schwartz AJ, Converso-Baran K, Michele DE, Shah YM. A Genetic Mouse Model of Severe Iron-Deficiency Anemia Reveals Tissue-Specific Transcriptional Stress Responses and Cardiac Remodeling, *Journal of Biological Chemistry*, 2019.

responses occur in which the heart shows little to no hypoxic and iron stress as compared to other peripheral organs. However, morphometric and echocardiographic analysis revealed massive cardiac hypertrophy and chamber dilation, albeit with increased cardiac output at very low basal heart rates. I propose that our intestine-specific ferroportin knockout mouse model of end-stage IDA could be used in future studies to investigate IDA progression and cell-specific responses to hypoxic and iron stress.

Introduction

Iron is an essential micronutrient to sustain life, from single-cell bacteria to complex, multi-cellular organisms. In mammals, systemic iron homeostasis requires multiple organs working in concert to maintain red blood cell (RBC) levels for oxygen transport and intracellular iron concentrations for redox and metabolic reactions (1). More than two billion people are affected by iron deficiency worldwide and one billion suffer from iron-deficiency anemia (IDA) (2). In IDA, iron absorption is limited to an extent that restricts the production of RBCs, ultimately leading to decreased transport of systemic oxygen and the development of intracellular iron stress (3). IDA is more common in developing countries, where it is mainly caused by the inadequate dietary consumption of iron, but also from blood loss due to intestinal worm colonization (4). In more developed countries, dietary eating habits, such as vegetarianism, as well as pathologic conditions that cause bleeding or malabsorption, are common causes (4). Patients with IDA are typically treated with dietary iron. A significant number of IDA patients are refractory to oral iron supplementation, known as iron-refractory IDA (IRIDA) (5). IRIDA patients require intravenous iron supplementation. If uncorrected, IDA can result in severe fatigue, weakness, and pathological cardiac complications (6,7).

Our group, among others, has unveiled that systemic iron homeostasis is regulated in mammals by a hetero-tissue crosstalk mechanism involving the liver-derived hormone hepcidin and the intestinal transcription factor hypoxia-inducible factor-2α (HIF-2α) (8-12). The function of hepcidin is to bind to the only mammalian iron exporter, ferroportin (Fpn), resulting in internalization from the plasma membrane,

intracellular degradation, and an increase in intracellular iron levels (13). Intestinal HIF-2α is a cellular iron sensor that transcriptionally activates machinery essential for iron absorption in normal physiology and in disease (14). I recently identified that these pathways are integrated, whereby HIF-2α activity is controlled by hepcidin/ferroportin dynamics in the intestine following downstream changes to intestinal epithelial iron concentrations (9). Therefore, in states of normal systemic iron and oxygen, hepatic hepcidin is abundantly produced and HIF-2α-mediated intestinal iron absorption is restricted. Conversely, during iron demand or systemic hypoxia, hepcidin production is repressed, intestinal ferroportin is stabilized, and intestinal HIF-2α becomes transcriptionally active and upregulates genes that drive iron absorption. The hepcidin/ferroportin/HIF-2α axis is perturbed in nearly all known iron related disorders (9,14). In the context of IDA, a genetic origin was recently discovered that is characterized by hyperactivation of this pathway following mutation to *TMPRSS6*, in both mice and humans (15,16). *TMPRSS6* is a negative regulator of hepcidin production that, when lost, leads to chronic degradation of ferroportin and progressive and robust IRIDA.

Despite the public health significance of IDA, very little is understood about the kinetics of disease progression and the impact that extreme iron and hypoxic stress exerts on different cell types. Several reports have investigated the role of low iron during development and in the early postnatal period (17,18), however, these manipulations result in developmental abnormalities and cognitive defects that confound analysis. Further, there are few and poorly characterized genetic models that give rise to severe IDA in mice. Long term dietary manipulation of iron levels in adult mice can

lead to IDA, but this model is variable and difficult to generate a state of end-stage IDA (11). Recent reports have uncovered organ-specific regulatory mechanism of iron homeostasis, particularly in the heart, where a local source of hepcidin is produced to specifically regulate cardiac ferroportin and organ-specific iron homeostasis (19). However, a systematic analysis of cardiac structure, function, and iron and hypoxia sensing during IDA has not been reported. It also remains unclear whether other organs respond similarly through unique mechanisms in IDA.

This paper established an inducible and novel model of progressive, end-stage IDA in mice in as little as three months. Through temporal in vivo deletion of ferroportin exclusively in the intestinal epithelium, this work characterized the kinetics by which IDA progresses following ablation of intestinal iron absorption. In end-stage IDA, tissue-specific hypoxic and iron stress responses were observed, whereby the heart shows relatively little direct hypoxic or iron stress responses, despite the development of cardiomegaly and cardiac chamber dilation. Echocardiogram analysis in these mice established that IDA decreases heart rate but with increased stroke volume, cardiac output, and ejection fraction. Collectively, these data characterized organ specific stress responses and the cardiac pathologies of IDA in detail. This novel model of IDA can be used to study disease progression and organ-specific responses to iron and hypoxic stress, as well as therapies for IRIDA.

Methods

Animals and treatments

Vil^{CreERT2}*;Fpn*$^{fl/fl}$ mice were described previously (9). Analysis began on mice that were either 2.5 weeks or 8 weeks of age, as indicated. Mice were injected with tamoxifen (Sigma-Aldrich, St. Louis, MO) at 100 mg/kg of body weight via i.p. for three consecutive days to ensure Cre-mediated recombination. All mice were fed with standard chow (Research Diets, New Brunswick, NJ) unless indicated as being fed a purified AIN-93G iron-replete (350 PPM) or low-iron (< 5 PPM) diet (Dyets, Bethlehem, PA). For intestinal protein and RNA analysis, duodenal epithelial scrapes were performed, whereby the intestine was opened flat and a microscope slide was used to scrape and collect epithelial cells, leaving behind the submucosa. All mice were housed at the Unit for Laboratory Animal Management (ULAM) at the University of Michigan (IACUC protocol number: PRO00008292).

Hematological and iron analysis

The Unit for Laboratory Animal Medicine Pathology Core at The University of Michigan performed complete blood count analysis. Non-heme iron was quantified as described previously (9). Briefly, tissues were homogenized at 100 µL/10 mg in de-ionized water and incubated with an equal volume of an acid digestion solution (i.e. 1M HCl and 10% trichloroacetic acid (Sigma-Aldrich, St. Louis, MO)) for one hour at 95°C. Homogenates were spun at full speed for 10 minutes and 50 µL of supernatant was mixed with 50 µL of a substrate containing 1:1 1 mM ferrozine: 3M sodium acetate and 1% mercaptoacetic acid. Reactions were read at 562 nm.

Quantitative reverse-transcription PCR

mRNA was extracted using Trizol (Thermo Scientific, Waltham, MA) per the manufacturer's instructions. The mRNA was measured by real-time RT-PCR (Life Technologies, Carlsbad, CA) using SYBR Green mix (Alkali Scientific, Fort Lauderdale, FL). Primers are listed in Table 3.1. Quantification cycle (Cq) values were normalized to β-actin and expressed as fold change.

Western blot

Whole-cell lysates were prepared in RIPA buffer as described previously (9). In brief, lysates were separated by SDS-PAGE, transferred to nitrocellulose membrane, and probed overnight at 4°C with antibodies for ferritin (FTN) (Cell Signaling, Danvers, MA) or GAPDH (Santa Cruz, Dallas, TX). Secondary antibodies were purchased from Santa Cruz (Dallas, TX) and membranes were developed using enhanced chemiluminescence substrate (Thermo Scientific, Waltham, MA).

Histological and immunohistochemical analysis

Bright-field histologic analysis was performed on H&E and Picrosirius red-stained formalin-fixed paraffin-embedded sections, using reagents from Sigma-Aldrich (St. Louis, MO). In brief, for Picrosirius red staining, slides were de-paraffinized and incubated with Picrosirius red for 1 hour and washed with an acid solution containing 0.5% acetic acid. Immunohistochemical analysis was performed on frozen sections, following fixation with 10% buffered formalin and blocking with 5% goat serum, using

antibodies against ferroportin (MTP11-A, ADI, San Antonio, TX) or HIF-2α (100-122, Novus, St. Louis, MO). For reticulocyte analysis, a 1% methylene blue (Sigma, St. Louis, MO) solution was mixed with equal volumes of blood and incubated at room temperature for 10 minutes and then smeared onto a microscope slide.

Echocardiogram analysis

Echocardiography was performed as previously described (37). Briefly, induction of anesthesia was performed in an enclosed container filled with 6% isoflurane. After induction, the mice were placed on a warming pad to maintain body temperature. 1 – 1.5% isoflurane was supplied via a nose cone to maintain a surgical plane of anesthesia. In all studies, the isoflurane was delivered with 100% oxygen carrier gas and the mice were anesthetized for less than 30 minutes total to collect the functional data and limit any isoflurane effect that may confound experimental results. The hair is removed from the upper abdominal and thoracic area with depilatory cream. ECG is monitored via non-invasive resting ECG electrodes**.** Transthoracic echocardiography was performed in the supine or left lateral position. Two-dimensional, M-mode, Doppler and tissue Doppler echocardiographic images were recorded using a Visual Sonics' Vevo 2100 high resolution in vivo micro-imaging system with a MS 550D transducer which has a center frequency of 40 MHz and a bandwidth of 22-55 MHz. I measured LV ejection fraction from the two-dimensional long axis view. I measured systolic and diastolic dimensions and wall thickness by M-mode in the parasternal short axis view at the level of the papillary muscles. Fractional shortening and ejection fraction were also calculated from the M-mode parasternal short axis view. Diastolic function was

assessed by conventional pulsed-wave spectral Doppler analysis of mitral valve inflow patterns (early [E] and late [A] filling waves). Doppler tissue imaging (DTI) was used to measure the early (Ea) diastolic tissue velocities of the septal annulus of the mitral valve in the apical 4-chamber view.

Statistics

Results are expressed as mean ± SEM. Significance between two groups was calculated by unpaired t test. Prism 7.0 software (GraphPad Software, La Jolla, CA) was used to conduct analyses.

Acknowledgements: This work was supported by grants from the NIH (R01CA148828 and R01DK095201 to Y.M.S.; F31DK116555 to A.J.S).

Conflict of interest: The authors declare that they have no conflicts of interest with the contents of this article.

Author contributions: A.J.S. and Y.M.S. conceived and designed the study. A.J.S. and K.C.B acquired the data. A.J.S., K.C.B., D.E.M., and Y.M.S. analyzed and interpreted the data. A.J.S. and Y.M.S. wrote the manuscript. Y.M.S. supervised the study.

Results

Inducible deletion of intestinal epithelial ferroportin in adult mice leads to end-stage iron-deficiency anemia

To study the kinetics by which IDA progresses in mice with loss of intestinal iron absorption, *Fpn*-floxed mice were bred to mice that express a tamoxifen-inducible, intestinal epithelium-specific Cre recombinase ($Vil^{CreERT2};Fpn^{fl/fl}$), giving rise upon tamoxifen treatment to mice null for ferroportin in the intestinal epithelium ($Fpn^{\Delta IE}$) (9). Adult, two-month old $Fpn^{fl/fl}$ and $Vil^{CreERT2};Fpn^{fl/fl}$ mice were injected with tamoxifen (n = 4, respectively), bled three months later to assess blood iron parameters, and then closely monitored until visible, phenotypic symptoms of IDA arose (Figure 3.1A). Six months following tamoxifen injection, $Fpn^{\Delta IE}$ mice began to lose their hair and develop white, translucent paws; all animals were therefore sacrificed at this time point (Figure 3.1B). The ferroportin protein was still absent in duodenal sections of $Fpn^{\Delta IE}$ mice six months following tamoxifen treatment, as compared to $Fpn^{fl/fl}$ mice (Figure 3.1C). Complete blood count analysis at three and six months following tamoxifen injection revealed robust, progressive IDA, as red blood cell (RBC) numbers, hemoglobin (HB) counts, and hematocrit (HCT) were significantly decreased in $Fpn^{\Delta IE}$ mice compared to $Fpn^{fl/fl}$ littermates, whereas mean corpuscular volume (MCV) and mean corpuscular hemoglobin (MCH) increased from the three to six month time point, indicating expansion of the reticulocyte pool (Figure 3.1D). Methylene blue staining confirmed a marked expansion of reticuluocytes and an overall decrease in cellularity in $Fpn^{\Delta IE}$ mice. (Figure 3.1E). These data demonstrate that complete ablation of intestinal iron

absorption by intestinal epithelial ferroportin deletion in adult mice results in severe IDA in six months.

Severe iron-deficiency anemia leads to inflammation and necrosis in the liver but spares other organs involved in iron homeostasis

To assess the effect of end-stage IDA on organs involved in maintaining systemic iron homeostasis, the liver, spleen, and duodenum were histologically analyzed by H&E. The spleen was devoid of its red pulp in $Fpn^{\Delta IE}$ mice (Figure 3.2A). Interestingly, the duodenum was unaffected, potentially explained by the short lifespan of the intestinal epithelium, which is approximately 3 to 5 days (Figure 3.2A). Interestingly, the liver exhibited robust morphological damage, including signs of inflammation and necrosis (Figure 3.2A). To further assess this phenotype, higher magnification images were taken of liver H&Es and coupled to picrosirius red staining to reveal collagen deposition and fibrosis. As shown in Fig. 2B, $Fpn^{\Delta IE}$ mice displayed marked collagen deposition, particularly surrounding and extended from central veins. Further assessment of the liver revealed inflammatory foci and necrotic areas (Figure 3.2C). An assessment of inflammatory transcripts indicated that IDA primarily activates *Tgfβ* and *Il6* expression in the liver (Figure 3.2D). Collectively, these data demonstrate that, among the major players in systemic iron homeostasis, end-stage IDA mostly impacts the liver, resulting in inflammation, necrosis, and activation of Tgfβ and Il6.

End-stage iron-deficiency anemia activates a hypoxic transcriptional response in the intestine

IDA starves tissues and cells of both iron and oxygen, which are substrates that control the protein stability of HIF-1α and HIF-2α (20). Intestinal iron absorption requires HIF-2α, the master intestinal transcriptional regulator of apical and basolateral iron transport. I recently showed that the canonical intestinal HIF-2α response is downstream of liver hepcidin kinetics during both iron deficiency and iron overload (9). This axis selectively activates HIF-2α during systemic iron demand, and not HIF-1α, via ferroportin-mediated iron efflux, a response that can be blunted by intracellular iron retention. This work suggests that intestinal epithelial iron levels are the primary stimulus that controls the oxygen-sensitive transcription factor, HIF-2α, during states of systemic hypoxia. In this present study, I sought to investigate the transcriptional response of intestinal hypoxic machinery in end-stage IDA. The duodenal ferroportin (*Fpn*) transcript was significantly reduced in $Fpn^{\Delta IE}$ mice (Figure 3.3A), confirming efficient recombination 6 months following tamoxifen treatment. Interestingly, activation of iron-absorptive HIF-2α-specific iron target genes was observed, *Dcytb*, *Dmt1,* and *Ankrd37*, while there was no change in the expression of duodenal transferrin receptor (*Tfrc)*, an indicator of cellular iron status (Figure 3.3A). Staining of duodenal sections revealed that the HIF-2α protein was massively stabilized in $Fpn^{\Delta IE}$ mice (Figure 3.3B). The intracellular iron storage protein ferritin (FTN) was elevated in $Fpn^{\Delta IE}$ mice, confirming iron retention despite systemic IDA (Figure 3.3C). HIF-1α-specific target genes, *Pdk1, Pgk1, Bnip3*, and *Ndufa4l2*, which are readouts of intracellular hypoxia, were all elevated (Figure 3.3D). Lastly, there was no change in HIF-2α-regulated inflammatory genes (Figure 3.3E). These data indicate that, despite intestinal epithelial iron retention, end-stage IDA generates a state of intestinal hypoxia that is sufficient to

activate HIF-2α-specific iron target genes and HIF-1α-specific target genes, but not HIF-2α-regulated inflammatory target genes.

Severe iron-deficiency anemia leads to tissue-specific hypoxic and iron stresses that spare the heart

In response to low intracellular oxygen, cells upregulate anaerobic glycolysis to sustain energy production, a process that is primarily mediated by the transcriptional upregulation of glycolytic genes via HIF-1α activity (21). The transcriptional response to low intracellular iron is regulated primarily by HIF-2α (14). I sought to address the HIF-1α and HIF-2α transcriptional response in peripheral tissues during IDA to assess relative oxygen and iron stress responses. In general, there was significant activation of HIF-1α and HIF-2α target genes in all tissues other than the heart (Figures 3.4A,B). Of note, erythropoietin expression (*Epo*), a hormonal signal that increases RBC production, was significantly elevated in the kidneys of $Fpn^{\Delta IE}$ mice, which is a process thought to be repressed during IDA (22-24). Recent literature has demonstrated that the heart maintains iron homeostasis by producing a local source of hepcidin that controls cell-autonomous ferroportin and cardiomyocyte iron levels. I did not observe a significant increase in hepcidin gene (*Hamp*) expression in the heart during IDA (Figure 3.4C). Collectively, these data demonstrate that IDA engenders hypoxic and iron stress across peripheral tissues other than the heart, which further confirms a unique, local mechanism of iron homeostasis in cardiomyocytes.

Iron-deficiency anemia leads to cardiac remodeling and pathologies in cardiac structure and function

Patients that suffer from IDA develop cardiac complications (6,7). Given the unique iron regulatory mechanisms in the heart, I sought to characterize this phenotype by in vivo echocardiogram technology 6 months after tamoxifen administration. Forty-eight hours before sacrifice, M-mode echocardiographic analysis revealed increases in septum and posterior wall thickness, as well as thickening of papillary muscles, in $Fpn^{\Delta IE}$ mice (Figure 3.5A). Quantitatively, cardiac structure was tremendously altered, with increases in left ventricular mass, left ventricular volume, interventricular septum, and posterior wall thickness at diastole, as well as ascending aorta diameter (Figure 3.5B). Interestingly, heart rate was decreased in the $Fpn^{\Delta IE}$ mice, despite increase in stroke volume, cardiac output, ejection fraction, and the peak velocity in the aorta, confirming disruption to cardiac function (Figure 3.5C). Heart iron content was decreased by about 50%, despite a quadrupling of left ventricular mass (Figure 3.5D). Decreases in liver, spleen, and kidney iron content were also observed (Figure 3.5D). These data, in connection with the data above, demonstrate that IDA does not lead to cardiac hypoxia or iron stress despite tremendous cardiomegaly and perturbation of cardiac function.

Ablation of intestinal epithelial ferroportin in young mice leads to a more rapid iron-deficiency anemia

To determine if there was an age effect on the development of IDA following loss of intestinal ferroportin, 2.5 week old $Fpn^{fl/fl}$ and $Vil^{CreERT2};Fpn^{fl/fl}$ mice were injected with

tamoxifen and closely monitored (Figure 3.6A). By three months following treatment, $Fpn^{\Delta IE}$ mice began to display similar phenotypic changes to the aforementioned adult cohort (e.g. hair loss, white paws, etc.) and were thus euthenized. The ferroportin protein was absent in duodenal sections of $Fpn^{\Delta IE}$ mice (Figure 3.6B). Furthermore, the ferroportin transcript was significantly decreased in this $Fpn^{\Delta IE}$ cohort (Figure 3.6C). Complete blood count analysis revealed robust IDA, as RBC, HB, HCT, MCH, and MCV were all significantly decreased in $Fpn^{\Delta IE}$ mice compared to $Fpn^{fl/fl}$ littermates, to the same extent as adult mice six months following treatment (Figure 3.6D). Furthermore, heart mass normalized to tibia length was increased already at 3 months post tamoxifen injection, indicating cardiac hypertrophy (Figure 3.6E). These data demonstrate that young mice progress to IDA more rapidly by intestinal ferroportin ablation than adult mice and this genetic model of severe IDA with cardiomegaly can be made more rapid by treating young $Vil^{CreERT2}$;$Fpn^{fl/fl}$ mice with tamoxifen.

Discussion

A constant influx of postnatal intestinal iron is critical to maintain intracellular iron concentrations for metabolism and erythropoiesis for systemic oxygen transport in mammals. However, iron deficiency remains the most common nutrient deficiency in humans, affecting nearly two billion people worldwide (4). Of these, over one billion people suffer from IDA, a state of iron insufficiency that limits the production of RBCs and results in systemic tissue hypoxia and intracellular iron stress (2). Few model systems exist to study the kinetics of IDA and the effect of extreme iron and oxygen stress on peripheral tissues. This present work demonstrates a temporal model of severe IDA in mice via the tamoxifen-inducible ablation of ferroportin in the intestinal epithelium. In as little as three months, severe, end-stage IDA is observed when 2.5 week old *Vil*^{CreERT2}*;Fpn*$^{fl/fl}$ mice are treated with tamoxifen. I discovered tissue-specific activation of hypoxic and iron transcriptional stress responses, whereby the heart is largely spared as compared to other peripheral organs. This transcriptional phenomenon was observed despite the quadrupling of left ventricular mass, significant increases in cardiac output, and the development of cardiomegaly as revealed by in vivo echocardiogram. I also demonstrate that severe IDA can activate the HIF-2α iron absorptive transcriptional program in the intestine despite a surplus of intracellular iron. Collectively, this work reveals a robust and reliable model to study IDA, tissue-specific responses to iron and oxygen stress, and the mechanisms of cardiac remodeling in iron related disorders.

Previous models that give rise to IDA in mice have utilized strategies of dietary iron manipulation or genetic deletion of iron handling in the embryo (6,11,17,18).

However, mice are extremely resistant to IDA when placed on iron deficient diets (9,11). This can be explained, at least in part, by iron contamination in proprietary diets. The ubiquitous nature of iron-containing proteins complicates the ability to remove iron from these diets, leaving behind sufficient iron levels to maintain systemic iron homeostasis for extended periods of time. Genetic models that manipulate intestinal iron absorption have relied on embryonic knockout strategies (18,25). These models dramatically disrupt embryonic and postnatal development, as disruption to iron homeostasis early in life can affect organ development and overall cognitive function (17). Our present model of IDA allows for postnatal development and the establishment of proper iron homeostasis before inducing a disease state. Surprisingly, mice survival appeared unaffected despite mean hemoglobin levels of <5g/dL and mean hematocrits <12%. The lowest observed hematocrit was 6.5%. Previous experiments in anesthetized animals with isovolumic anemia have shown that oxygen delivery can be maintained to approximately similar Hb concentrations (3-5g/DL) and hematocrits (10-15%), but organ function starts to decline near these values and is correlated with development of lactic acidosis (26). Furthermore, the progressive nature of this genetic model allows for the temporal characterization of IDA in ways never executed before. This model is limited, however, because it recapitulates IRIDA, a rare phenotype of IDA that is refractory to oral iron supplementation due to the inability to absorb intestinal iron. Future work will need to carefully describe IDA progression and more clearly define the mechanisms behind disparate intracellular stress responses in peripheral tissues.

In addition to the hepcidin/ferroportin/HIF-2α axis that regulates systemic iron homeostasis, there exists a ubiquitous cell-autonomous mechanism of intracellular iron

sensing and regulation via iron-regulatory protein (IRP) and iron response element (IRE) machinery. This system controls cellular iron homeostasis by modulating the translation of mRNAs involved in iron handling via the binding of IRPs with IREs in the 5'- or 3'- untranslated region (UTR) of these transcripts. Erythropoietin (EPO), an endocrine hormone produced by the kidney to drive RBC production in the bone marrow, is a classical HIF-2α-target gene regulated by systemic hypoxia (24,27). HIF-2α contains a 5′-UTR IRE that is responsible for translational inhibition during states of iron deficiency (22-24). This IRP/IRE interaction is thought to serve as a molecular brake on HIF-2α-mediated kidney EPO expression to restrict RBC production when iron levels are limited for hemoglobin synthesis. Surprisingly, I find in this work that the *Epo* transcript is induced 1000-fold, despite severe kidney iron deficiency in IDA. This finding might indicate that the IRP/IRE system is an insufficient mechanism to dampen HIF-2α in the kidney during the severe disease state of IDA. Moreover, high EPO production in IDA is likely a pathological feature in which red blood cell production is continually attempted despite insufficient circulating iron levels. This finding may explain the expansion of reticulocytes that I observe in this manuscript. In addition to IRE/IRP machinery, HIF-2α is also regulated at the post-transcriptional level by PHD enzymes, whereby intracellular iron deficiency limits PHD enzyme activity to stabilize the HIF-2α protein (9). It is therefore possible that a hepcidin/ferroportin/PHD axis may exist in EPO producing cells in the kidney, similar to the intestine, whereby the hepcidin/ferroportin/PHD induction of HIF-2α outweighs the IRP/IRE break on HIF-2α in contexts when both pathways are active. In the intestine, the dominance of the hepcidin/ferroportin/PHD axis over IRP/IRE machinery enables HIF-2α protein

stabilization and an increase in iron absorption during states of iron deficiency. However, in the kidney during IDA, the interplay between these pathways appears to be pathological given the inappropriate, sustained, and paradoxical production of EPO. More work will need to be done to understand the complete molecular mechanisms of *Epo* expression during normal physiology and in disease states such as IDA.

Transcriptional stress responses to states of low intracellular oxygen are mediated by the family of hypoxia inducible factors, namely HIF-1α and HIF-2α. These transcription factors activate unique and overlapping target genes to upregulate anaerobic glycolysis and modulate cellular metabolism in order to survive in low oxygen environments (14,20,21). Our lab, among others, has shown that HIF-2α, but not HIF-1α, is a direct cellular iron sensor (10,12). More recently, I revealed that intestinal HIF-2α is primarily regulated by intracellular iron levels during states of systemic iron demand, whereby the canonical and physiological HIF-2α response can be blunted by a state of intracellular iron excess (9). Interestingly, I show in this present work that the intestinal HIF-2α iron absorptive transcriptional program is active during severe IDA, despite excess intracellular iron following ferroportin ablation. This finding suggests that, while intestinal HIF-2α is mainly responsive to intracellular iron levels in physiological iron demand, HIF-2α maintains an oxygen sensing capacity during severe tissue hypoxia in IDA. Interestingly, HIF-2α transcriptional targets involved in inflammation were not active, despite activation of iron absorptive genes. This finding is in line with recent work to show that HIF-2α functions with cofactors and other transcriptional partners to regulate subsets of target genes once the protein is stabilized (28,29). Future work will need to define how specific HIF target genes are regulated during

unique environmental ques, as well as the relative contribution of HIF-2α oxygen and iron sensing in different cells and tissues.

Cardiac structure and function is perturbed in iron related disorders, including iron deficiency, iron overload, and anemia. In IDA in humans, the heart undergoes massive cardiac hypertrophy and remodeling to increase cardiac output and prolong survival when systemic oxygen transport becomes limiting (30,31). A recent study comparing genetic models of sickle cell anemia with diet induced IDA in adult mice showed that after 3 months of anemia (5-9 g/dL Hb with a IDA target of 7.5 g/dL Hb) both models develop a high output functional state in the heart (32). However, while the sickle cell anemia produced a more severe restrictive cardiomyopathy with fibrotic remodeling, this study reported 3 months of IDA beginning at 5 months of age failed to produce significant cardiac hypertrophy (32). This is consistent with our findings of a more slowly progressive IDA phenotype in adult mice and suggests hemoglobin concentrations <5g/DL and hematocrits <15% in IDA are required for inducing significant cardiac hypertrophy. Interestingly, the cardiac hypertrophy in IDA can be explained, at least in part, simply by decreases in cardiac iron stores because genetic disruption to the serum uptake of iron exclusively in cardiomyocytes leads to cardiac hypertrophy (33). Using in vivo echocardiogram, I detail in this present work the structural and functional changes that occur in the heart during severe IDA. I observed structural changes that include the quadrupling of left ventricular mass and increases in left ventricular volume and posterior wall thickness at diastole. I also observed increases in cardiac output and stroke volume, despite a decrease in heart rate and total heart iron content. Interestingly, in spite of these pathophysiological changes, the

heart was largely spared from transcriptional stress responses downstream of HIF that would demonstrate tissue hypoxia and iron stress. Recent literature has revealed that cardiomyocytes rely on cell-autonomous mechanisms to control iron homeostasis in the heart that are distinct from systemic mechanisms of iron homeostasis (19). While normal mice do not normally show lower arterial blood oxygen saturation or heart rate under the 1-1.5% isoflurane conditions used here for the cardiac functional studies (34-36), I cannot rule out that IDA mice are more susceptible to subtle effects of isoflurane on arterial blood oxygen saturation. I note that the mice in this present work were maintained on 1-1.5% isoflurane delivered in 100% oxygen carrier gas even though room air is sufficient to maintain arterial oxygen saturation in isoflurane anesthetized wild-type mice (35). Taken together, these data might suggest that cell-autonomous mechanisms of cardiac iron handling are sufficient to prevent overt iron and oxygen stress during IDA. Moreover, it is possible that the heart is somehow spared by peripheral organs and that serum iron and oxygen are redirected to the heart during stress. Future work will need to identify the signaling pathways that mediate the robust cardiac remodeling that is observed in IDA, as well as the complete molecular mechanisms of cardiac iron homeostasis that prevent hypoxic and iron transcriptional stress responses.

In conclusion, our work demonstrates a novel, robust, and inducible model of IDA in mice. I provide new insights into the molecular mechanisms of HIF signaling and IRP/IRE kinetics. I also characterize the cardiac changes of IDA and unveil unique tissue-specific transcriptional stress responses across peripheral tissues during hypoxic and iron stress.

References

1. Drakesmith, H., Nemeth, E., and Ganz, T. (2015) Ironing out Ferroportin. *Cell Metab* 22, 777-787
2. McLean, E., Cogswell, M., Egli, I., Wojdyla, D., and de Benoist, B. (2009) Worldwide prevalence of anaemia, WHO Vitamin and Mineral Nutrition Information System, 1993-2005. *Public Health Nutr* 12, 444-454
3. Muckenthaler, M. U., Rivella, S., Hentze, M. W., and Galy, B. (2017) A Red Carpet for Iron Metabolism. *Cell* 168, 344-361
4. Camaschella, C. (2015) Iron-deficiency anemia. *N Engl J Med* 372, 1832-1843
5. Heeney, M. M., and Finberg, K. E. (2014) Iron-refractory iron deficiency anemia (IRIDA). *Hematol Oncol Clin North Am* 28, 637-652, v
6. Chung, Y. J., Luo, A., Park, K. C., Loonat, A. A., Lakhal-Littleton, S., Robbins, P. A., and Swietach, P. (2019) Iron-deficiency anemia reduces cardiac contraction by downregulating RyR2 channels and suppressing SERCA pump activity. *JCI Insight* 4
7. Sutil-Vega, M., Rizzo, M., and Martinez-Rubio, A. (2019) Anemia and iron deficiency in heart failure: a review of echocardiographic features. *Echocardiography* 36, 585-594
8. Anderson, E. R., Xue, X., and Shah, Y. M. (2011) Intestinal hypoxia-inducible factor-2alpha (HIF-2alpha) is critical for efficient erythropoiesis. *J Biol Chem* 286, 19533-19540
9. Schwartz, A. J., Das, N. K., Ramakrishnan, S. K., Jain, C., Jurkovic, M. T., Wu, J., Nemeth, E., Lakhal-Littleton, S., Colacino, J. A., and Shah, Y. M. (2019) Hepatic hepcidin/intestinal HIF-2alpha axis maintains iron absorption during iron deficiency and overload. *J Clin Invest* 129, 336-348
10. Shah, Y. M., Matsubara, T., Ito, S., Yim, S. H., and Gonzalez, F. J. (2009) Intestinal hypoxia-inducible transcription factors are essential for iron absorption following iron deficiency. *Cell Metab* 9, 152-164
11. Taylor, M., Qu, A., Anderson, E. R., Matsubara, T., Martin, A., Gonzalez, F. J., and Shah, Y. M. (2011) Hypoxia-inducible factor-2alpha mediates the adaptive increase of intestinal ferroportin during iron deficiency in mice. *Gastroenterology* 140, 2044-2055
12. Mastrogiannaki, M., Matak, P., Keith, B., Simon, M. C., Vaulont, S., and Peyssonnaux, C. (2009) HIF-2alpha, but not HIF-1alpha, promotes iron absorption in mice. *J Clin Invest* 119, 1159-1166
13. Nemeth, E., Tuttle, M. S., Powelson, J., Vaughn, M. B., Donovan, A., Ward, D. M., Ganz, T., and Kaplan, J. (2004) Hepcidin regulates cellular iron efflux by binding to ferroportin and inducing its internalization. *Science* 306, 2090-2093
14. Shah, Y. M., and Xie, L. (2014) Hypoxia-inducible factors link iron homeostasis and erythropoiesis. *Gastroenterology* 146, 630-642
15. Finberg, K. E., Heeney, M. M., Campagna, D. R., Aydinok, Y., Pearson, H. A., Hartman, K. R., Mayo, M. M., Samuel, S. M., Strouse, J. J., Markianos, K., Andrews, N. C., and Fleming, M. D. (2008) Mutations in TMPRSS6 cause iron-refractory iron deficiency anemia (IRIDA). *Nat Genet* 40, 569-571

16. Guo, S., Casu, C., Gardenghi, S., Booten, S., Aghajan, M., Peralta, R., Watt, A., Freier, S., Monia, B. P., and Rivella, S. (2013) Reducing TMPRSS6 ameliorates hemochromatosis and beta-thalassemia in mice. *J Clin Invest* 123, 1531-1541
17. Ramakrishnan, S. K., Anderson, E. R., Martin, A., Centofanti, B., and Shah, Y. M. (2015) Maternal intestinal HIF-2alpha is necessary for sensing iron demands of lactation in mice. *Proc Natl Acad Sci U S A* 112, E3738-3747
18. Donovan, A., Lima, C. A., Pinkus, J. L., Pinkus, G. S., Zon, L. I., Robine, S., and Andrews, N. C. (2005) The iron exporter ferroportin/Slc40a1 is essential for iron homeostasis. *Cell Metab* 1, 191-200
19. Lakhal-Littleton, S., Wolna, M., Chung, Y. J., Christian, H. C., Heather, L. C., Brescia, M., Ball, V., Diaz, R., Santos, A., Biggs, D., Clarke, K., Davies, B., and Robbins, P. A. (2016) An essential cell-autonomous role for hepcidin in cardiac iron homeostasis. *Elife* 5
20. Keith, B., Johnson, R. S., and Simon, M. C. (2011) HIF1alpha and HIF2alpha: sibling rivalry in hypoxic tumour growth and progression. *Nat Rev Cancer* 12, 9-22
21. Semenza, G. L. (2013) HIF-1 mediates metabolic responses to intratumoral hypoxia and oncogenic mutations. *J Clin Invest* 123, 3664-3671
22. Sanchez, M., Galy, B., Muckenthaler, M. U., and Hentze, M. W. (2007) Iron-regulatory proteins limit hypoxia-inducible factor-2alpha expression in iron deficiency. *Nat Struct Mol Biol* 14, 420-426
23. Anderson, S. A., Nizzi, C. P., Chang, Y. I., Deck, K. M., Schmidt, P. J., Galy, B., Damnernsawad, A., Broman, A. T., Kendziorski, C., Hentze, M. W., Fleming, M. D., Zhang, J., and Eisenstein, R. S. (2013) The IRP1-HIF-2alpha axis coordinates iron and oxygen sensing with erythropoiesis and iron absorption. *Cell Metab* 17, 282-290
24. Wilkinson, N., and Pantopoulos, K. (2013) IRP1 regulates erythropoiesis and systemic iron homeostasis by controlling HIF2alpha mRNA translation. *Blood* 122, 1658-1668
25. Chen, A. C., Donovan, A., Ned-Sykes, R., and Andrews, N. C. (2015) Noncanonical role of transferrin receptor 1 is essential for intestinal homeostasis. *Proc Natl Acad Sci U S A* 112, 11714-11719
26. Viele, M. K., and Weiskopf, R. B. (1994) What can I learn about the need for transfusion from patients who refuse blood? The experience with Jehovah's Witnesses. *Transfusion* 34, 396-401
27. Wang, G. L., and Semenza, G. L. (1993) General involvement of hypoxia-inducible factor 1 in transcriptional response to hypoxia. *Proc Natl Acad Sci U S A* 90, 4304-4308
28. Ma, X., Das, N. K., Castillo, C., Gourani, A., Perekatt, A. O., Verzi, M. P., and Shah, Y. M. (2019) SMAD family member 3 (SMAD3) and SMAD4 repress HIF2alpha-dependent iron-regulatory genes. *J Biol Chem* 294, 3974-3986
29. Xue, X., Ramakrishnan, S., Anderson, E., Taylor, M., Zimmermann, E. M., Spence, J. R., Huang, S., Greenson, J. K., and Shah, Y. M. (2013) Endothelial PAS domain protein 1 activates the inflammatory response in the intestinal epithelium to promote colitis in mice. *Gastroenterology* 145, 831-841

30. Hayashi, R., Ogawa, S., Watanabe, Z., and Yamamoto, M. (1999) Cardiovascular function before and after iron therapy by echocardiography in patients with iron deficiency anemia. *Pediatr Int* 41, 13-17
31. Zhou, Q., Shen, J., Liu, Y., Luo, R., Tan, B., and Li, G. (2017) Assessment of left ventricular systolic function in patients with iron deficiency anemia by three-dimensional speckle-tracking echocardiography. *Anatol J Cardiol* 18, 194-199
32. Bakeer, N., James, J., Roy, S., Wansapura, J., Shanmukhappa, S. K., Lorenz, J. N., Osinska, H., Backer, K., Huby, A. C., Shrestha, A., Niss, O., Fleck, R., Quinn, C. T., Taylor, M. D., Purevjav, E., Aronow, B. J., Towbin, J. A., and Malik, P. (2016) Sickle cell anemia mice develop a unique cardiomyopathy with restrictive physiology. *Proc Natl Acad Sci U S A* 113, E5182-5191
33. Xu, W., Barrientos, T., Mao, L., Rockman, H. A., Sauve, A. A., and Andrews, N. C. (2015) Lethal Cardiomyopathy in Mice Lacking Transferrin Receptor in the Heart. *Cell Rep* 13, 533-545
34. Loeven, A. M., Receno, C. N., Cunningham, C. M., and DeRuisseau, L. R. (2018) Arterial blood sampling in male CD-1 and C57BL/6J mice with 1% isoflurane is similar to awake mice. *J Appl Physiol (1985)* 125, 1749-1759
35. Wilding, L. A., Hampel, J. A., Khoury, B. M., Kang, S., Machado-Aranda, D., Raghavendran, K., and Nemzek, J. A. (2017) Benefits of 21% Oxygen Compared with 100% Oxygen for Delivery of Isoflurane to Mice (Mus musculus) and Rats (Rattus norvegicus). *J Am Assoc Lab Anim Sci* 56, 148-154
36. Adelsperger, A. R., Bigiarelli-Nogas, K. J., Toore, I., and Goergen, C. J. (2016) Use of a Low-flow Digital Anesthesia System for Mice and Rats. *J Vis Exp*
37. Zolov, S. N., Bridges, D., Zhang, Y., Lee, W. W., Riehle, E., Verma, R., Lenk, G. M., Converso-Baran, K., Weide, T., Albin, R. L., Saltiel, A. R., Meisler, M. H., Russell, M. W., and Weisman, L. S. (2012) In vivo, Pikfyve generates PI(3,5)P2, which serves as both a signaling lipid and the major precursor for PI5P. *Proc Natl Acad Sci U S A* 109, 17472-17477

Table 3.1. Chapter 3 qPCR Primers.

Gene	*Primer Sequence*
Dcytb F	CATCCTCGCCATCATCTC
Dcytb R	GGCATTGCCTCCATTTAGCTG
DMT1 F	TTGGCAATCATTGGTTCTGA
DMT1 R	CTTCCGCAAGCCATATTTGT
Ferroportin F	ATGGGAACTGTGGCCTTCAC
Ferroportin R	TCCAGGCATGAATACGGAGA
Ankrd37 F	CGGCCTTGCGTGCTTT
Ankrd37 R	TGGTTGAGGTCAGCACCTGTT
Transferrin Receptor F	CAGTCCAGCTGGCAAAGATT
Transferrin Receptor R	GTCCAGTGTGGGAACAGGTC
PDK1 F	TTACTCAGTGGAACACCGCC
PDK1 R	GTTTATCCCCCGATTCAGGT
PGK1 F	CAAATTTGATGAGAATGCCAAGACT
PGK1 R	TTCTTGCTGCTCTCAGTACCACA
Bnip3 F	TGAAGTGCAGTTCTACCCAGG
Bnip3 R	CCTGTCGCAGTTGGGTTC
Ndufa4l2 F	AGTCTAGGGACCCGCTTCTAC
Ndufa4l2 R	TGTACTGGTCATTGGGACTCA
STEAP4 F	GGAAACTCATCTGCATGTGCT
STEAP4 R	CTAGAAGGCAGAGCCCACC
CXCL1 F	TCTCCGTTACTTGGGGACAC
CXCL1 R	CCACACTCAAGAATGGTCGC
Erythropoietin F	CATCTGCGACAGTCGAGTTCTG
Erythropoietin R	CACAACCCATCGTGACATTTTC
Hamp1 F	CTATCTCCATCAACAGATGAGACAGA

Hamp1 R	AACAGATACCACACTGGGAA
Tnfα F	AGGGTCTGGGCCATAGAACT
Tnfα R	CCACCACGCTCTTCTGTCTAC
Tgfβ F	CAACCCAGGTCCTTCCTAAA
Tgfβ R	GGAGAGCCCTGGATACCAAC
CXCL5 F	TGCATTCCGCTTAGCTTTCT
CXCL5 R	CAGAAGGAGGTCTGTCTGGA
Cox 2 F	GGCGCAGTTTATGTTGTCTGT
Cox 2 R	CAAGACAGATCATAAGCGAGGA
Il6 F	ACCAGAGGAAATTTTCAATAGGC
Il6 R	TGATGCACTTGCAGAAAACA
Il1β F	AAGAGCTTCAGGCAGGCAGTATCA
Il1β R	TGCAGCTGTCTAGGAACGTCA
Il22 F	TCGCCTTGATCTCTCCACTC
Il22 R	GCTCAGCTCCTGTCACATCA
IL23 F	GCTCCCCTTTGAAGATGTCA
Il23 R	GACCCACAAGGACTCAAGGA

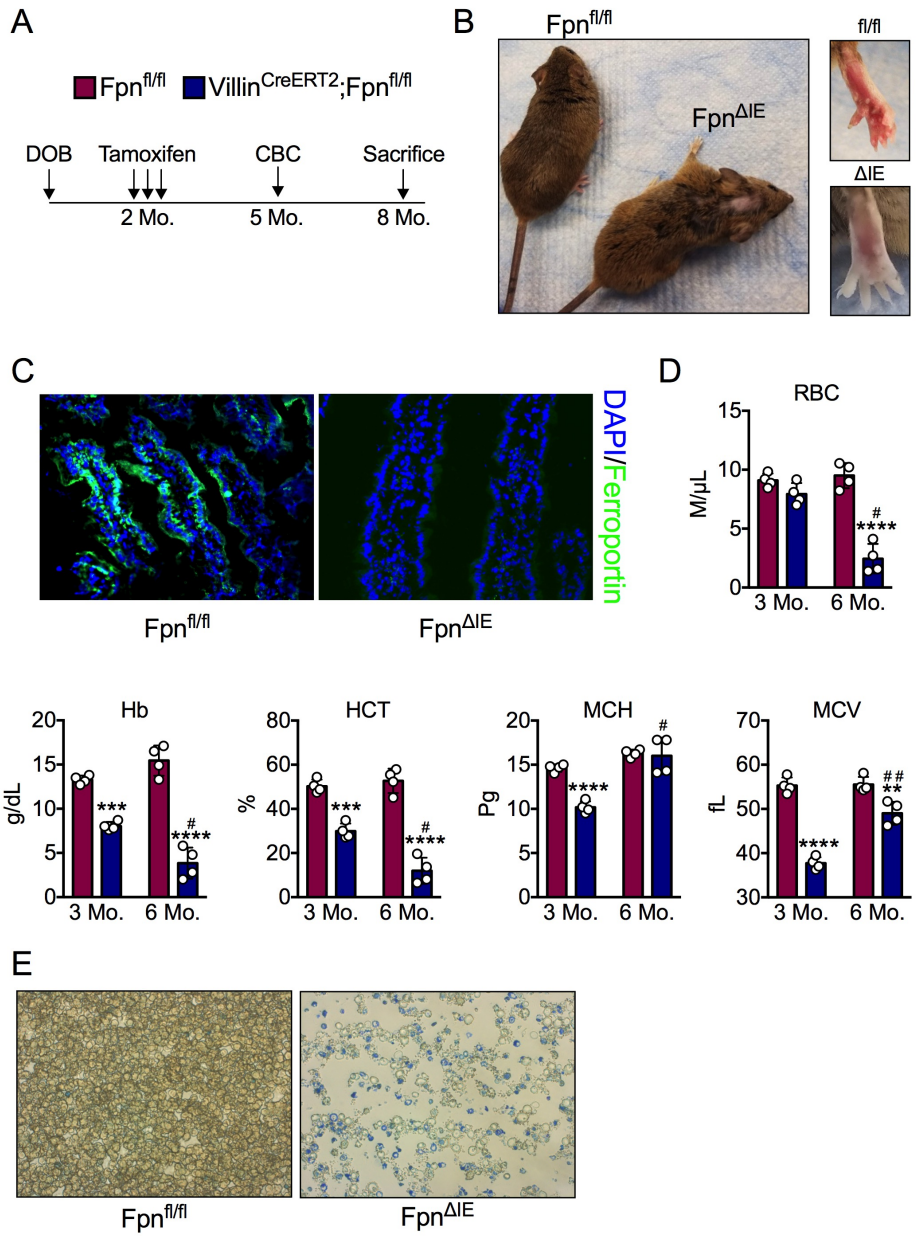

Figure 3.1. Intestinal epithelial ferroportin deletion in adult mice gives rise to progressive and end-stage iron-deficiency anemia. (A) Schematic of experimental design, (B) Gross images of *Fpn*$^{fl/fl}$ and *Fpn*$^{\Delta IE}$ mice 6 months after tamoxifen administration, (C) Representative ferroportin staining in duodenal sections of *Fpn*$^{fl/fl}$ and *Fpn*$^{\Delta IE}$ mice, images at 40x, (D) Analysis of red blood cells (RBC), hemoglobin (HB), hematocrit (HCT), mean corpuscular hemoglobin (MCH), and mean corpuscular volume (MCV) at 3 and 6 months following tamoxifen injection, (E) Representative methylene blue staining for reticulocytes, images at 60x. Mean ± SEM are plotted. **p < 0.01; ***p < 0.001; ****p < 0.0001 compared between *Fpn*$^{fl/fl}$ and *Fpn*$^{\Delta IE}$ cohorts within each time point, using 2-tailed unpaired t test. #p < 0.05; # #p < 0.01 compared between individual *Fpn*$^{\Delta IE}$ mice at 3 month and 6 month time points, using 2-tailed paired t test.

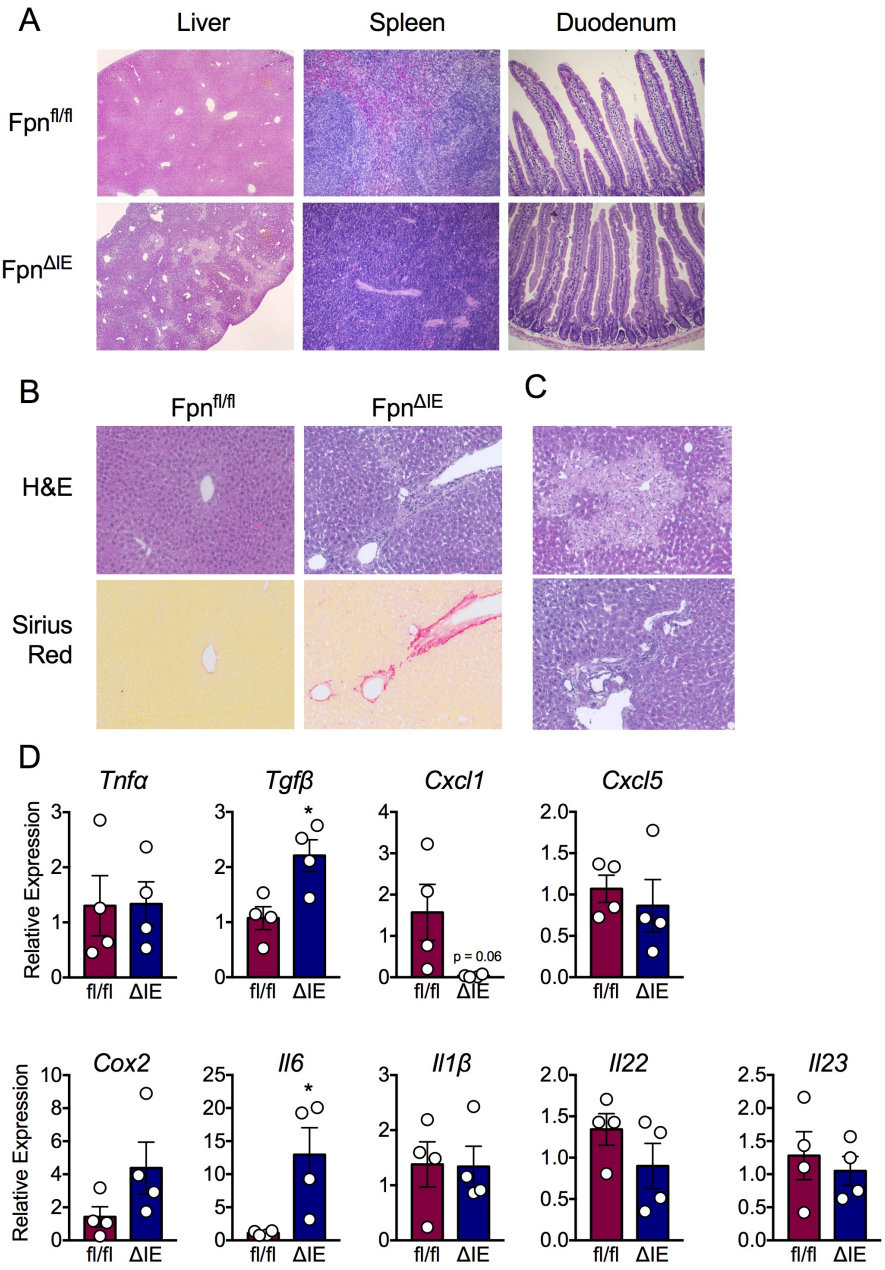

Figure 3.2. Histological analysis of peripheral organs involved in iron homeostasis reveals inflammation and necrosis in the liver. (A) Representative H&E analysis of liver at 5x and spleen and duodenum at 20x from *Fpn*$^{fl/fl}$ and *Fpn*$^{\Delta IE}$ cohorts, (B) Representative H&E and Picrosirius Red analysis of liver from *Fpn*$^{fl/fl}$ and *Fpn*$^{\Delta IE}$ cohorts, images at 20x, (C) Additional representative H&E images of liver from *Fpn*$^{\Delta IE}$ cohorts, images at 20x (D) qPCR analysis of inflammatory genes in livers of *Fpn*$^{fl/fl}$ and *Fpn*$^{\Delta IE}$ cohorts. All data here is from mice 6 months post-tamoxifen treatment. Mean ± SEM are plotted. Significance determined using 2-tailed unpaired t test. *p < 0.5 compared between *Fpn*$^{fl/fl}$ and *Fpn*$^{\Delta IE}$ cohorts.

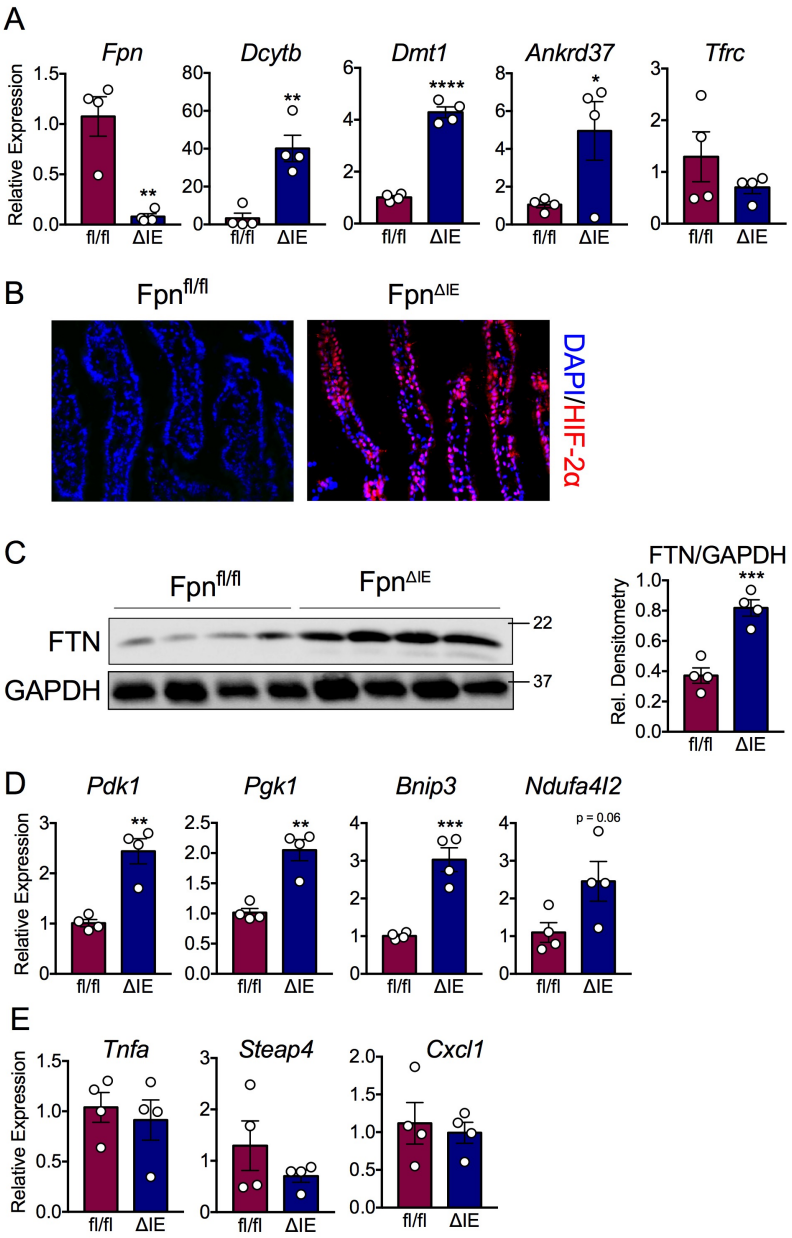

Figure 3.3. Iron-deficiency anemia leads to transcriptional activation of iron and hypoxic target genes in the intestine despite intestinal epithelial iron retention. (A) qPCR analysis for duodenal HIF-2α-specific and iron-handling transcripts, (B) Representative HIF-2α staining in duodenal sections of *Fpn*$^{fl/fl}$ and *Fpn*$^{\Delta IE}$ mice, images at 40x, (C) Western blot analysis and quantification for duodenal ferritin (FTN) abundance, (D) qPCR analysis for duodenal HIF-1α-specific transcripts, (E) qPCR analysis for duodenal HIF-2α-specific and inflammatory transcripts. All data here is from mice 6 months post-tamoxifen treatment. Mean ± SEM are plotted. Significance determined using 2-tailed unpaired t test. *p < 0.5; **p < 0.01; ***p < 0.001; ****p < 0.0001 compared between *Fpn*$^{fl/fl}$ and *Fpn*$^{\Delta IE}$ cohorts.

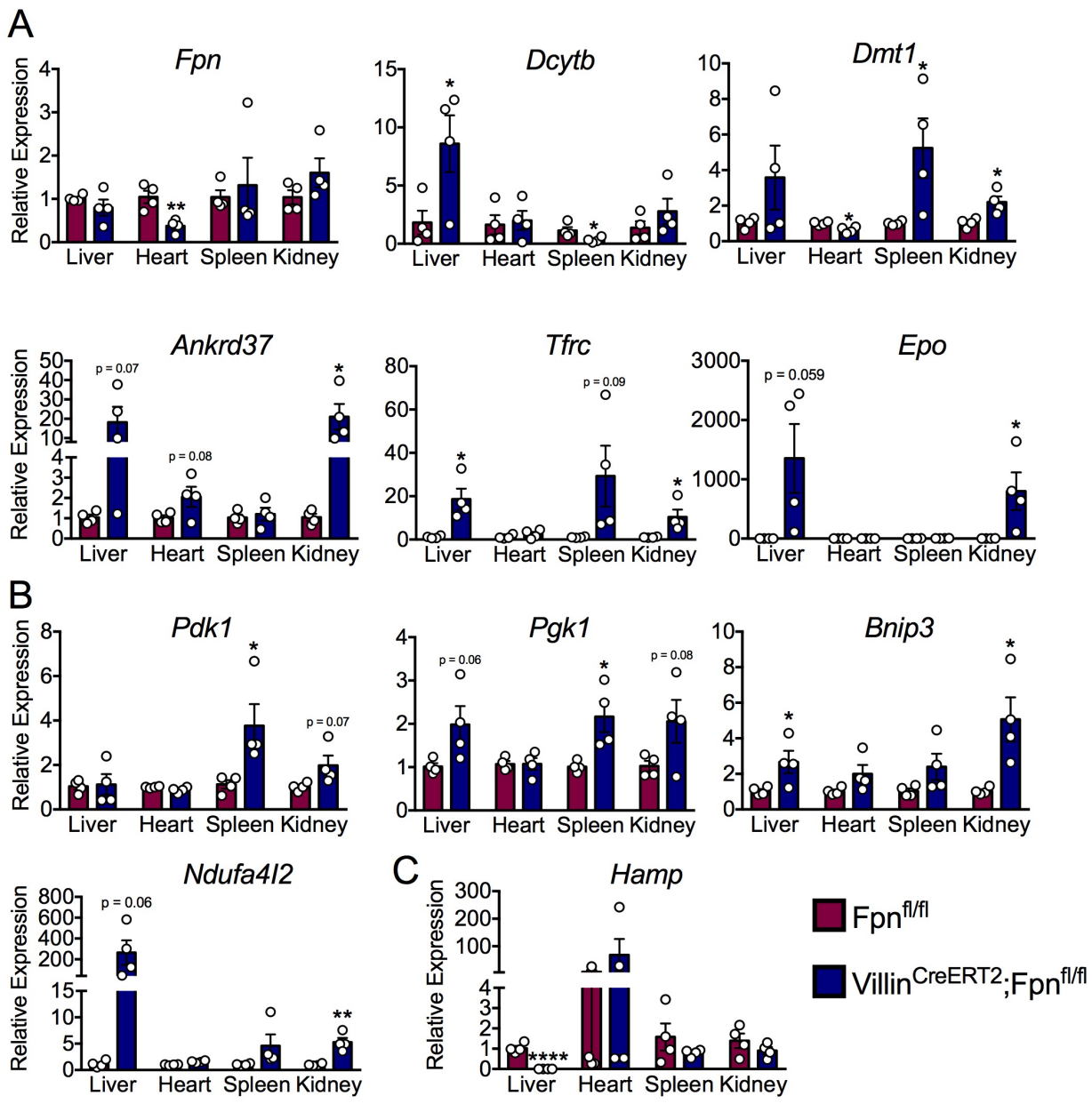

Figure 3.4. The heart is spared from hypoxic and iron stresses that affect peripheral tissues during iron-deficiency anemia. (A) qPCR analysis for HIF-2α-specific and iron-handling transcripts in liver, heart, spleen, and kidney, (B) qPCR analysis for HIF-1α-specific transcripts in liver, heart, spleen, and kidney, (C) qPCR analysis for hepcidin (*Hamp*) in liver, heart, spleen, and kidney. All data here is from mice 6 months post-tamoxifen treatment. Mean ± SEM are plotted. Significance determined using 2-tailed unpaired t test. *p < 0.5; **p < 0.01; ****p < 0.0001 compared between $Fpn^{fl/fl}$ and $Fpn^{\Delta IE}$ cohorts within each tissue group.

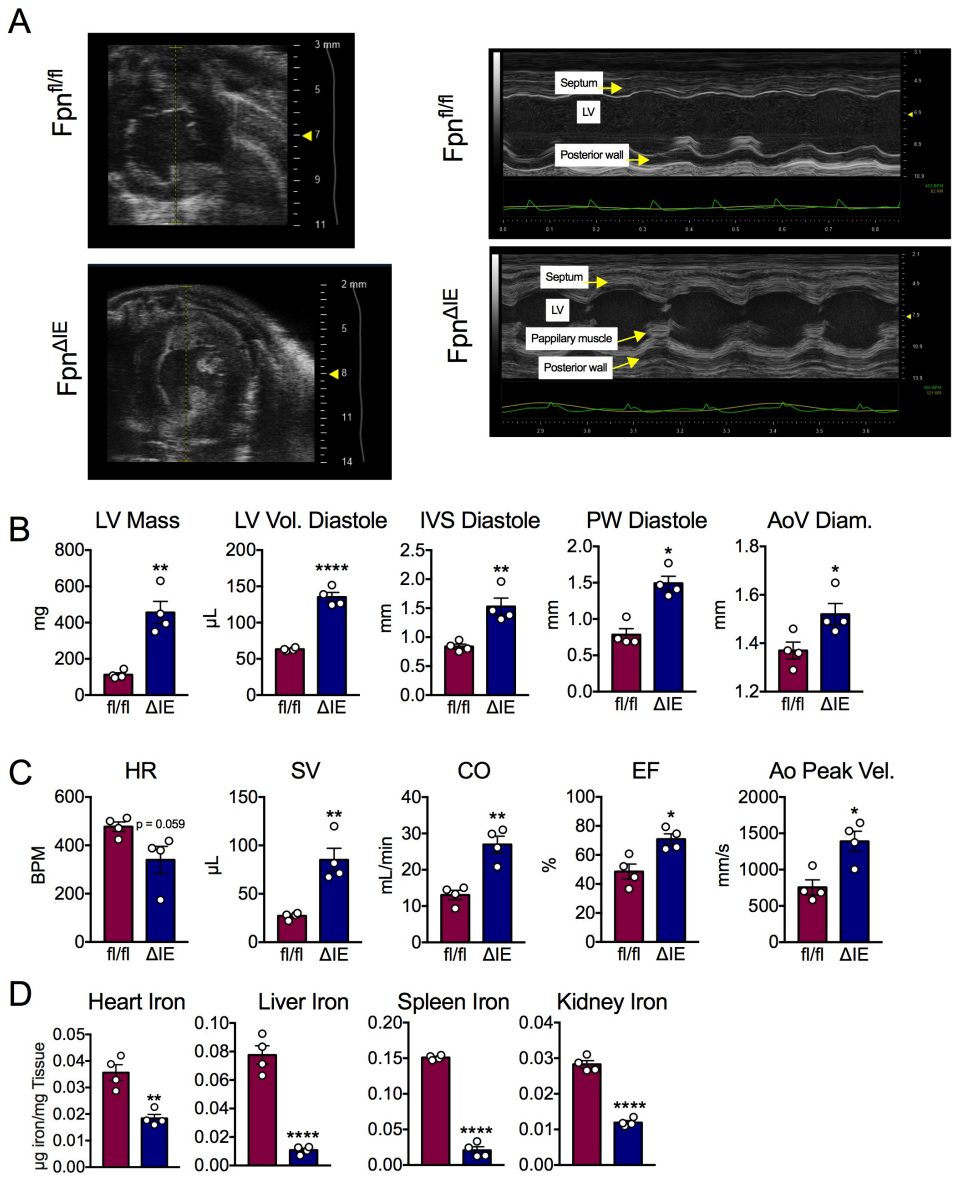

Figure 3.5. Echocardiogram analysis of iron-deficiency anemia reveals cardiomegaly and disruption to cardiac function. (A) M-mode images from echocardiogram analysis in *Fpn*$^{fl/fl}$ and *Fpn*$^{\Delta IE}$ mice at end-stage iron-deficiency anemia, (B) Quantification of cardiac structure parameters, left ventricular mass (LV Mass), left ventricular volume at diastole (LV Vol. Diastole), interventricular septum width at diastole (IVS Diastole), posterior wall thickness at diastole (PW Diastole), and ascending aorta diameter (AoV Diam.), (C) Quantification of cardiac function parameters, heart rate (HR), stroke volume (SV), cardiac output (CO), ejection fraction (EF), and aorta velocity peak gradient (Ao Peak Vel.), (D) heart, liver, spleen, and kidney iron content. All data here is from mice 6 months post-tamoxifen treatment. Mean ± SEM are plotted. Significance determined using 2-tailed unpaired t test. *p < 0.5; **p < 0.01; ****p < 0.0001 compared between *Fpn*$^{fl/fl}$ and *Fpn*$^{\Delta IE}$ cohorts.

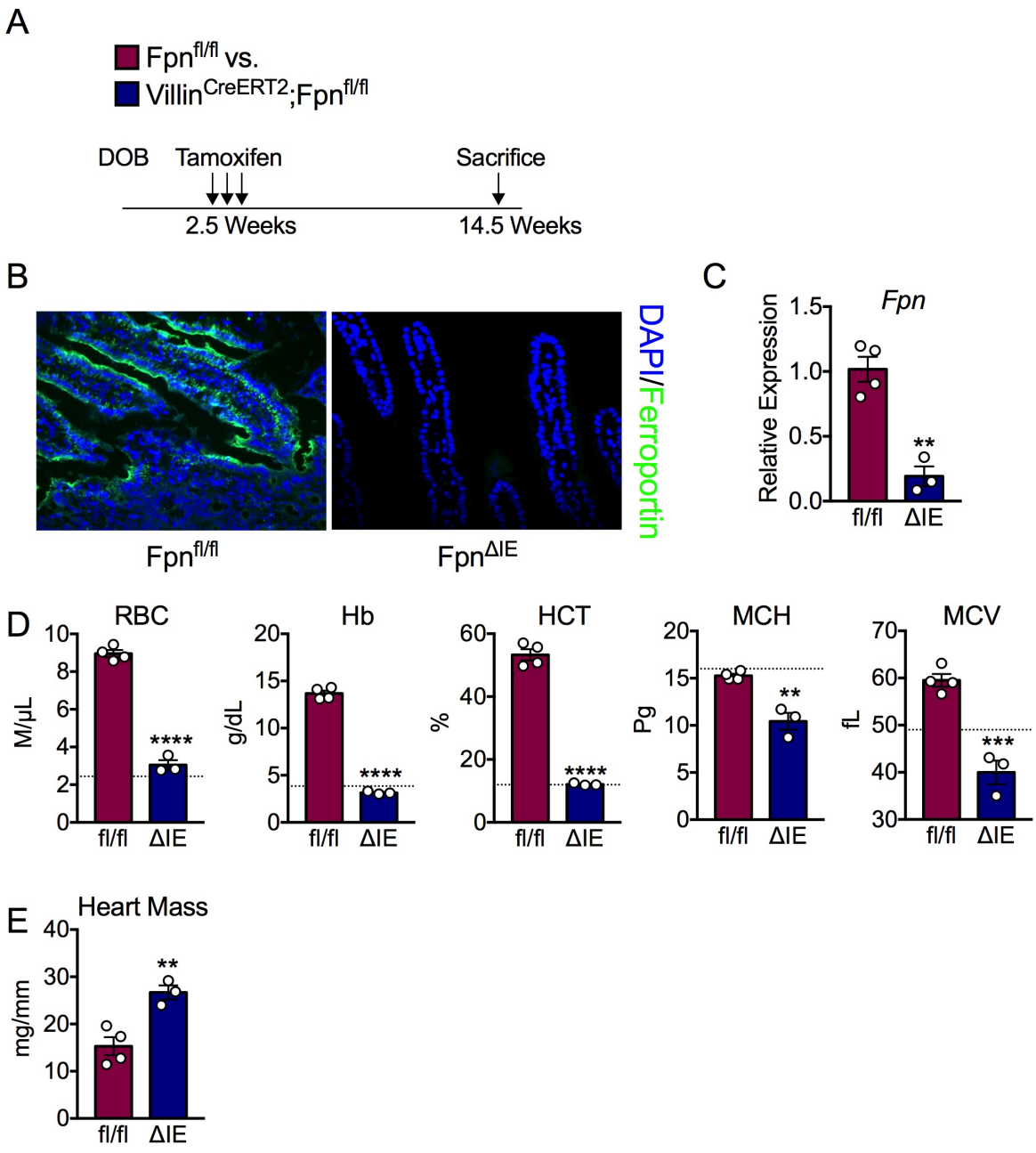

Figure 3.6. End-stage iron-deficiency anemia develops more rapidly when induced in young mice. (A) Schematic of experimental design, (B) Representative ferroportin staining in duodenal sections of *Fpn*$^{fl/fl}$ and *Fpn*$^{\Delta IE}$ mice, images at 40x, (C) qPCR analysis of the duodenal ferroportin (*Fpn*) transcript in *Fpn*$^{fl/fl}$ and *Fpn*$^{\Delta IE}$ mice, (D) Analysis of red blood cells (RBC), hemoglobin (HB), hematocrit (HCT), mean corpuscular hemoglobin (MCH), and mean corpuscular volume (MCV), dashed line indicate six month values observed in experiment in *Fpn*$^{\Delta IE}$ adult mice reported in Figure 1, (E) heart mass normalized to tibia length. All data here is from mice 3 months post-tamoxifen treatment. Mean ± SEM are plotted. Significance determined using 2-tailed unpaired t test. **p < 0.01; ***p < 0.001; ****p < 0.0001 compared between *Fpn*$^{fl/fl}$ and *Fpn*$^{\Delta IE}$ cohorts.

Chapter 4

The Colon Tumor Epithelium Produces an Ectopic Source of Hepcidin that Controls Iron-Dependent Cancer Cell Metabolism and Tumorigenesis

Abstract

Human epidemiological studies have shown a correlation between dietary iron intake and/or systemic iron levels and colorectal cancer (CRC) risk. Iron is sequestered in colorectal tumor tissue, leading to massive intratumoral iron stores that are essential for growth and survival. However, the complete molecular mechanisms of local iron handling in CRC remain largely unknown. At the systemic level, iron homeostasis is maintained by the liver-derived, endocrine hormone, hepcidin. Hepcidin binds to the only known mammalian iron exporter, ferroportin, resulting in internalization and degradation of ferroportin. The present work revealed that the ferroportin protein is expressed in adjacent normal colon tissue but is absent in colon tumor tissue. A cellular enrichment strategy demonstrated that tumor epithelial cells produce a major source of ectopic, intratumoral hepcidin in CRC that portends poor patient survival. Mice deficient for the hepcidin gene specifically in colon tumor epithelium exhibited significant decreases in tumor number, burden, and size compared to wild-type littermates in a sporadic model of CRC, whereas hepcidin overexpression increased tumor size in an orthotopic model. Hepcidin promoter analysis demonstrated that hypoxia and its

downstream transcription factor, hypoxia inducible (HIFs) factors-2α, are sufficient to activate the hepcidin promoter in CRC-derived cell lines. Furthermore, intratumoral hepcidin was necessary for iron-dependent activation of the STAT3 pathway. These data suggest that the HIF-2α induction of hepcidin in the tumor epithelium establishes an axis to degrade ferroportin and sequester iron in colorectal tumors in order to maintain iron-dependent cancer cell metabolism and drive tumorigenesis.

Introduction

Colorectal cancer (CRC) is the third most common type of cancer and it is the third leading cause of cancer-related death in the United States (1). A hallmark of CRC is the process by which these tumors deregulate cellular energetics in ways that afford a growth and survival advantage (2). Tremendous attention has been given to understanding how macromolecules, such as glucose, lipids, proteins, and nucleic acids, are used differently by CRC cells than adjacent normal cells (3-5). However, the production of macromolecules is achieved via redundant systems that offer tumors a multitude ways to evolve resistance to therapeutics that target these pathways. Micronutrients are exogenously derived, essential elements that are required by organisms in small quantities for ubiquitous cellular processes (6). Despite the fact that micronutrients are central to cellular metabolism and growth promoting pathways, very little is known about the direct molecular role of micronutrients in cancer cell metabolism.

Iron is a metal micronutrient that is required by all living organisms, from single cell bacteria to complex, multicellular organisms that include humans (7). On the cellular level, iron orchestrates basic energy metabolism, mitochondrial function, and DNA synthesis, among other functions (8, 9). Interestingly, epidemiological data has correlated iron levels with CRC risk. Individuals with high red meat intake, which contains large quantities of heme iron, and patients with disease of iron overload are at an increased risk of developing CRC (10-12). Moreover, CRC cells sequester massive iron stores relative to adjacent normal cells (13). CRC is the only malignancy that maintains access to two sources of iron acquisition: i) systemic uptake from iron in

circulation, and ii) intestinal lumen iron uptake. Accordingly, human colon tumors capitalize on this unique environment by upregulating iron import from the intestinal lumen via overexpression of the apical iron transporter, divalent metal transporter-1 (DMT1) (13, 14). In addition to hyper-activating the many physiological metabolic pathways that require iron, cancers can also use iron in unique ways to directly activate oncogenic STAT3 pathways, WNT signaling, DNA-synthesis, reactive oxygen species, and modulate P53 (13, 15-18). Intratumoral iron stores and iron-dependent oncogenic signaling pathways are essential to CRC growth and survival, as genetic disruption to CRC iron uptake decreases tumor number, burden, and size (13, 14).

Despite these data, an important, unaddressed paradox is the molecular mechanism by which CRC sequesters massive iron stores. On the systemic level, iron handling is regulated by a liver-derived, endocrine hormone, hepcidin (19). The molecular function of hepcidin is to bind to the only mammalian iron exporter, ferroportin, resulting in ferroportin internalization from the membrane, intracellular degradation, and an increase in intracellular iron concentrations (20). Ferroportin is predominately expressed on cells that regulate systemic iron handling, namely hepatocytes, intestinal enterocytes, and macrophages of the reticuloendothelial system (8). Therefore, in the presence of hepcidin, ferroportin is continually internalized from the membrane and iron mobilization into circulation is limited; in the absence of hepcidin, ferroportin is rapidly stabilized and iron is exported into plasma.

Interestingly, in addition to these canonical sources of hepcidin and ferroportin, recent reports have shown that these proteins can be produced at lower levels in peripheral tissues that are not involved in systemic iron metabolism (8). Moreover, a

recent investigation unveiled that hepcidin can be produced locally by cardiomyocytes to establish a cell-autonomous axis that regulates cardiac ferroportin and maintains cardiomyocyte iron levels for cardiac function (21). In the context of cancer, reports have also begun to speculate whether hepcidin and/or ferroportin are utilized to modulate local iron handling inside of tumors (22-25). In this report, I demonstrate that colon tumors produce a local source of extra-hepatic hepcidin that controls iron-dependent tumorigenesis and cancer cell metabolism. High levels of intratumoral hepcidin expression portend a significant decrease in overall patient survival and correlate with a decrease in ferroportin protein abundance. Using a cellular enrichment strategy in combination with genetic mouse models, I confirm that the majority of local, intratumoral hepcidin in CRC is produced by epithelial cells. Unlike hepatocytes, intratumoral hepcidin in CRC is not regulated by iron, but is a direct target of hypoxia inducible factor-2α. Lastly, hepcidin is necessary and sufficient to drive tumorigenesis and activation of iron-dependent STAT3 signaling in CRC. Collectively, these findings unveil basic mechanisms by which local iron handling is modulating in CRC and unveil potential avenues for adjuvant therapeutics in cancer treatment.

Methods

Animals

For embryonic, colon epithelial-specific disruption of hepcidin, mice floxed for *Hamp1* (*Hamp*$^{fl/fl}$) were crossed to mice harboring Cre recombinase under the control of the CDX2 promoter (*CDX2*^{Cre}) to generate *CDX2*^{Cre};*Hamp*$^{fl/fl}$ mice. This line was then crossed to APC$^{fl/+}$ mice to generate a sporadic model of CRC with concomitant hepcidin deletion (i.e. *CDX2*^{Cre};*APC*$^{fl/+}$;*Hamp*$^{fl/fl}$ mice). All other mouse models (i.e. CDX2^{CreER};APC$^{fl/fl}$;KRAS^{G12DLSL};p53$^{fl/fl}$, CDX2^{ER}; HIF-2α^{OE}, CDX2^{ER};APC$^{fl/fl}$;HIF-2α^{OE}, CDX2^{ER};APC$^{fl/+}$;HIF-2$\alpha^{fl/fl}$) have been previously used (13, 26, 27). Littermates wild-type for the gene of interest were used as controls for all animal studies and analysis began on mice that were between 2 and 2.5 months of age for each of the respective experiments. Mice were injected i.p. with tamoxifen (Sigma-Aldrich) at a dose of 100 mg/kg BW for 3 consecutive days to ensure Cre-mediated recombination. For the inflammation-associated model of colorectal cancer, animals were injected intraperitoneally with 10 mg/ kg azoxythmethane, then cycled on and off 2% (weight/volume) dextran sulfate sodium in their drinking water for 100 days, as previously described (28). For the orthotopic tumor model, colon cancer CT26 cells were injected subcutaneously at 6 × 106 cells in BABL/C mice and animals were euthanized 14 days after implantation. All mice were fed ad libitum and maintained under a 12-hour light/12-hour dark cycle. All mice were fed either a standard chow diet (Research Diets) or a purified AIN-93G iron-replete (350 ppm) or low- iron (<5 ppm) diet (Dyets). All mice were housed in the Unit for Laboratory Animal Management (ULAM) at the University of Michigan.

Cell culture

Doxycycline-inducible FPNGFP HEK293 and IEC6 cells were generated previously (19). To generate stable doxycycline- inducible human FPNGFP colon cancer-derived cell lines, pLenti rtTA3 (Addgene) and pLVX-Tight-Puro hFpnGFP plasmids were prepared into lentivirus by the University of Michigan Vector Core, coinfected into cells, and selected with 10 μg/ml blasticidin and 1 μg/ml puromycin. Stable, hepcidin overexpressing cell lines were generated by transfecting a mouse hepcidin pLentiLoxIres construct into CT26 cells and selection with 1 μg/ml puromycin. Cell growth analysis was performed using live cell imaging (BioSpa, BioTek, Winooksi, VT). The truncated human hepcidin luciferase promoter construct disrupted for hypoxia response elements was generated using primers listed in Supplemental Table 4.1. The following concentrations were used for cell treatments: 250 ng/ml doxycycline, 100 μM FG4592 (Selleckchem), 1 mg/ml human recombinant hepcidin (Bachem), 200 μM DFO (Sigma-Aldrich), 10 μM 5AZA (Cayman, Ann Arbor, MI), 10 ng/mL LPS (Sigma-Aldrich). Cells were maintained at 37°C in 5% CO2 and 21% O2. Cells were cultured in DMEM supplemented with 10% FBS and 1% antibiotic/antimycotic.

Luciferase assay

Cells were lysed in reporter lysis buffer (Promega) and firefly luciferase activity was measured as described previously (19).

Quantitative reverse transcription PCR

mRNA was measured by quantitative reverse transcription PCR (qPCR) (Life

Technologies, Thermo Fisher Scientific). The primers used are listed in Table 4.1. Quantification cycle (Cq) values were normalized to β-actin and expressed as the fold change.

Western blot analysis

Lysates were generated as previously described (19). In brief, lysates were separated by SDS-PAGE, transferred onto nitrocellulose membranes, and probed overnight at 4°C with antibodies against GFP (66002-1-Ig, Proteintech, Rosemont, IL), phospho-STAT3 (9145 Cell Signaling, Danvers, MA) or Actin (66009-1-Ig, Proteintech, Rosemont, IL).

Epithelial enrichment

The mice were sacrificed and the tumors were pooled from each respective mouse. All plasticware was precoated with 0.1% bovine serum albumin (BSA) and all steps were carried out on ice unless otherwise specified. The tissue was homogenized with a scalpel and then was incubated in 10 mM DTT for 15 min at room temperature, changing to fresh DTT every 5 min. The tissue was rinsed in DPBS, rinsed once with 8 mM EDTA, and then incubated/rotated in 8 mM EDTA at 4°C for 75 min. The EDTA was removed and the tissue was washed three times with DPBS. The tissue was then “snap-shaken” 10 times to manually separate the colon tumor epithelium. The epithelium-containing supernatant was immediately added to 1.5 ml of cold FBS in a BSA-coated 50-ml tube, and the shaking step was repeated twice more. The epithelium was spun at 40 × *g* for 2 min at 4°C. The tissue that was not broken free into the supernatant was considered the stromal fraction. The epithelial pellet was washed in

DPBS and spun again at 40 × *g* for 2 min at 4°C. Both cell pellets were then directly resuspended in Trizol for RNA analysis.

Mouse- and patient-derived enteroids

Mouse- and patient-derived colorectal tumor enteroids were generated as previously described (29).

Meta-analysis of CRC samples

CRC gene expression data sets along with the patient survival were identified in GEO using the search keywords “colon,” “cancer,” and “microarray” (**www.ncbi.nlm.nih.gov/geo/**). Only publications providing raw data and clinical survival information and containing at least 30 patients were included. The gene chips were MAS 5.0–normalized in the R statistical environment (**www.R-project.org**) using the Bioconductor package affy (**www.bioconductor.org**). Survival analysis using Cox proportional hazards regression was performed as previously described (30). The most reliable probe sets for each gene were selected using Jetset. Kaplan-Meier survival plots were generated using WinSTAT for Excel (Robert K. Fitch Software). Methylation data was generated from the online UALCAN resource (**www.ualcan.path.uab.edu/analysis**).

Histology, tissue iron staining, and immunohistochemistry

Tissue iron detection was performed in formalin-fixed, paraffin-embedded sections stained with Prussian blue and signal was enhanced with 3,3′-

Diaminobenzidine tetrahydrochloride (DAB). For immunohistochemical analysis, frozen sections were probed with polyclonal rabbit anti–ferroportin antibody (21502, Novus).

Metabolite extraction and bacteria treatment

Metabolites from mouse feces were extracted by 80% methanol [methanol:water (80:20; v/v)] extraction as described previously (31). For treatment with live and heat-killed bacteria, one mouse fecal pellet was suspended in 1 mL of PBS. For heat-killed, this homogenate was boiled for 5 minutes. Either live or heat-killed bacteria were then added to cell culture media at 20 µL/mL.

Statistics

Results are expressed as the mean ± SEM. Significance between 2 groups was tested using a 2-tailed, unpaired or paired *t* test, as indicated. Significance among multiple groups was tested using a 1-way ANOVA followed by Tukey's post hoc test for multiple comparisons. A *P* value of less than 0.05 was considered statistically significant. GraphPad Prism 7.0 was used to conduct the statistical analyses.

Study approval

All animal procedures were approved by the IACUC of the University of Michigan.

Results

Local hepcidin expression is increased in many cancers, including colorectal cancer

We sought to investigate which cancer types express an ectopic, local source of hepcidin using human microarray data made available through The Cancer Genome Atlas. Comparing hepcidin mRNA abundance (encoded by *HAMP*) between normal and tumor tissue, I found that hepcidin was significantly upregulated in colorectal cancer, as well as brain, breast, kidney, lung, ovarian, and prostate cancer (Figure 4.1). No change was observed in bladder, cervical, head/neck, leukemia, liver, lymphoma, and pancreas cancer (Figure 4.1). These data indicate that human colorectal tumors, among several other cancer types, upregulate local *HAMP* expression relative to adjacent normal tissue. Collectively, these data suggest that specific cancers might rely on a local source of hepcidin to modulate intratumoral iron handling.

The colon tumor epithelium produces a local source of hepcidin that associates with decreased patient survival

To assess the role of iron in CRC, primary human CRC biopsies were stained for iron. CRC tumor tissue exhibited a significant increase in iron content when compared to adjacent normal tissue (Figure 4.2A and B). To address the mechanism by which iron sequestration occurs in CRC, I found that the iron exporter, ferroportin, was completely absent from tumor tissue, but highly present in adjacent normal tissue using samples from a sporadic mouse model of CRC (Figures 4.2C). Tumor-specific ferroportin protein depletion suggested that this was due to local, intratumoral mechanisms and not

endocrine action by the circulating, liver-derived ferroportin ligand, hepcidin. Kaplan-Meier survival analysis generated from 530 human CRC biopsies showed that high levels of intratumoral hepcidin expression portend a significant decrease in overall patient survival (Figure 4.2D). This increase in local, extra-hepatic hepcidin mRNA was phenocopied in mouse models of both sporadic and inflammation-associated CRC (Figures 4.2E and F). To determine which cell type is responsible for driving intratumoral hepcidin expression in CRC, I first utilized immunohistochemistry approaches using hepcidin antibodies. However, these antibodies could never be validated using primary hepatocytes from *Hamp*$^{fl/fl}$ mice treated with a Cre-expressing adenovirus in vitro, despite a significant decrease in *Hamp* transcript abundance (Figure S4.1A and B). This non-specific signaling was also seen in liver samples from mice treated with a low-iron diet (< 5 PPM) for 7 days, which is known to potently decrease liver *Hamp* transcription (Figure S4.1C). To circumvent antibody-based approaches, I utilized an epithelial enrichment strategy (Figure 4.2G). In three separate experiments, the *Hamp* transcript was highest in the tumor epithelium fraction (Figure 4.2H). *Epcam* mRNA, a marker of epithelial cells, was higher in our epithelial fraction, which confirmed the efficiency of this strategy (Figure 4.2H). These data collectively demonstrate that the colon tumor epithelium produces a local, extra-hepatic source of hepcidin that correlates with decreased ferroportin protein abundance and portends poor patient survival.

Hypoxia signaling via HIF-2α drives hepcidin expression in CRC

We next sought to address the molecular mechanism by which extra-hepatic hepcidin is activated in CRC. Hepatic hepcidin is canonically regulated via iron sensing

machinery. To address whether colon hepcidin is regulated by iron levels, mice were placed a low-iron diet (< 5 PPM) for three months and compared to an iron-replete diet (350 PPM). Interestingly, there was no change in *Hamp* expression (Figure 4.3A). The most common genetic mutations that are selected for in human CRC are loss of function for APC and p53 and gain of function to KRAS. Mice harboring a tamoxifen-inducible Cre recombinase under the control of a colon-specific promoter ($CDX2^{CreER}$) were bred to mice floxed for APC and p53 and knocked-in for a constitutively active $KRAS^{G12D}$ construct in the *ROSA26* locus, preceded by a loxP-STOP-loxP cassette (i.e. $CDX2^{CreER}$;$APC^{fl/fl}$;$KRAS^{G12DLSL}$;$p53^{fl/fl}$), referred to as $CDX2^{TripleMutant}$. To determine if dysplasia and/or mutation to canonical oncogenic pathways in CRC are sufficient to activate colonic hepcidin, $CDX2^{TripleMutant}$ mice were treated with tamoxifen and sacrificed 10 days later. Massive colonic dysplasia was observed when pathways were acutely altered in the colon epithelium of mice, by as quickly as 10 days. However, no change in *Hamp* mRNA was observed (Figure 4.3B). Therefore, I deduced that some element of the bona fide tumor microenvironment must be responsible for activating hepcidin, as dysplasia alone was not sufficient. A hallmark of the tumor microenvironment is hypoxia. Hypoxia promotes the activation of hypoxia-inducible transcription factors (HIF)s. HIFs are transcription factors that consist of a heterodimer of an oxygen-sensitive α subunit (HIF-1α, HIF-2α, and HIF-3α) and a constitutively expressed β subunit (ARNT). Previous studies have shown that exclusively HIF-2α, but not other HIFs, plays an important role in CRC tumorigenesis and progression. Interestingly, using a sporadic model of CRC, mice deficient for HIF-2α in the colon epithelium exhibited significantly lower intratumoral *Hamp* mRNA as compared to wild-

type littermates (Figure 4.3C). To address whether this was a direct effect by HIF-2α, I generated a luciferase reporter construct consisting of 1.7 kb of the human hepcidin promoter fused to a luciferase construct. Of note, there are three canonical hypoxia response elements (HREs) within this region of the human hepcidin promoter (Figure 4.3D). Exposure of CRC-derived cell lines to hypoxia (1% oxygen) for 16 hours significantly activated the *HAMP* promoter, as compared normoxic cells (21% oxygen) (Figure 4.3E). Transfection of an oxygen stable HIF-2α construct also significantly activated the human hepcidin promoter in two CRC-derived cell lines (Figure 4.3F). Furthermore, this effect appeared to be a direct response, as truncation of the luciferase reporter construct to remove canonical HREs prevented activation by HIF-2α (Figure 4.3G). However, treatment of CRC-derived cells with FG4592 for 16 hours, which is a chemical activator of HIF, did not induce endogenous *HAMP* transcription (Figure S4.2A). Enteroids are three-dimensional intestinal models derived from the intestinal epithelium that recapitulate the in vivo intestinal microenvironment better than traditional two-dimensional cell culture techniques. I therefore generated colon enteroids from $CDX2^{TripleMutant}$ mice and treated these cultures with FG4592 for 16 hours, but failed to induce endogenous *Hamp* transcription when compared to vehicle treatment (Figure S4.2B).

To determine if there is some element of the in vivo colon that is lost using these in vitro systems, I bred mice in which Cre recombinase is expressed under the control of an intestinal epithelial-specific promoter ($Villin^{Cre}$) to mice knocked-in for an oxygen stable HIF-2α construct in the *ROSA26* locus, preceded by a loxP-STOP-loxP cassette ($HIF\text{-}2\alpha^{LSL}$), giving rise to intestinal epithelial HIF-2α overexpressing mice (referred to

as HIF-2α^{OE} following tamoxifen induction). However, there was no change in the *Hamp* transcript in HIF-2α^{OE} mice as compared to wild-type, littermate controls (Figure S4.2C). I next considered that some additional element of the CRC environment must be necessary for HIF-2α to activate endogenous hepcidin transcription. About 80-90% of CRC patients present with mutation to APC (32). I therefore overexpressed HIF-2α in the colon epithelium in combination with loss of APC (i.e. CDX2^{ER};APC$^{fl/fl}$;HIF-2α^{OE}), however, there was no change in hepcidin expression (Figure S4.2D). Hepatic hepcidin is increased by a range of inflammatory stimuli that includes IL6, IL1β, among others (7). To determine in an unbiased fashion if canonical inflammatory molecules are sufficient to activate hepcidin in CRC-derived cells, I generated conditioned media (CM) from RAW macrophages stimulated with LPS for 16 hours and then treated CRC cells with this CM for 24 hours. However, there was no change in *Hamp* mRNA abundance, as compared to control RPMI media (Figure S4.2E). Hepcidin was originally discovered because of its cystine-rich structure, which is a hallmark of the defensin and protegrin antimicrobial peptide families. To determine if hepcidin is regulated by bacteria in CRC, I treated CRC-derived cells with live bacteria and heat-killed bacteria, but failed to observed any induction of the human hepcidin luciferase promoter construct (Figure S4.2F). In vivo, bacteria of the intestinal microbiome secrete an array of metabolites that affect host metabolism and cellular function. Treatment of CRC-derived cells with bacterial-derived metabolites did not activate the human hepcidin luciferase promoter construct (Figure S4.2G). DNA methylation is a canonical mechanism by which promoters are regulated and plasmids such as the luciferase reporter used in these studies are typically hypomethylated relative to endogenous DNA. Interestingly, the

human hepcidin promoter is significantly hypomethylated in CRC (Figure S4.2H). To determine if DNA methylation status could explain activation of the endogenous hepcidin promoter by hypoxia signaling, I treated CRC-derived cells with 5AZA, which inhibits DNA methyltransferase and results in significant reduction of DNMT1 protein abundance over a 72 hour treatment (Figure S4.2I). However, co-treatment of CRC-derived cells with 5AZA and FG4592 still did not induce transcription of *HAMP* (Figure S4.2J). Lastly, I sought to investigate *HAMP* regulation in human-derived CRC enteroids. I collected human CRC normal adjacent and tumor tissue (Figure 4.3H). As I observed in the TCGA, *HAMP* expression was elevated in paired normal adjacent and tumor samples (Figure 4.3I). However, when comparing matched in vivo tumor tissue with tumor enteroids generated from the same patient, I observed a significant reduction in *HAMP* mRNA abundance (Figure 4.3I). Furthermore, there was no change in *HAMP* expression when comparing unpaired enteroids generated from normal adjacent and tumor tissue (Figure 4.3I). These data indicate that *HAMP* expression is lost when the tumor epithelium is isolated alone and place in culture, suggesting that there is a non-epithelial element of the tumor microenvironment that acts in a cell non-autonomous fashion to drive epithelial *HAMP* expression. Collectively, all of these data demonstrate that HIF-2α is necessary but not sufficient to drive the endogenous intratumoral hepcidin response and that there is likely a non-epithelial paracrine factor that is required by HIF-2α to drive *HAMP* transcription.

Inducible ferroportin-mediated iron efflux decreases cell growth and blunts STAT3 signaling

High levels of intratumoral hepcidin serve to downregulate the hepcidin-target, ferroportin. I therefore sought to inducibly overexpress ferroportin in CRC-derived cells to mimic an environment of low hepcidin and to determine the functional effect of iron efflux on CRC cell growth. I attempted to generate doxycycline inducible, ferroportin^{GFP} overexpressing cells (i.e. FPN^{GFP}) in various human and mouse CRC-derived cell lines, as described previously (19). Interestingly and consistently, I observed doxycycline induction of FPN^{GFP} in early passages in these cells, which was completely lost in subsequent “late” passages (Figure 4.4A). This effect was not observed in two normal, non-CRC cell lines, which continued to overexpress the FPN^{GFP} construct following doxycycline treatment in late passages (Figure 4.4B). Analysis for ferroportin expression in these cell lines revealed that all CRC-derived cell lines expressed markedly lower ferroportin mRNA following doxycycline treatment as compared to the two normal, non-CRC cell lines (Figure 4.4C). Although induction of the FPN^{GFP} plasmid is doxycycline dependent, a lower, basal expression most likely occurs in the absence of doxycycline treatment, as these constructs tend to be somewhat leaky. Collectively, these observations suggest that CRC-derived cells are exquisitely more sensitive to iron loss via FPN^{GFP} than normal cells. Generation of CRC-derived stable cells was initially successful, but as these lines are passaged cells with a lower copy number of FPN^{GFP} integration likely outcompeted those with high copy number because they retained intracellular iron more efficiently. Therefore, the FPN^{GFP} protein and mRNA response was lost over time, per our observation. To assess the overall effect of ferroportin-mediated iron efflux on general cell growth, I utilized stable, doxycycline inducible IEC6 FPN^{GFP} cells, which is a normal intestinal epithelial cell line. Doxycycline treatment

decreased cell growth by as quickly as 36 hours following treatment, a response that was completely rescued by co-treatment with recombinant hepcidin (Figure 4.4D). I also treated these cells with the iron chelator, deferoxamine (DFO), which decreased cell growth more quickly and efficiently than FPN^{GFP} overexpression (Figure 4.4D). Previous research has shown that intratumoral iron in CRC activates the phosphorylation of STAT3, a known oncogenic factor in CRC (13). Overexpression of FPN^{GFP} decreased phospho-STAT3 levels by as quickly as 16 hours in IEC6 FPN^{GFP} cells. In total, these data demonstrate that CRC-derived cell lines are more sensitive to iron loss than normal cells and that hepcidin/ferroportin signaling is essential to maintain overall proliferation and STAT3 activation.

Colon epithelial hepcidin is necessary and sufficient for CRC tumorigenesis and is required for STAT3 target gene activation

To determine the functional role of hepcidin in CRC formation and progression in vivo, mice harboring Cre recombinase under the control of a colon-specific promoter ($CDX2^{Cre}$) were bred to mice floxed for both *Hamp1* ($Hamp^{fl/fl}$) and for one allele of APC ($APC^{fl/+}$), giving rise to $CDX2^{Cre}$; $APC^{fl/+}$;$Hamp^{fl/fl}$ mice (Figure 4.5A). This is a sporadic model of CRC, whereby mice spontaneously develop colon tumors by four months of age. Mice deficient for colon epithelial hepcidin exhibited decreased tumor number, burden, and size, as compared to wild-type litter mates (Figure 4.5B). Importantly, the *Hamp* transcript was significantly elevated in wild-type tumors, a response that was abrogated in the hepcidin-deficient mice, confirming that the majority of intratumoral *Hamp* is produced by the colon tumor epithelium (Figure 4.5C). There was no observed

change in the *Ferroportin* transcript, suggesting that ferroportin is regulated at the protein level by hepcidin (Figure 4.5C). Previous work has shown that intratumoral iron in CRC affects the local immune response (13). I observed a decrease in expression of the macrophage marker, *F480*, in hepcidin-deficient tumors while no other immune marker was different between these groups (Figure 4.5D). However, I did observe blunted activation of the STAT3 target genes, *CyclinD1* and *Bcl2*, in hepcidin-deficient tumors, which are iron-dependent in CRC (Figure 4.5E). To investigate whether increased hepcidin expression is sufficient to increase tumorigenesis in CRC, I generated stable CT26 hepcidin overexpressing cells (Figure 4.5F). Subcutaneous implantation of these cells in vivo in BALB/C mice led to an increased tumor weight by as quickly as 14 days (Figure 4.5G). Collectively, these data demonstrate that epithelial hepcidin is necessary and sufficient to drive tumorigenesis in CRC and activates iron-dependent STAT3 signaling.

Discussion

Cancers such as CRC evolve an array of mechanisms to enable efficient growth and survival in the nutrient scarce tumor microenvironment. Research efforts have largely focused on understanding how macronutrients, such as glucose, lipids, proteins, and nucleic acids, are metabolized differently in CRC to rewire intracellular energetics (32-34). However, very little is known about micronutrients, which are exogenously derived elements that are essential in a multitude of metabolic pathways. Iron is a metal micronutrient that is required for energy metabolism, mitochondrial function, and DNA synthesis, among other functions (35). Epidemiological data has correlated systemic iron levels with CRC risk, namely red meat intake and in patients that have iron overload (10-12). Colon tumor tissue also sequesters massive intracellular iron stores that are required for cancer cell growth (13, 14). The present work demonstrates that CRC modulates local, oncogenic iron handling by ectopically expressing the liver-derived, iron-regulatory hormone, hepcidin, in order to downregulate ferroportin. High levels of intratumoral hepcidin expression portend a significant decrease in overall patient survival. Using a cellular enrichment strategy, the majority of local, intratumoral hepcidin in CRC is produced by epithelial cells. Using a genetic mouse model of sporadic CRC, and an orthoptic model of CRC, I show that CRC-derived hepcidin is necessary and sufficient to drive tumor number, size, and burden. Unlike hepatocytes, intratumoral hepcidin in CRC is not regulated by iron, but is a direct target of the hypoxia sensitive HIF-2α transcription factor. Hepcidin/ferroportin signaling is also necessary and sufficient to drive tumorigenesis and activation of iron-dependent STAT3 signaling in CRC. In combination with previous work, this current model reveals that

HIF-2α is utilized by CRC cells to simultaneously increase intestinal lumen iron uptake via DMT1 overexpression and to decrease iron export by activating autocrine/paracrine hepcidin-mediated ferroportin degradation. Collectively, this work unveils the pathways of local iron handling in CRC, provides insight into mechanisms of ectopic hepcidin transcriptional activation, and reveals nutrient vulnerabilities in CRC that can be targeted therapeutically.

Since the discovery of hepcidin/ferroportin signaling, this interaction has primarily been thought of as a liver-derived, endocrine system that acts on major ferroportin expressing cells to control systemic iron mobilization (i.e. hepatocytes, intestinal enterocytes, and splenic macrophages) (8). However, recent reports have started to reveal extra-hepatic, functional sources of hepcidin that act in paracrine and/or autocrine fashions on local ferroportin. This new paradigm was catalyzed by reports showing that ferroportin is expressed on cardiomyocytes and it is primarily regulated by a local, cell-autonomous source of hepcidin (21). Embryonic deletion of cardiomyocyte hepcidin in mice leads to intracellular iron depletion, contractile defects, and metabolic alterations that decrease mitochondrial activity, all of which results in massively decrease survival (21). A similar model has been proposed in cancer, as ferroportin protein abundance is reduced in breast cancer cells compared to nonmalignant breast epithelial cells (23). Several additional reports have shown that both breast and prostate cancers can activate their own source of local hepcidin, while investigators have observed increases in hepcidin mRNA and protein in human CRC (24, 36, 37). These investigations of cancer hepcidin/ferroportin kinetics are mostly correlative and have been limited by a lack of genetic and functional data. I definitively

show that ectopic hepcidin exerts a functional role in CRC tumorigenesis, growth, and survival by regulating intratumoral iron handling. I also demonstrate that cell proliferation is markedly decreased following ferroportin-mediated iron efflux by as quickly as 36 hours. While I observe dampening of known iron-dependent oncogenic signaling pathways in this model (i.e. STAT3), future work will need to carefully understand the mechanisms by which iron metabolism integrates with general cancer cell metabolism. Moreover, it will be important to understand whether iron is a necessary cofactor for enzymes involved in cell division, or whether there is a central iron sensor in cells that halts proliferation when intracellular iron stores are limited.

Another key question in the field of extra-hepatic hepcidin/ferroportin signaling is understanding the transcriptional regulation of hepcidin in non-hepatocytes. Reports have implicated a range of intratumoral molecules, including BMP4/7, IL6, Wnt, and GDF15, however, none of these findings have been functionally verified in vivo (22, 24, 36). A hallmark of the tumor microenvironment is hypoxia, as tumors outgrow their blood supply and are challenged by increased metabolic demand and inflammation (38). Interestingly, reports have shown that hypoxia can activate cardiac hepcidin mRNA in rats following 24 hour exposure to 6% oxygen (39). Furthermore, although systemic hypoxia inhibits hepatocyte hepcidin, reports have shown that this mechanism is indirect via erythropoietin action on hepatocytes and that hypoxia signaling actually activates hepcidin in erythropoietin-deficient mice (40). The hypoxia-inducible factor, HIF-2α, maintains essential roles in both iron metabolism and CRC progression (13). Using a luciferase reporter construct, I show in this present work that HIF-2α is necessary to activate the human hepcidin promoter in vitro and in vivo. However, HIF-

2α is not sufficient to drive transcription of the endogenous hepcidin gene in CRC-derived cell lines, three-dimensional intestinal mini gut enteroid models, or in mice that overexpress colon epithelial HIF-2α. These findings suggest that there is a cell non-autonomous molecule that is necessary for HIF-2α-mediated activation of hepcidin in CRC. Future work will need to explore the mechanism by which hypoxia activates local hepcidin/ferroportin signaling in CRC and to determine if there are similar mechanisms that take place in physiological cell-autonomous hepcidin regulation, namely in the heart.

Previous work has established that HIF-2α, but not other HIFs, is necessary and sufficient to drive CRC tumorigenesis (26, 41). HIF-2α exerts both iron-independent and –dependent mechanisms in CRC. HIF-2α transcriptionally upregulates the chemokine CXCL1 to promote the influx of pro-tumorigenic, intratumoral neutrophils in CRC (26). HIF-2α has also been shown to potentiate oncogenic yes-associated protein 1 (YAP1) activity and drive oncogenic cyclooxgenase-2 (COX2) expression in CRC (42, 43). In the context of iron metabolism, HIF-2α has been shown to drive tumor iron uptake via DMT1 hyper-transcription (13, 14). HIF-2α-dependent intratumoral iron stores are used to directly activate a CDK1/JAK1/STAT3 axis that is necessary for CRC growth (13). Iron has also been implicated in STAT3 signaling in glioblastoma (44). I show in this work that, in addition to DMT1, HIF-2α also drives the transcription of hepcidin in CRC to downregulate ferroportin and trap intratumoral iron stores. Moreover, HIF-2α actively increases iron uptake and decreases iron export in CRC to maintain intracellular iron concentrations that are necessary for STAT3 activation. Work has shown that there are nearly 200 uncharacterized iron-related HIF-2α-target genes in the intestine (45).

Therefore, future work must characterize the complete iron metabolic transcriptional program of HIF-2α in CRC.

In conclusion, this work shows that the colon tumor epithelium produces an ectopic, extra-hepatic source of local hepcidin that is necessary and sufficient for CRC growth. Intratumoral hypoxia via HIF-2α drives this source of hepcidin, which maintains intracellular iron levels and activates oncogenic STAT3 signaling. Finally, these data demonstrate the molecular mechanisms by which colon tumors modulate local iron handling and reveal vulnerabilities that can be targeted for therapeutic benefit in CRC.

References

1. Siegel R, Ma J, Zou Z, and Jemal A. Cancer statistics, 2014. *CA Cancer J Clin.* 2014;64(1):9-29.
2. Hanahan D, and Weinberg RA. Hallmarks of cancer: the next generation. *Cell.* 2011;144(5):646-74.
3. Kroemer G, and Pouyssegur J. Tumor cell metabolism: cancer's Achilles' heel. *Cancer Cell.* 2008;13(6):472-82.
4. Thomson TM, Balcells C, and Cascante M. Metabolic Plasticity and Epithelial-Mesenchymal Transition. *J Clin Med.* 2019;8(7).
5. Lee S, and Schmitt CA. The dynamic nature of senescence in cancer. *Nat Cell Biol.* 2019;21(1):94-101.
6. Xue X, and Shah YM. Intestinal iron homeostasis and colon tumorigenesis. *Nutrients.* 2013;5(7):2333-51.
7. Muckenthaler MU, Rivella S, Hentze MW, and Galy B. A Red Carpet for Iron Metabolism. *Cell.* 2017;168(3):344-61.
8. Drakesmith H, Nemeth E, and Ganz T. Ironing out Ferroportin. *Cell Metab.* 2015;22(5):777-87.
9. Coffey R, and Ganz T. Iron homeostasis: An anthropocentric perspective. *J Biol Chem.* 2017;292(31):12727-34.
10. Cross AJ, Ferrucci LM, Risch A, Graubard BI, Ward MH, Park Y, et al. A large prospective study of meat consumption and colorectal cancer risk: an investigation of potential mechanisms underlying this association. *Cancer Res.* 2010;70(6):2406-14.
11. Nelson RL. Iron and colorectal cancer risk: human studies. *Nutr Rev.* 2001;59(5):140-8.
12. Osborne NJ, Gurrin LC, Allen KJ, Constantine CC, Delatycki MB, McLaren CE, et al. HFE C282Y homozygotes are at increased risk of breast and colorectal cancer. *Hepatology.* 2010;51(4):1311-8.
13. Xue X, Ramakrishnan SK, Weisz K, Triner D, Xie L, Attili D, et al. Iron Uptake via DMT1 Integrates Cell Cycle with JAK-STAT3 Signaling to Promote Colorectal Tumorigenesis. *Cell Metab.* 2016;24(3):447-61.
14. Xue X, Taylor M, Anderson E, Hao C, Qu A, Greenson JK, et al. Hypoxia-inducible factor-2alpha activation promotes colorectal cancer progression by dysregulating iron homeostasis. *Cancer Res.* 2012;72(9):2285-93.
15. Brookes MJ, Boult J, Roberts K, Cooper BT, Hotchin NA, Matthews G, et al. A role for iron in Wnt signalling. *Oncogene.* 2008;27(7):966-75.
16. Dixon SJ, and Stockwell BR. The role of iron and reactive oxygen species in cell death. *Nat Chem Biol.* 2014;10(1):9-17.
17. Le NT, and Richardson DR. The role of iron in cell cycle progression and the proliferation of neoplastic cells. *Biochim Biophys Acta.* 2002;1603(1):31-46.
18. Shen J, Sheng X, Chang Z, Wu Q, Wang S, Xuan Z, et al. Iron metabolism regulates p53 signaling through direct heme-p53 interaction and modulation of p53 localization, stability, and function. *Cell Rep.* 2014;7(1):180-93.

19. Schwartz AJ, Das NK, Ramakrishnan SK, Jain C, Jurkovic MT, Wu J, et al. Hepatic hepcidin/intestinal HIF-2alpha axis maintains iron absorption during iron deficiency and overload. *J Clin Invest.* 2019;129(1):336-48.
20. Nemeth E, Tuttle MS, Powelson J, Vaughn MB, Donovan A, Ward DM, et al. Hepcidin regulates cellular iron efflux by binding to ferroportin and inducing its internalization. *Science.* 2004;306(5704):2090-3.
21. Lakhal-Littleton S, Wolna M, Chung YJ, Christian HC, Heather LC, Brescia M, et al. An essential cell-autonomous role for hepcidin in cardiac iron homeostasis. *Elife.* 2016;5.
22. Blanchette-Farra N, Kita D, Konstorum A, Tesfay L, Lemler D, Hegde P, et al. Contribution of three-dimensional architecture and tumor-associated fibroblasts to hepcidin regulation in breast cancer. *Oncogene.* 2018;37(29):4013-32.
23. Pinnix ZK, Miller LD, Wang W, D'Agostino R, Jr., Kute T, Willingham MC, et al. Ferroportin and iron regulation in breast cancer progression and prognosis. *Sci Transl Med.* 2010;2(43):43ra56.
24. Zhang S, Chen Y, Guo W, Yuan L, Zhang D, Xu Y, et al. Disordered hepcidin-ferroportin signaling promotes breast cancer growth. *Cell Signal.* 2014;26(11):2539-50.
25. Xue D, Zhou CX, Shi YB, Lu H, and He XZ. Decreased expression of ferroportin in prostate cancer. *Oncol Lett.* 2015;10(2):913-6.
26. Triner D, Xue X, Schwartz AJ, Jung I, Colacino JA, and Shah YM. Epithelial Hypoxia-Inducible Factor 2alpha Facilitates the Progression of Colon Tumors through Recruiting Neutrophils. *Mol Cell Biol.* 2017;37(5).
27. Solanki S, Devenport SN, Ramakrishnan SK, and Shah YM. Temporal induction of intestinal epithelial hypoxia-inducible factor-2alpha is sufficient to drive colitis. *Am J Physiol Gastrointest Liver Physiol.* 2019;317(2):G98-G107.
28. Triner D, Devenport SN, Ramakrishnan SK, Ma X, Frieler RA, Greenson JK, et al. Neutrophils Restrict Tumor-Associated Microbiota to Reduce Growth and Invasion of Colon Tumors in Mice. *Gastroenterology.* 2019;156(5):1467-82.
29. Dame MK, Jiang Y, Appelman HD, Copley KD, McClintock SD, Aslam MN, et al. Human colonic crypts in culture: segregation of immunochemical markers in normal versus adenoma-derived. *Lab Invest.* 2014;94(2):222-34.
30. Gyorffy B, Surowiak P, Budczies J, and Lanczky A. Online survival analysis software to assess the prognostic value of biomarkers using transcriptomic data in non-small-cell lung cancer. *PLoS One.* 2013;8(12):e82241.
31. Bennett BD, Yuan J, Kimball EH, and Rabinowitz JD. Absolute quantitation of intracellular metabolite concentrations by an isotope ratio-based approach. *Nat Protoc.* 2008;3(8):1299-311.
32. Fearon ER. Molecular genetics of colorectal cancer. *Annu Rev Pathol.* 2011;6:479-507.
33. O'Keefe SJ. Diet, microorganisms and their metabolites, and colon cancer. *Nat Rev Gastroenterol Hepatol.* 2016;13(12):691-706.
34. Terzic J, Grivennikov S, Karin E, and Karin M. Inflammation and colon cancer. *Gastroenterology.* 2010;138(6):2101-14 e5.
35. Shah YM, and Xie L. Hypoxia-inducible factors link iron homeostasis and erythropoiesis. *Gastroenterology.* 2014;146(3):630-42.

36. Tesfay L, Clausen KA, Kim JW, Hegde P, Wang X, Miller LD, et al. Hepcidin regulation in prostate and its disruption in prostate cancer. *Cancer Res.* 2015;75(11):2254-63.
37. Ward DG, Roberts K, Brookes MJ, Joy H, Martin A, Ismail T, et al. Increased hepcidin expression in colorectal carcinogenesis. *World J Gastroenterol.* 2008;14(9):1339-45.
38. Triner D, and Shah YM. Hypoxia-inducible factors: a central link between inflammation and cancer. *J Clin Invest.* 2016;126(10):3689-98.
39. Merle U, Fein E, Gehrke SG, Stremmel W, and Kulaksiz H. The iron regulatory peptide hepcidin is expressed in the heart and regulated by hypoxia and inflammation. *Endocrinology.* 2007;148(6):2663-8.
40. Liu Q, Davidoff O, Niss K, and Haase VH. Hypoxia-inducible factor regulates hepcidin via erythropoietin-induced erythropoiesis. *J Clin Invest.* 2012;122(12):4635-44.
41. Xue X, Ramakrishnan SK, and Shah YM. Activation of HIF-1alpha does not increase intestinal tumorigenesis. *Am J Physiol Gastrointest Liver Physiol.* 2014;307(2):G187-95.
42. Xue X, and Shah YM. Hypoxia-inducible factor-2alpha is essential in activating the COX2/mPGES-1/PGE2 signaling axis in colon cancer. *Carcinogenesis.* 2013;34(1):163-9.
43. Ma X, Zhang H, Xue X, and Shah YM. Hypoxia-inducible factor 2alpha (HIF-2alpha) promotes colon cancer growth by potentiating Yes-associated protein 1 (YAP1) activity. *J Biol Chem.* 2017;292(41):17046-56.
44. Schonberg DL, Miller TE, Wu Q, Flavahan WA, Das NK, Hale JS, et al. Preferential Iron Trafficking Characterizes Glioblastoma Stem-like Cells. *Cancer Cell.* 2015;28(4):441-55.
45. Taylor M, Qu A, Anderson ER, Matsubara T, Martin A, Gonzalez FJ, et al. Hypoxia-inducible factor-2alpha mediates the adaptive increase of intestinal ferroportin during iron deficiency in mice. *Gastroenterology.* 2011;140(7):2044-55.

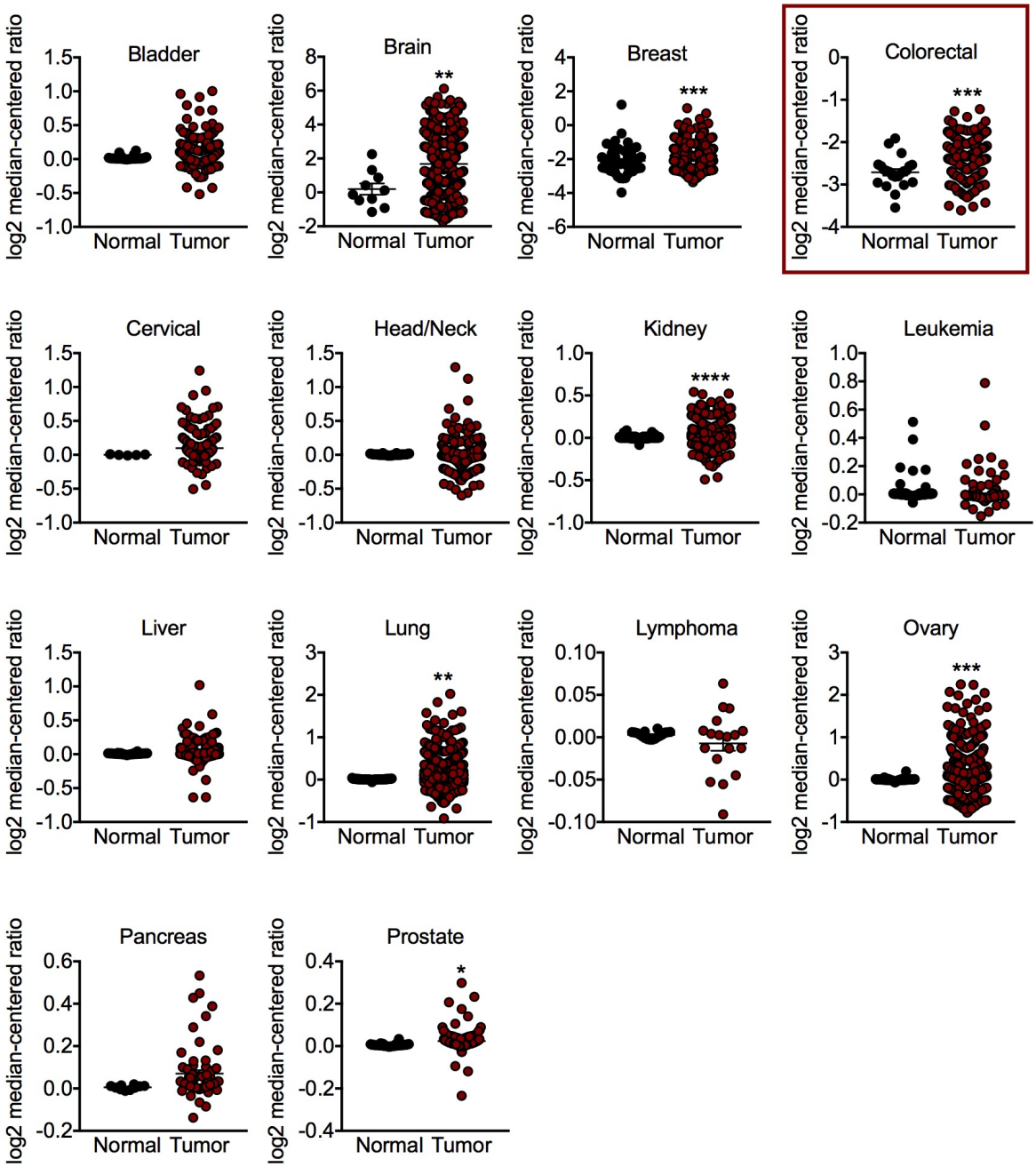

Figure 4.1. Hepcidin expression is increased across many cancer types. Hepcidin transcript abundance in normal and tumor tissue across 14 cancers, made available via microarray data through The Cancer Genome Atlas. Log2 median centered ratio is plotted. Data represent the mean ± SEM. Significance was determined by 2-tailed, unpaired *t* test. **P* < 0.05, ***P* < 0.01, ****P* < 0.001, and *****P* < 0.0001 compared to normal tissue.

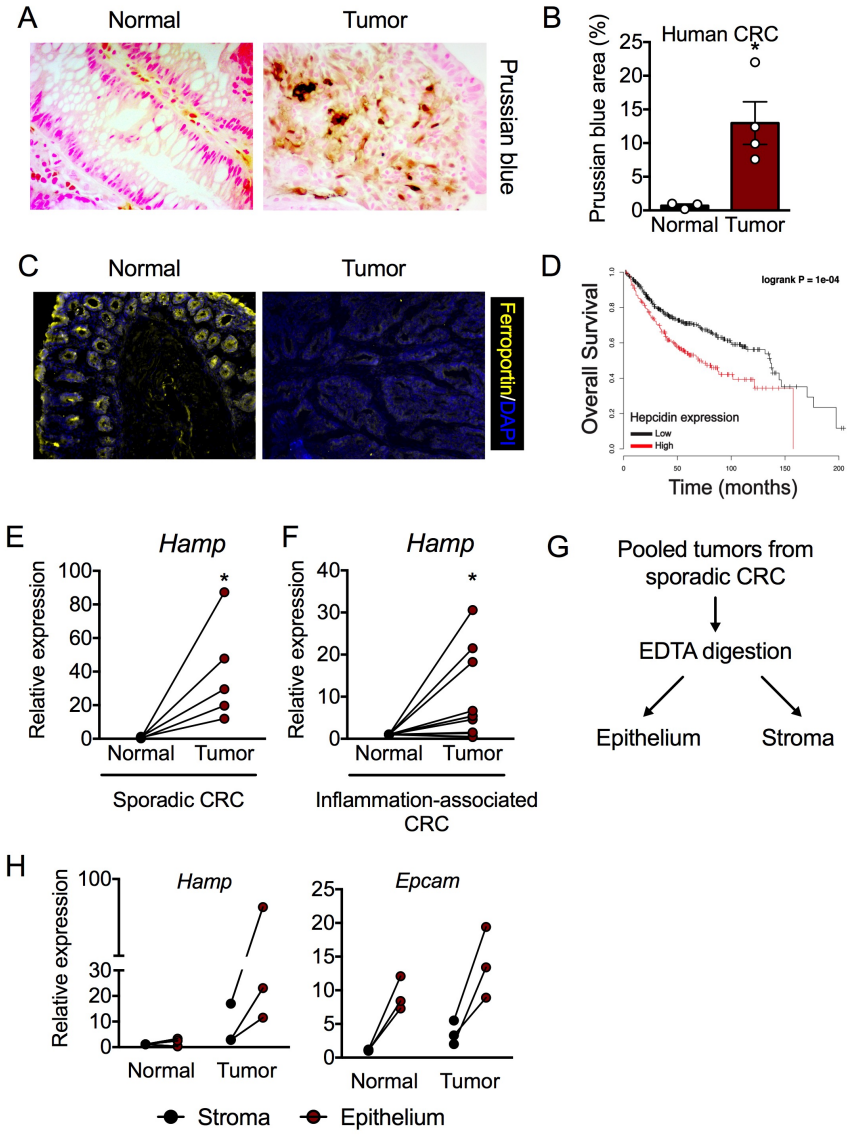

Figure 4.2. Colorectal cancer produce an extra-hepatic source of hepcidin that portends decreased patient survival. (A) Representative DAB-enhanced Prussian blue iron staining of human colorectal tumor and normal adjacent tissue, images 20x. (B) Quantification of Prussian blue area as a percent of total tissue. (C) Representative staining for ferroportin in colorectal tumor and normal adjacent tissue from a mouse model of sporadic colorectal cancer, images 20x. (D) Kaplan-Meier survival analysis generated from 530 human CRC biopsies, stratified on high vs. low hepcidin transcript from the median. (E and F) qPCR analysis for hepcidin (*Hamp*) expression in normal and tumor tissue in sporadic (E) and inflammation-associated (F) mouse models of colorectal cancer. (G) Experimental design for tumor epithelium vs. stroma enrichment. (H) qPCR analysis for *Hamp* in epithelium vs stroma compartments of normal and tumor tissue from three independent mice with sporadic colorectal cancer. Data represent the mean ± SEM. Significance was determined by 2-tailed, unpaired (B) or paired (E and F) *t* test. $*P < 0.05$

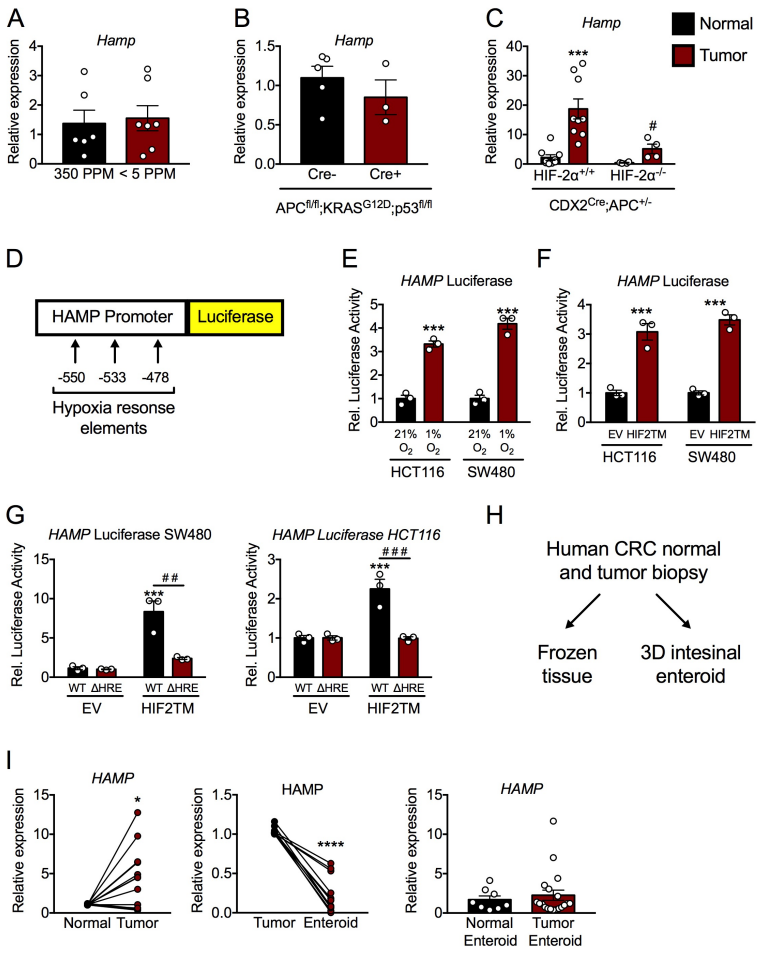

Figure 4.3. Hypoxia via HIF-2α activates hepcidin expression in CRC. (A) qPCR analysis for hepcidin *(Hamp*) in the colon of mice that were on iron replete (350 PPM) or low iron (< 5 PPM) diets for three months. (B) qPCR analysis for *Hamp* in the colon of mice with inducible, colon epithelial deletion of APC and p53 and activation of KRAS for ten days. (C) qPCR analysis for *Hamp* in normal and tumor tissue from a sporadic model of colorectal cancer in mice that were either wild-type for or deficient of HIF-2α. (D) Schematic of luciferase reporter construct of 1.7 kb of the human hepcidin promoter, indicating location of hypoxia response elements (HREs). (E and F) Hepcidin luciferase reporter activity in colorectal cancer-derived HCT116 and SW480 cells treated with either normoxia (21% oxygen)/hypoxia (1% oxygen) for 16 hours (E) or an oxygen stable HIF-2α construct (HIF2TM) (F). (G) Relative luciferase activity of the hepcidin promoter following transfection with HIF2TM as wild-type (WT) or deleted for HREs (ΔHRE) in SW480 and HCT116 cells. (H) Schematic of sample collection and utilization from primary colorectal cancer (CRC) patients. (I) qPCR analysis for *HAMP* in paired human normal and tumor tissue, paired tumor tissue and enteroid line generated from the same patient, and between all primary normal and tumor enteroid lines. Data represent the mean ± SEM. Significance was determined by 2-tailed, unpaired (A and B) or paired (I) *t* test, or by 1-way ANOVA with Tukey's post hoc (C, E-G). **P* < 0.05, ****P* < 0.001, and *****P* < 0.0001 comparing within a treatment group. # *P* < 0.05, # # *P* < 0.05, # # # *P* < 0.001 comparing between treatment groups.

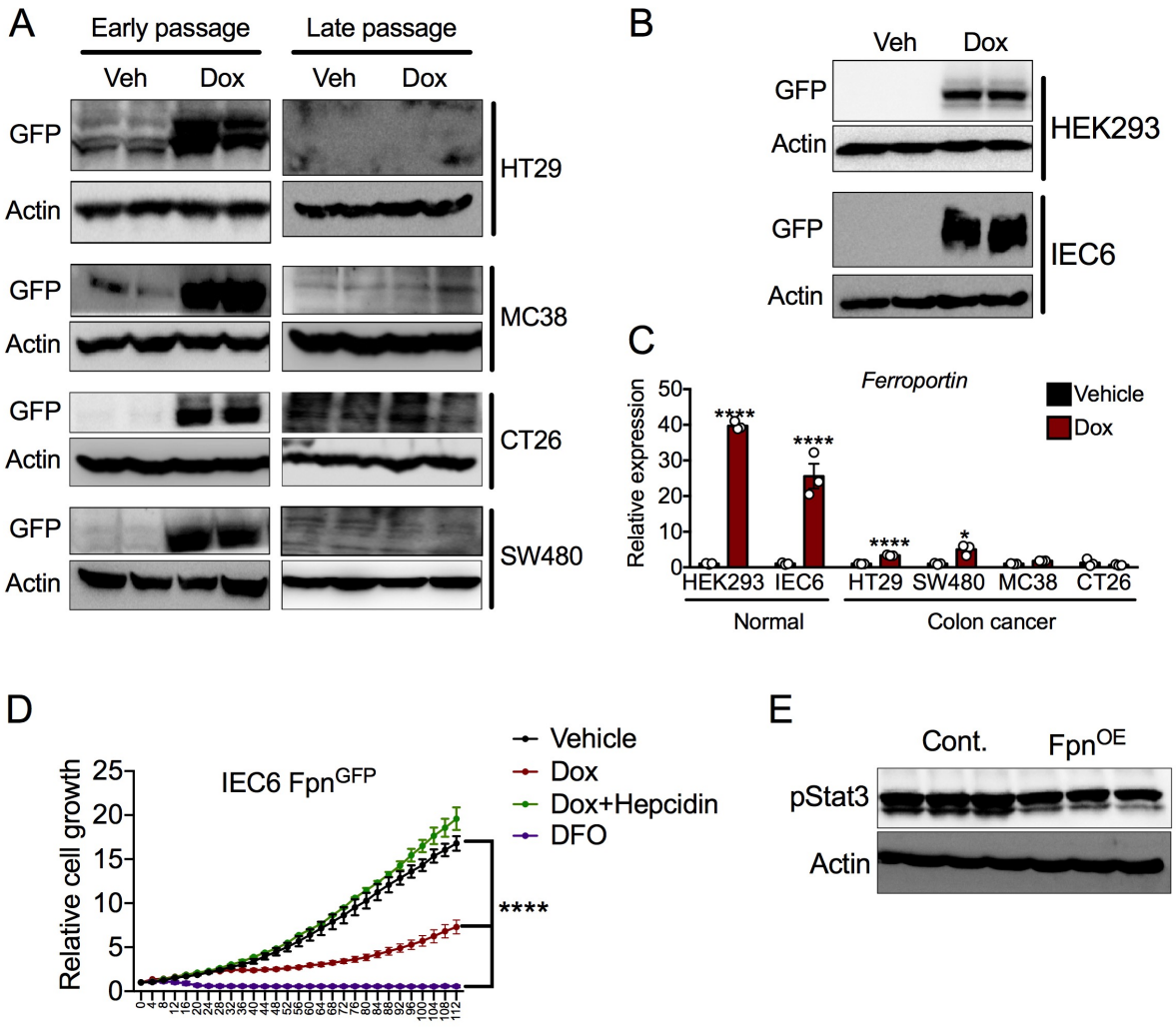

Figure 4.4. Colon cancer-derived cell lines are exquisitely sensitive to ferroportin-mediated iron loss, which decreases cell growth and blunts STAT3 signaling. (A) Western blot analysis for GFP in early and late passages of colon cancer-derived cell lines that were made stable for a doxycycline (dox) inducible ferroportin^{GFP} overexpression construct, following 16 hour treatment with dox (250 ng/mL). (B) Western blot analysis for GFP in stable, normal ferroportin^{GFP} overexpressing cell lines following 16 hour treatment with dox (250 ng/mL). (C) qPCR analysis for the ferroportin transcript in late passages cells that were made stable for a doxycycline (dox) inducible ferroportin^{GFP} overexpression construct, following 16 hour treatment with dox (250 ng/mL). (D) Cell growth assay in intestinal IEC6 ferroportin (FPN)^{GFP} cells treated with vehicle, dox (250 ng/mL), dox (250 ng/mL) and recombinant hepcidin (1 µg/mL), or deferoxamine (DFO) 200 µM [we need to out in significance]. (E) Western blot analysis for phospho-STAT3 in IEC6 FPN^{GFP} cells overexpressing ferroportin (Fpn^{OE}) following dox (250 ng/mL) treatment for 16 hours. Data represent the mean ± SEM. Significance was determined by 2-tailed, unpaired *t* test. **P* < 0.05 and *****P* < 0.0001 comparing within each cell line (C), or by by 1-way ANOVA with Tukey's post hoc, *****P* < 0.0001 comparing to vehicle (D).

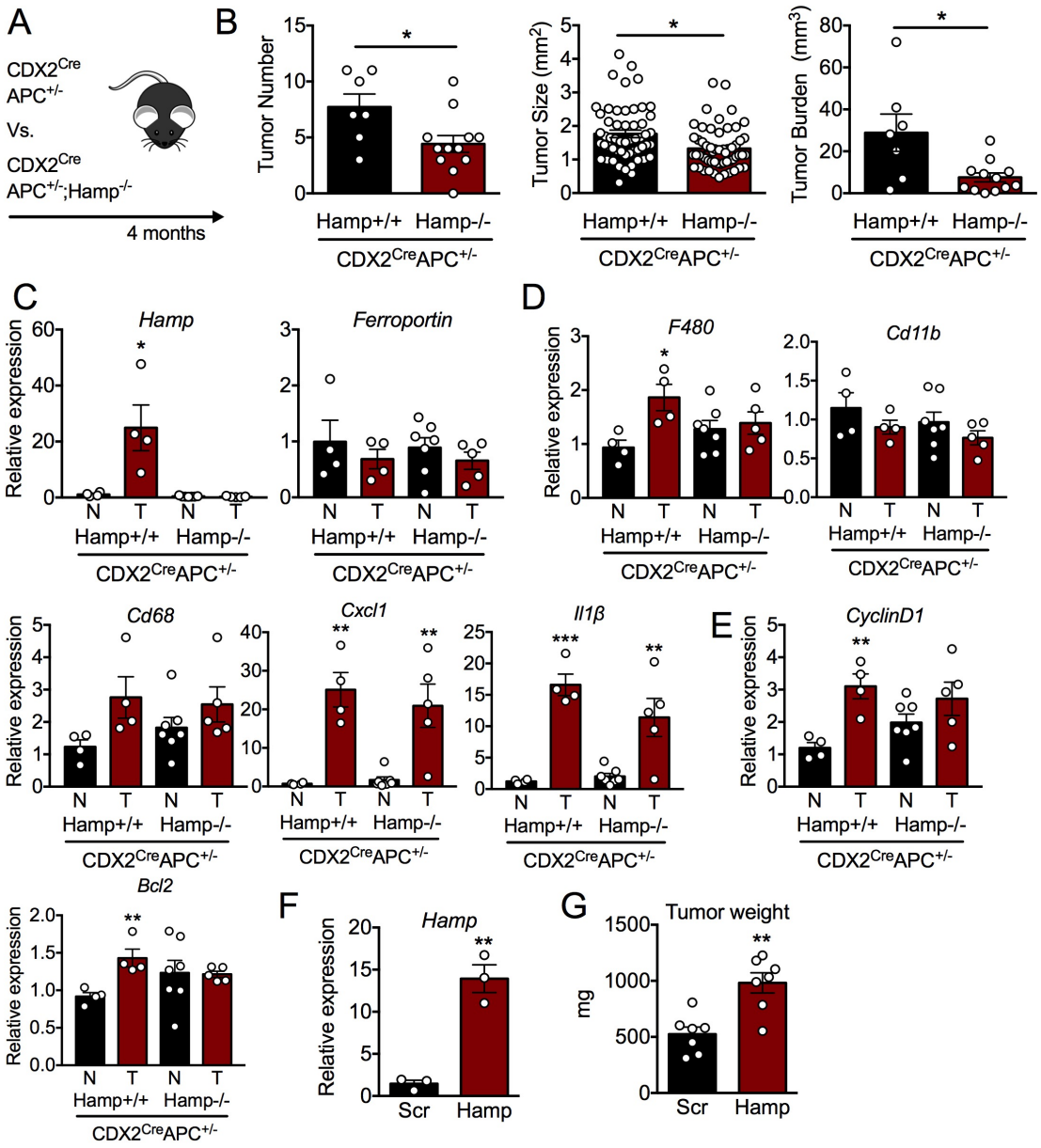

Figure 4.5. Hepcidin is necessary and sufficient to drive colon cancer growth. (A) Schematic of experimental design in this figure, using a sporadic model of colon cancer in mice deficient or wild-type for hepcidin in the colon epithelium four months after birth. (B) Tumor number, size, and burden in these mice. (C-E) qPCR analysis in normal and tumor tissue of mice deficient or wild-type for hepcidin, (C) iron genes, hepcidin (*Hamp*) and ferroportin, (D) inflammatory mediators, F480, Cd11b, Cd68, Cxcl, and Il1β, and (E) STAT3 target genes, CyclinD1 and Bcl2. (F) *Hamp* expression in mouse colon cancer-derived CT26 cells that stably overexpress hepcidin or a scrambled construct. (G) Tumor weight (mg) of CT26 orthotopic tumors that were implanted in BALB/C mice for 14 days. Significance was determined by 2-tailed, unpaired *t* test. **P* < 0.05, ***P* < 0.01 and ****P* < 0.001 comparing with each genotype or treatment group.

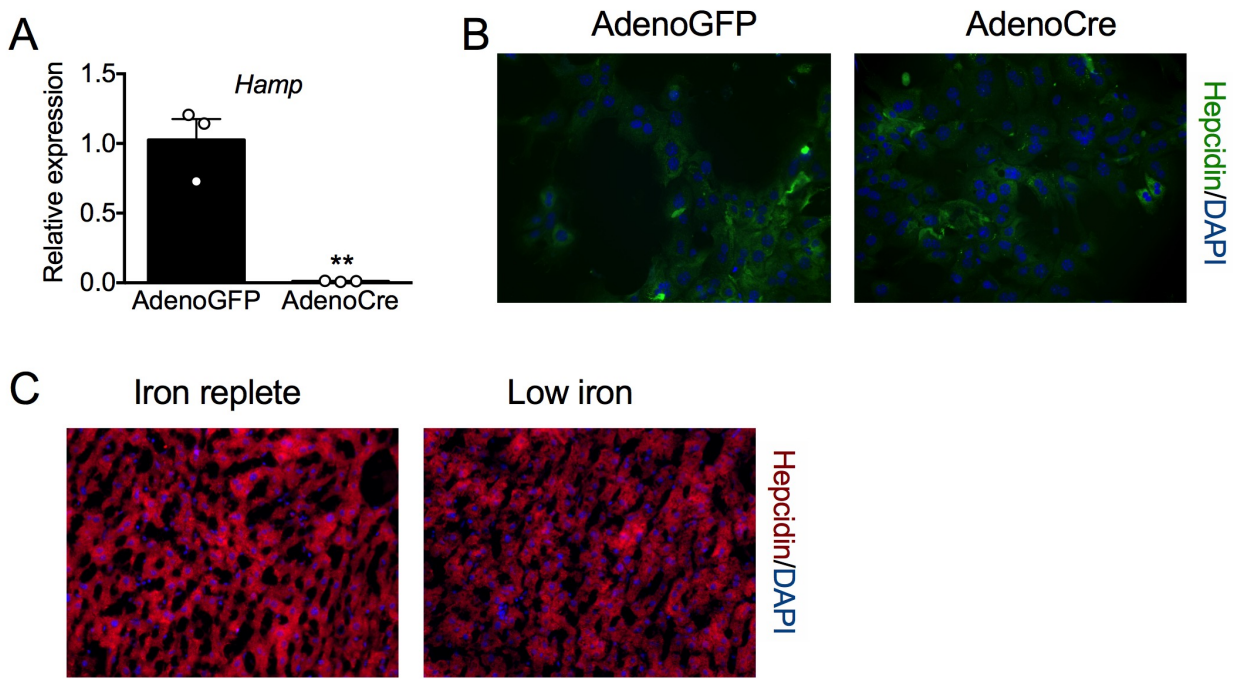

Figure S4.1. Detection of the hepcidin protein by immunohistochemistry is ineffective. (A and B) Primary hepatocytes were generated from *Hamp*$^{fl/fl}$ mice and treated in vitro with adenoviruses expressing either GFP or Cre recombinase for 48 hours. These cells were analyzed for hepcidin (*Hamp*) expression by qPCR analsysis (A) and were stained for hepcidin protein, images 40x (B). (C) Hepcidin staining in mice that were placed on either an iron replete (350 PPM) or low iron (< 5 PPM) for seven days. Data represent the mean ± SEM. Significance was determined by 2-tailed, unpaired *t* test. $^{**}P < 0.01$.

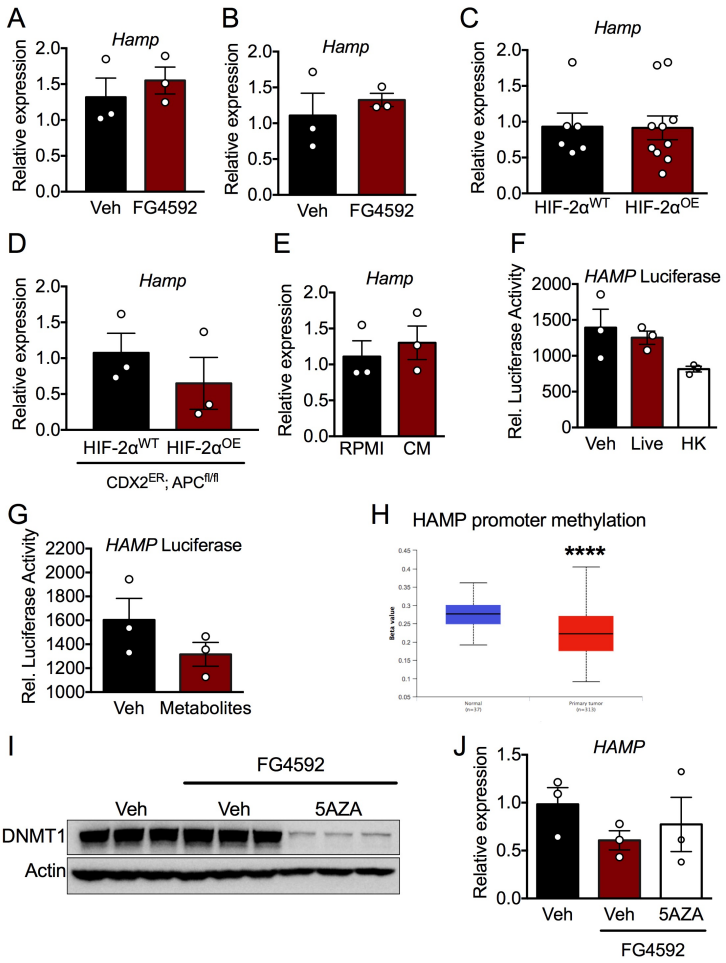

Figure S4.2. Activation of HIF-2α is not sufficient to drive hepcidin expression in vitro or in vivo, nor is inflammatory stimuli, bacteria, or DNA de-methylation. (A and B) qPCR analysis for hepcidin (*Hamp*) after treatment with FG4592 (100 μM) or vehicle for 16 hours in (A) colorectal cancer-derived HCT116 cells and (B) enteroids generated from mice with inducible, colon epithelial deletion of APC and p53 and activation of KRAS. (C) qPCR analysis of *Hamp* in the colon of mice with embryonic, intestinal epithelial-specific overexpression of HIF-2α (HIF-2α^{OE}) compared to wild-type mice (HIF-2α^{WT}). (C) qPCR analysis of *Hamp* in the colon of colon epithelial-specific HIF-2α^{WT} and HIF-2α^{OE} mice that are also deficient for APC for 30 days. (E) qPCR analysis of *Hamp* in HCT116 cells treated for 24 hours with conditioned media (CM) from RAW 264.7 macrophages that had been treated with 10 ng/mL LPS for 16 hours. (F and G) Relative luciferase activity of the human hepcidin promoter treated with (F) vehicle (Veh), live bacteria (Live), or heat-killed bacteria (HK), or (G) vehicle (Veh) or bacteria-derived metabolites (metabolites). (H) Methylation status of the human hepcidin promoter in human colorectal cancer tissue. (I and J) HCT116 cells were treated with vehicle (Veh) or 5AZA (10 μM) for 72 hours and then treated with vehicle (Veh) and/or FG4592 (100 μM) for 16 hours and analyzed via (I) Western blot analysis for DNA methyltransferase 1 (DNMT1) and (J) qPCR analysis for *HAMP* expression. Data represent the mean ± SEM. Significance was determined by 2-tailed, unpaired *t* test. ****$P < 0.0001$.

Table 4.1. Chapter 4 qPCR and cloning primers.

Gene	Primer sequence
mβ-Actin F	GTTGTCGACGACGAGCG
mβ-Actin R	GCACAGAGCCTCGCCTT
mHamp1 F	CTATCTCCATCAACAGATGAGACAGA
mHamp1 R	AACAGATACCACACTGGGAA
hHAMP F	CTCCTTCGCCTCTGGAACAT
hHAMP R	AGTGGCTCTGTTTTCCCACA
mEpcam F	CCAGTTTGGAGCAAATGACA
mEpcam R	CCGCGGCTCAGAGAGACT
mFerroportin F	ATGGGAACTGTGGCCTTCAC
mFerroportin R	TCCAGGCATGAATACGGAGA
mF480 F	AGGACTGGAAGCCCATAGCCAA
mF480 F	GCATCTAGCAATGGACAGCTG
mCd11b F	ATGGACGCTGATGGCAATACC
mCd11b R	TCCCCATTCACGTCTCCCA
mCd68 F	ACCGCCATGTAGTCCAGGTA
mCd68 R	ATCCCCACCTGTCTCTCTCA
mCxcl1 F	TCTCCGTTACTTGGGGACAC
mCxcl1 R	CCACACTCAAGAATGGTCGC
m1l1β F	AAGAGCTTCAGGCAGGCAGTATCA
m1l1β R	TGCAGCTGTCTAGGAACGTCA
CyclinD1 F	GGGTGGGTTGGAAATGAAC
CyclinD1 R	TCCTCTCCAAAATGCCAGAG
mBcl2 F	GGTCTTCAGAGACAGCCAGG
mBcl2 F	GATCCAGGATAACGGAGGCT
Hepcidin HRE truncation F	ATACAT**CTCGAG**GGCTCCCCAGATGGCTG
Hepcidin HRE truncation F	ATACAT**AAGCTT**CTTGAGCTTGCTCTGGT

Chapter 5

Conclusion

5.1 Summary

Iron is a fundamental metal micronutrient that sustains life, from single cell bacteria to complex multicellular organisms that include humans. On the cellular level, iron is utilized for an array of biochemical processes that maintain energy balance, mitochondrial function, DNA synthesis, and redox homeostasis. On the systemic level, iron controls tissue oxygen delivery within the heme of hemoglobin in RBCs. As a whole, mammalian iron metabolism depends on multiple organs working in concert to maintain iron concentrations for these physiological and biological functions. Advances in the understanding of tissue- and cell-type specific mechanisms of iron metabolism have begun to redefine the ways in which peripheral organs participate in systemic iron homeostasis while also protecting organ function via cell-autonomous mechanisms during states of iron overload and deficiency. Furthermore, recent investigations have unveiled intimate links between iron and oxygen sensing pathways that explain the molecular mechanisms of intracellular iron trafficking and oxygen consumption.

5.2 Hepcidin and HIF-2α in iron homeostasis

The work presented in Chapter 2 redefines the way in which systemic iron homeostasis and iron handling is understood. Research over the past decade has shown that, i) systemic iron handling is centrally regulated by the endocrine source of

hepatic hepcidin, and ii) intestinal iron absorption is necessary for the maintenance of postnatal systemic iron levels. Chapter 2 demonstrates that the liver controls the intestine through a hepatic hepcidin/intestinal HIF- 2α axis that regulates physiological iron uptake during systemic iron deficiency and drives pathological iron absorption during iron overload caused by hepcidin deficiency. High-throughput RNA-Seq revealed that the transcriptional responses in the intestine to systemic iron deficiency and hepcidin deficiency–mediated iron overload are largely the same. Both physiological repression of hepcidin and the genetic perturbation of hepcidin directly trigger iron efflux through intestinal ferroportin to limit the activity of iron-dependent PHD enzymes. This stabilizes intestinal HIF-2α to activate genes that are necessary and sufficient for intestinal iron absorption.

Interestingly, I reveal in Chapter 2 that acute loss of hepatic hepcidin gives rise to a HIF-2α-dependent expansion of the RBC pool (Figure 2.7C). Possible explanations for this observation include that, i) hepatocyte deletion of hepcidin triggers HIF-2α-dependent intestinal iron hyperabsorption; therefore, increases in systemic iron levels enhance RBC production and/or survival, or ii) similar to the intestine, hepcidin dampens HIF-2α activation in the bone marrow or in another peripheral cell type; therefore, deletion of hepcidin leads to a HIF-2α-dependent transcriptional response that triggers an increase in RBC production and/or survival. To test the first hypothesis, I executed a pilot experiment and generated systemic iron overload in wild-type mice by weekly intraperitoneal injections of iron dextran coupled to complete blood count analysis at 1, 3, and 5 weeks (Figure 5.1A). Contrary to the hepcidin deletion experiments, I find that there is no change in RBC numbers when comparing vehicle to

iron dextran treatment over time (Figure 5.1B). There was also no change in other blood parameters, namely hemoglobin, hematocrit, mean corpuscular hemoglobin, and mean corpuscular volume (Figure 5.1C). To confirm that this model successfully generated systemic iron overload, I assessed liver iron content, which was about 20-fold higher in the iron dextran treated group than the vehicle group (Figure 5.1D). This level of liver iron overload is similar to what was observed in the hepcidin deletion experiments in Chapter 2. Lastly, I observed no change in kidney erythropoietin transcript abundance (Figure 5.1E). These data collectively demonstrate that increases in systemic iron concentrations are not sufficient to trigger expansion of the RBC pool. Moreover, in combination with the data in Chapter 2, it appears that a hepcidin/HIF-2α axis might exist in a peripheral cell type(s) that regulates RBCs. Recent data has shown that RBCs express the ferroportin protein and that ferroportin-mediated iron efflux controls RBC survival (1, 2). It is therefore possible that an interaction exists between ferroportin and HIF-2α in RBCs to increase RBC survival. It will be critical in future work to understand the molecular mechanisms by which hepcidin/HIF-2α control RBCs and whether this axis operates in other peripheral cell types as well.

Another unanswered paradox in the regulation of HIF-2α is the mechanism by which ferroportin stabilization selectively activates HIF-2α over HIF-1α. As shown in Figures 2.6I and S2.6G, ferroportin overexpression in intestinal epithelial IEC6 cells leads to marked stabilization of the HIF-2α protein but no induction of HIF-1α. HIFs are regulated by post-translational hydroxylation of proline residues by PHDs that are enzymatically dependent on oxygen, iron, and 2-oxoglutarate for their function. HIF hydroxylation leads to association with the von-Hippel Lindau (VHL) tumor

suppressor/E3 ubiquitin ligase complex, ubiquitin conjugation, and 26s proteasomal degradation. In contexts that limit PHD activity, such as intracellular oxygen or iron depletion, HIF protein becomes stabilized. Given the current dogma of HIF protein regulation, intracellular depletion of iron should stabilize both HIF-1α and HIF-2α due to inhibition of PHD activity, however, this was not observed following ferroportin overexpression. Moreover, treatment of IEC6 cells with the iron chelator, deferoxamine, massively stabilized HIF-1α, suggesting that intracellular iron depletion, but not ferroportin overexpression, is sufficient to activate HIF-1α (Figure S2.6G).

Several biological phenomena could explain this observation, including, i) an intestinal PHD isoform that is both selective for HIF-2α over HIF-1α hydroxylation and is exquisitely sensitive to decreases in intracellular iron concentrations, ii) a ferroportin-interacting protein that directly activates HIF-2α over HIF-1α following ferroportin stabilization, and/or iii) a ferroportin-independent iron-sensing protein that directly activates HIF-2α over HIF-1α. To begin to address these paradigms in vivo, I have preliminary data using a genetic mouse model that is devoid of the VHL protein exclusively in the intestinal epithelium ($Vhl^{\Delta IE}$). VHL is downstream of PHDs and is the rate limiting protein in HIF-1α and HIF-2α post-translational regulation, whereby deletion of VHL leads to maximal stabilization of HIFs and activation of all downstream target genes. I placed $Vhl^{\Delta IE}$ mice on 350 PPM (iron replete) and <5 PPM (iron deficient) iron diets for two weeks and compared to $Vhl^{f/lfl}$ wild-type littermates on a 350 PPM diet. Interestingly and surprisingly, I found that the canonical HIF-2α iron-sensitive target genes, *Dcytb*, *Dmt1*, and *Fpn*, were potentiated in the iron deficient group compared to the iron replete group (Figure 5.2A). No potentiation was observed for canonical HIF-1α

target genes, *Pdk1*, *Pgk1*, and *Aldoc* (Figure 5.2B). These data confirm that there are VHL-independent mechanisms by which HIF-2α is selectively activated by a drop in intracellular iron levels. Moreover, seeing as VHL is downstream of PHDs, PHD selectively/sensitivity to iron cannot explain these observation in $Vhl^{\Delta IE}$. Recent work has revealed that SMAD3 and SMAD4 repress HIF-2α-dependent iron-regulatory genes through an unknown mechanism (3). Future work needs to carefully interrogate the complete molecular mechanisms by which HIF-2α is activated by intracellular iron deficiency. Collectively, these questions will provide insight into the mechanisms by which basic intracellular oxygen and iron sensing pathways are integrated.

5.3 Organ-specific transcriptional stress responses to iron and oxygen deficiency

Research over the last few years has reshaped ways to think about local iron handling and oxygen metabolism. The work presented in Chapter 3 builds upon previous work by characterizing a novel genetic mouse model of iron-deficiency anemia (IDA). Our data reveal a robust phenotype of progressive IDA that develops in as little as three months following disruption to intestinal iron absorption. At end-stage IDA, tissue-specific transcriptional stress responses were observed, whereby the heart shows little to no hypoxic or iron stress as compared to other peripheral organs. However, morphometric and echocardiographic analysis revealed massive cardiac hypertrophy and chamber dilation, albeit with increased cardiac output at very low basal heart rates. Collectively, these data demonstrate a rapid mouse model of end-stage IDA that can be used to study disease progression and cell-specific responses to iron and oxygen stress.

There are several experimental findings from Chapter 3 that need to be addressed in future work, including the observation that erythropoietin (encoded by *Epo*) was induced 1000-fold, despite severe kidney iron deficiency in IDA (Figure 3.4A). *Epo* is a classical HIF-2α-target gene regulated by systemic hypoxia (4). HIF-2α contains a 5′-UTR iron response element (IRE) that is responsible for translational inhibition during states of iron deficiency (5). This iron regulatory protein (IRP)/IRE interaction is thought to serve as a molecular brake on HIF-2α-mediated kidney EPO expression, to restrict RBC production when iron levels are limited for hemoglobin synthesis. The finding that *Epo* is massively induced in IDA might indicate that the IRP/IRE system is an insufficient mechanism to dampen HIF-2α in the kidney during the severe disease state of IDA. It is also possible that a mechanism of hepcidin/ferroportin sensing may exist in EPO producing cells in the kidney similar to the intestine, whereby the hepcidin/ferroportin induction of HIF-2α outweigh the IRP/IRE break on HIF-2α in contexts when both pathways are active. More work is needed to understand the complete molecular mechanisms of *Epo* expression during normal physiology and in disease states such as IDA.

Future experiments must also follow up on the observation that the heart is spared from severe iron and oxygen stress in IDA. Recent investigations have shown the heart controls cell-autonomous iron handling by establishing a local hepcidin/ferroportin axis (6). However, the molecular mechanisms that govern this local axis are still poorly defined. It is also unclear as to why a hypoxic transcriptional program is not activated in the heart during IDA, as was the case in other peripheral organs. It is possible that the heart is somehow spared by peripheral organs and that

serum iron and oxygen are redirected to the heart during stress. These are all important areas of investigation in the contexts of iron and oxygen biology that must be addressed in the coming years.

5.4 Cell-autonomous mechanisms of iron handling in cancer

In Chapter 4, I revealed that colon tumors can produce their own source of ectopic hepcidin to control ferroportin and trap intratumoral iron levels. Iron becomes sequestered in colorectal tumor tissue, leading to massive intratumoral iron stores that are essential for growth and survival. Human data from epidemiological studies have shown a correlation between dietary iron intake and/or systemic iron levels and CRC risk. I revealed in Chapter 4 that the ferroportin protein is highly expressed in adjacent normal colon tissue but is absent in colon tumor tissue. Furthermore, intratumoral hepcidin in CRC that portends poor patient survival. Kaplan-Meier survival analysis generated from 530 human CRC biopsies showed that high levels of intratumoral hepcidin expression portend a significant decrease in overall patient survival. Mice deficient for the hepcidin gene specifically in colon epithelium exhibited significant decreases in tumor number, burden, and size compared to wild-type littermates in a sporadic model of CRC, whereas hepcidin overexpression increased tumor size in an orthotopic model. A luciferase-based reporter construct of the human hepcidin promoter revealed that HIF-2α is sufficient to activate the hepcidin promoter in CRC-derived cell lines. Furthermore, intratumoral hepcidin was necessary for iron-dependent activation of the STAT3 pathway. These data suggest that intratumoral hypoxia in CRC activates HIF-2α to drive hepcidin transcription in the tumor epithelium. This ectopic hepcidin

establishes an axis to degrade ferroportin and sequester iron in colorectal tumors in order to maintain iron-dependent cancer cell metabolism. These data advance our understanding about how cancer cells use iron handling mechanisms differently than normal cells to enhance their growth and survival. Furthermore, these data provide insight into the mechanisms by which ectopic, extra-hepatic hepcidin is regulated, which might provide information into basic physiological processes that take place in other organs, namely the heart.

One major unanswered question from this work is in the mechanism by which iron metabolism links to general cancer cell metabolism. There is strong evidence to show that iron is necessary to activate oncogenic STAT3 signaling in CRC (7). However, intracellular iron is utilized for an array of biochemical processes and it will be important to define the complete iron metabolome in cancer. To begin to address this question, I have preliminary data from two non-cancerous, doxycycline inducible ferroportin overexpressing cell lines (i.e. HEK293 and IEC6 Ferroportin^{GFP}), as I were unsuccessful in generating stable ferroportin overexpressing CRC-derived cells in Chapter 4. I treated these cell lines with doxycycline for 16 hours. Using snapshot metabolomics, I found that nearly two-thirds of the metabolites with differential abundance in both cell lines following ferroportin overexpression were involved in nucleotide metabolism (Figure 5.3A and B). Furthermore, I found that many key metabolites that are involved in de novo pyrimidine biosynthesis are significantly lower following doxycycline treatment, but completely rescued by co-treatment with recombinant hepcidin. Figure 5.3C outlines these changes, using representative data from IEC6 cells that were also observed in HEK293 cells. De novo pyrimidine

biosynthesis converges with a salvage, “recycling” pathway at uridine 5-monophosphate, which was significantly elevated following ferroportin overexpression in both HEK293 and IEC6 cells (Figure 5.3C). These data collectively indicate that ferroportin-mediated iron efflux selectively decreases de novo pyrimidine production and activates the pyrimidine salvage pathway because uridine 5-monophostphate is elevated. However, salvage pathways are inefficient mechanisms to maintain nucleotide metabolism, and overall cell proliferation is halted in each of these cell lines when ferroportin is stabilized. It will be essential in future work to determine if these iron-dependent mechanisms are also observed in CRC-derived cell lines and in in vivo tumors. Furthermore, on a mechanistic basis, it will also be important to understand how intracellular iron depletion via ferroportin disrupts nucleotide metabolism. Possible explanations include, i) iron is a necessary substrate for enzymes involved in de novo nucleotide production, or ii) there is an iron sensing protein that directly inhibits nucleotide production following ferroportin stabilization. These findings will provide key insights into cancer cell metabolism and may reveal vulnerabilities to launch therapeutics against for cancer treatment.

5.5 Hepcidin-mediated ferroportin degradation

One essential but unanswered paradox in iron biology is the complete molecular mechanism by which hepcidin initiates ferroportin-mediated degradation. Previous work has shown that the hepcidin/ferroportin interaction results in rapid ubiquitination, internalization, and intracellular degradation of ferroportin. Due to the retraction of a key seminal paper in understanding this mechanism, zero papers have been published that

provide mechanistic insight into how ferroportin is degraded by hepcidin (8). Studying the molecular mechanisms of the hepcidin/ferroportin degradation axis is fundamental to understanding i) hepcidin/HIF-2α crosstalk, which depends on ferroportin degradation, and ii) basic processes of systemic and cellular iron handling in mammals. Several species of ferroportin have been described in the literature, which is likely due to a posttranslational modification on ferroportin (7). In our system of doxycycline inducible ferroportin^{GFP} overexpression, I observe a functional difference between the two protein species: the higher molecular weight ferroportin is sensitive to hepcidin-mediated degradation as quickly as two hours following treatment, while the lower molecular weight ferroportin remains hepcidin-resistant (Figure 5.4A).

Our preliminary data on the larger, hepcidin-sensitive band demonstrates that hepcidin-mediated ferroportin degradation occurs within the lysosome (Figure 5.4B). The lysosomal degradation of cellular content is canonically thought to occur through a process known as macroautophagy (9). Interestingly, our data suggests that the lysosomal degradation of ferroportin occurs independent of canonical macroautophagic machinery, as treatment with known pharmacological inhibitors of this process do not rescue ferroportin in the presence of hepcidin (Figure 5.4C). To address the complete mechanism of hepcidin-mediated ferroportin degradation in an unbiased manner, I have performed co-immunoprecipitation and mass spectrometry-based proteomic experiments using anti-GFP beads in our Ferroportin^{GFP} cells following vehicle or hepcidin treatment. I identified heat shock 70 kDa protein 8 (HSC70), which is the rate limiting cargo protein involved in a process of selective and substrate-specific lysosomal degradation that is discrete from macroautophagy, known as chaperone-mediated

autophagy (CMA) (9). CMA has received much attention over the last few decades as a targeted pathway for lysosomal degradation that is responsive to many of the broad metabolic and cellular cues that are known to regulate macroautophagy (10, 11). In CMA, factors such as metabolic and nutrient deprivation trigger HSC70 to seek a conserved motif in its target substrates (10). HSC70 then transports its cargo directly to the lysosome for docking with the rate-limiting receptor in this pathway, lysosome-associated membrane protein type 2A (LAMP2A), at which point cargo is internalized and degraded in the lysosomal lumen (10). I have confirmed using an exogenous HSC70-V5 expression construct that ferroportin interacts with HSC70 (Figure 5.4D). Future work will need to define the role of CMA machinery in hepcidin-mediated degradation of ferroportin by the lysosome. Furthermore, more research will need to investigate the mechanisms by which iron, oxygen, and autophagic pathways integrate in cellular homeostasis.

5.6 Perspectives

Through a collection of three experimental works, this dissertation advances the field of iron biology forward by enhancing our understanding of systemic and cellular iron metabolism. This dissertation defines the basic processes of iron metabolism inside of cells and the ways in which organs communicate across the body, expanding on previous work and defining new ways to understand iron homeostasis during physiology and in various disease states. The work presented in this dissertation also shifts our understanding of, i) direct liver/intestinal dynamics that regulate systemic iron levels, ii) organ and cell-type specific iron and/or oxygen stress responses, and iii) the ways in which iron and oxygen metabolism are alerted in cancer to enable efficient growth and

survival. These data will serve as a framework to define new approaches for the design and implementation of therapies to treat diseases of iron metabolism and cancer.

References

1. Zhang DL, Ghosh MC, Ollivierre H, Li Y, and Rouault TA. Ferroportin deficiency in erythroid cells causes serum iron deficiency and promotes hemolysis due to oxidative stress. *Blood.* 2018;132(19):2078-87.
2. Zhang DL, Wu J, Shah BN, Greutelaers KC, Ghosh MC, Ollivierre H, et al. Erythrocytic ferroportin reduces intracellular iron accumulation, hemolysis, and malaria risk. *Science.* 2018;359(6383):1520-3.
3. Ma X, Das NK, Castillo C, Gourani A, Perekatt AO, Verzi MP, et al. SMAD family member 3 (SMAD3) and SMAD4 repress HIF2alpha-dependent iron-regulatory genes. *J Biol Chem.* 2019;294(11):3974-86.
4. Wang GL, and Semenza GL. General involvement of hypoxia-inducible factor 1 in transcriptional response to hypoxia. *Proc Natl Acad Sci U S A.* 1993;90(9):4304-8.
5. Sanchez M, Galy B, Muckenthaler MU, and Hentze MW. Iron-regulatory proteins limit hypoxia-inducible factor-2alpha expression in iron deficiency. *Nat Struct Mol Biol.* 2007;14(5):420-6.
6. Lakhal-Littleton S, Wolna M, Chung YJ, Christian HC, Heather LC, Brescia M, et al. An essential cell-autonomous role for hepcidin in cardiac iron homeostasis. *Elife.* 2016;5.
7. Xue X, Ramakrishnan SK, Weisz K, Triner D, Xie L, Attili D, et al. Iron Uptake via DMT1 Integrates Cell Cycle with JAK-STAT3 Signaling to Promote Colorectal Tumorigenesis. *Cell Metab.* 2016;24(3):447-61.
8. De Domenico I, Lo E, Yang B, Korolnek T, Hamza I, Ward DM, et al. The role of ubiquitination in hepcidin-independent and hepcidin-dependent degradation of ferroportin. *Cell Metab.* 2011;14(5):635-46.
9. Jiang X, Overholtzer M, and Thompson CB. Autophagy in cellular metabolism and cancer. *J Clin Invest.* 2015;125(1):47-54.
10. Kaushik S, Bandyopadhyay U, Sridhar S, Kiffin R, Martinez-Vicente M, Kon M, et al. Chaperone-mediated autophagy at a glance. *J Cell Sci.* 2011;124(Pt 4):495-9.
11. Tasset I, and Cuervo AM. Role of chaperone-mediated autophagy in metabolism. *FEBS J.* 2016;283(13):2403-13.

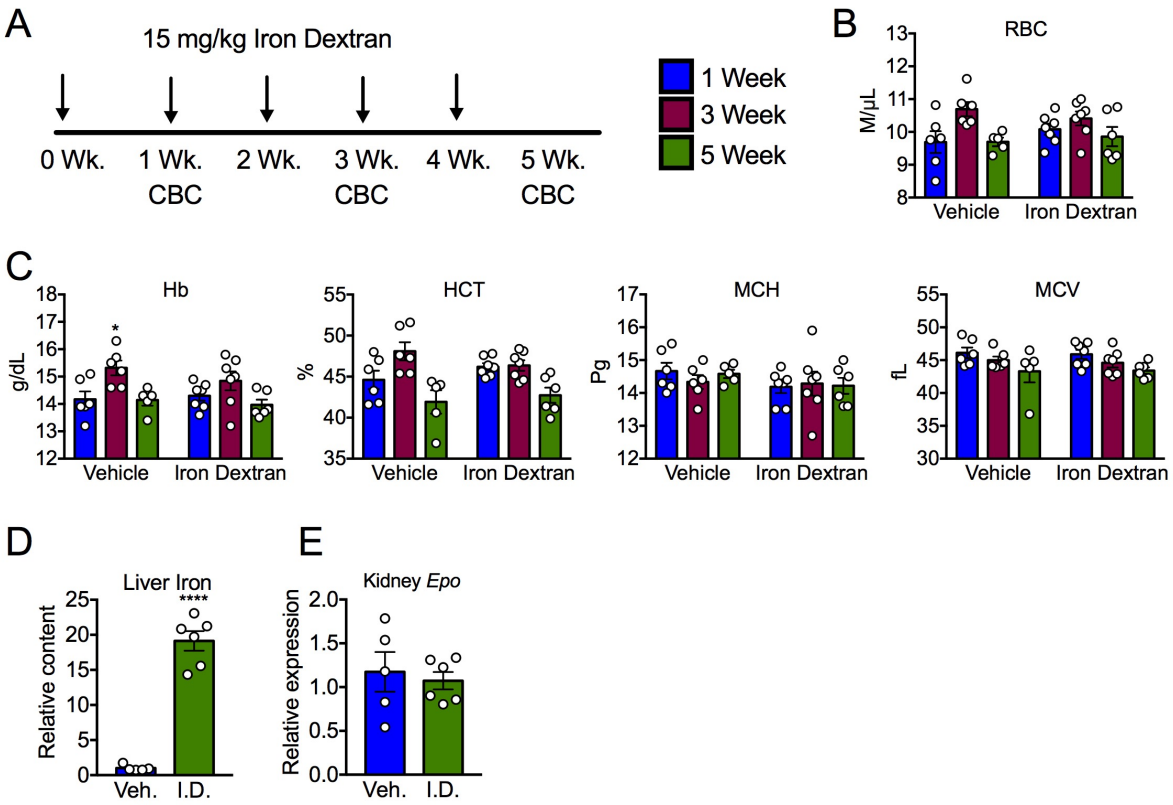

Figure 5.1. Iron overload does not trigger an increase in red blood cell numbers. (A) Schematic of iron dextran-induced iron overload in wild-type mice. (B and C) Time course analysis of complete blood count parameters in vehicle and iron dextran treated groups, showing (B) red blood cell count (RBC), and (C) hemoglobin (Hb), hematocrit (HCT), mean corpuscular hemoglobin (MCH), and mean corpuscular volume (MCV). (D) Liver iron concentrations. (E) qPCR analysis for erythropoietin (*Epo*). Data represent the mean ± SEM. Significance was determined by 2-tailed, unpaired *t* test or one-way ANOVA followed by Tukey's post hoc. **P* < 0.05, *****P* < 0.0001 compared to 1 week vehicle or vehicle groups.

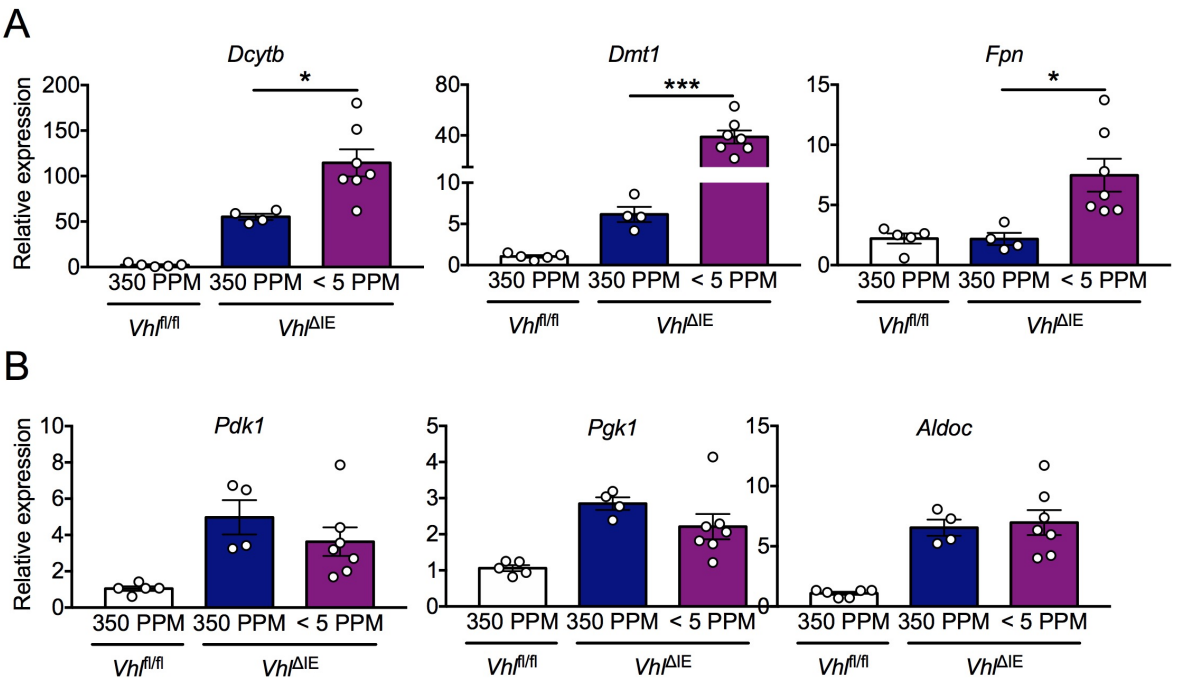

Figure 5.2. A VHL-independent mechanism for activation of intestinal HIF-2α but not HIF-1α during iron demand. Mice deficient for the VHL protein exclusively in the intestinal epithelium (*VHL*$^{\Delta IE}$) were placed on iron-replete (350 PPM iron) or iron-deficient (< 5PPM iron) diets for two weeks and compared to wild-type *Vhl*$^{fl/fl}$ littermates on a 350PPM diet. (A) qPCR analysis of canonical HIF-2α-specific iron absorptive genes. (B) qPCR analysis of canonical HIF-1α glycolytic genes. Data represent the mean ± SEM. Significance was determined by one-way ANOVA followed by Tukey's post hoc. **P* < 0.05, ****P* < 0.001 compared to 350 PPM *VHL*$^{fl/fl}$ mice.

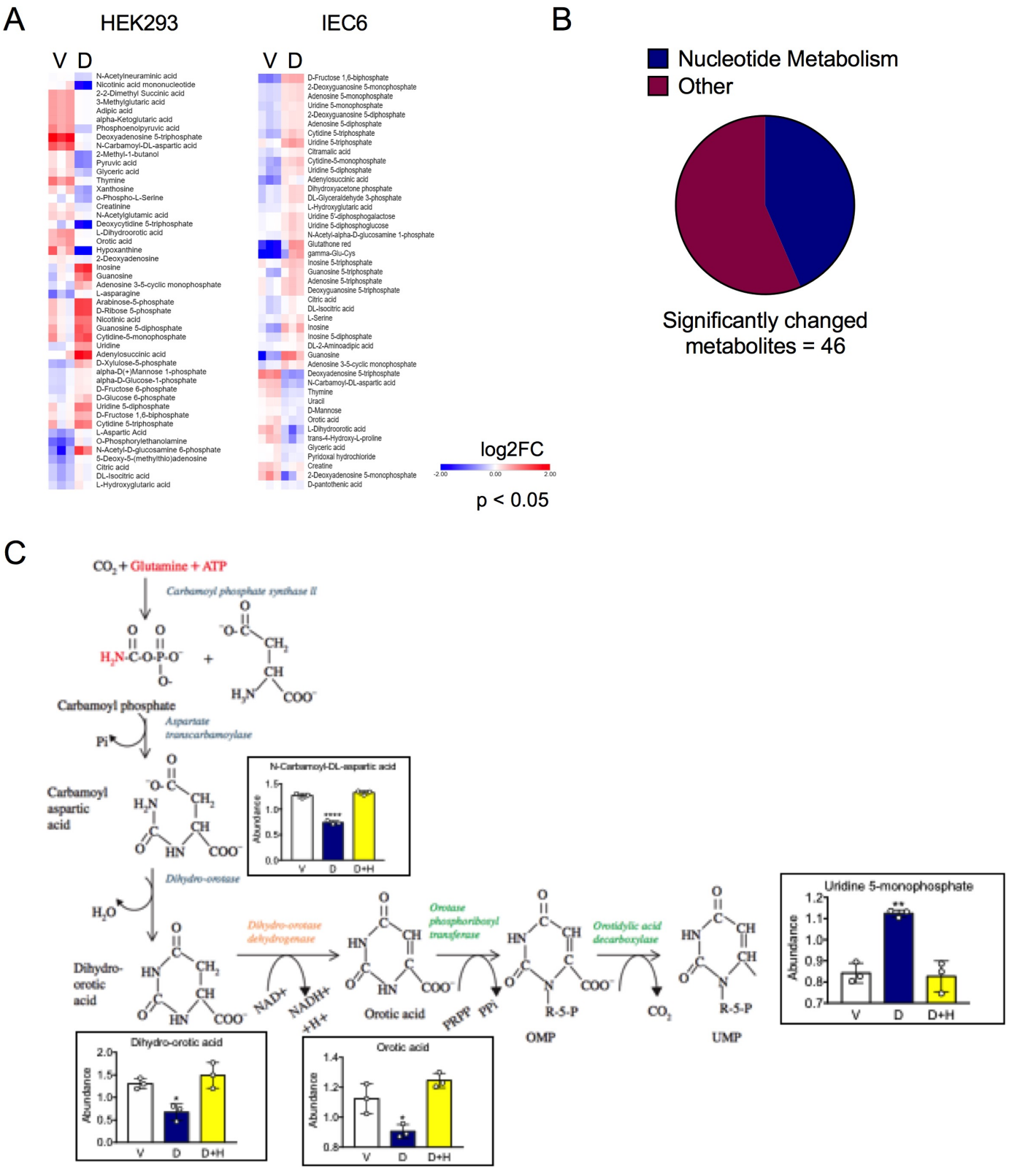
A
HEK293
IEC6
V D
V D
N-Acetylneuraminic acid
Nicotinic acid mononucleotide
2-2-Dimethyl Succinic acid
3-Methylglutaric acid
Adipic acid
alpha-Ketoglutaric acid
Phosphoenolpyruvic acid
Deoxyadenosine 5-triphosphate
N-Carbamoyl-DL-aspartic acid
2-Methyl-1-butanol
Pyruvic acid
Glyceric acid
Thymine
Xanthosine
o-Phospho-L-Serine
Creatinine
N-Acetylglutamic acid
Deoxycytidine 5-triphosphate
L-Dihydroorotic acid
Orotic acid
Hypoxanthine
2-Deoxyadenosine
Inosine
Guanosine
Adenosine 3-5-cyclic monophosphate
L-asparagine
Arabinose-5-phosphate
D-Ribose 5-phosphate
Nicotinic acid
Guanosine 5-diphosphate
Cytidine-5-monophosphate
Uridine
Adenylosuccinic acid
D-Xylulose-5-phosphate
alpha-D(+)Mannose 1-phosphate
alpha-D-Glucose-1-phosphate
D-Fructose 6-phosphate
D-Glucose 6-phosphate
Uridine 5-diphosphate
D-Fructose 1,6-biphosphate
Cytidine 5-triphosphate
L-Aspartic Acid
O-Phosphorylethanolamine
N-Acetyl-D-glucosamine 6-phosphate
5-Deoxy-5-(methylthio)adenosine
Citric acid
DL-Isocitric acid
L-Hydroxyglutaric acid
D-Fructose 1,6-biphosphate
2-Deoxyguanosine 5-monophosphate
Adenosine 5-monophosphate
Uridine 5-monophosphate
2-Deoxyguanosine 5-diphosphate
Adenosine 5-diphosphate
Cytidine 5-triphosphate
Uridine 5-triphosphate
Citramalic acid
Cytidine-5-monophosphate
Uridine 5-diphosphate
Adenylosuccinic acid
Dihydroxyacetone phosphate
DL-Glyceraldehyde 3-phosphate
L-Hydroxyglutaric acid
Uridine 5'-diphosphogalactose
Uridine 5-diphosphoglucose
N-Acetyl-alpha-D-glucosamine 1-phosphate
Glutathione red
gamma-Glu-Cys
Inosine 5-triphosphate
Guanosine 5-triphosphate
Adenosine 5-triphosphate
Deoxyguanosine 5-triphosphate
Citric acid
DL-Isocitric acid
L-Serine
Inosine
Inosine 5-diphosphate
DL-2-Aminoadipic acid
Guanosine
Adenosine 3-5-cyclic monophosphate
Deoxyadenosine 5-triphosphate
N-Carbamoyl-DL-aspartic acid
Thymine
Uracil
D-Mannose
Orotic acid
L-Dihydroorotic acid
trans-4-Hydroxy-L-proline
Glyceric acid
Pyridoxal hydrochloride
Creatine
2-Deoxyadenosine 5-monophosphate
D-pantothenic acid
log2FC
-2.00
0.00
2.00
p < 0.05
B
Nucleotide Metabolism
Other
Significantly changed metabolites = 46
C
CO2 + Glutamine + ATP
Carbamoyl phosphate synthase II
Carbamoyl phosphate
Aspartate transcarbamoylase
Pi
Carbamoyl aspartic acid
N-Carbamoyl-DL-aspartic acid
Abundance
V
D
D+H
Dihydro-orotase
H2O
Dihydro-orotic acid
Dihydro-orotate dehydrogenase
NAD+
NADH+ +H+
Orotic acid
Orotate phosphoribosyl transferase
PRPP
PPi
OMP
R-5-P
Orotidylic acid decarboxylase
CO2
UMP
Uridine 5-monophosphate
Dihydro-orotic acid
Orotic acid

Figure 5.3. Ferroportin-mediated iron efflux blunts de novo pyrimidine synthesis. (A) Heatmap of metabolites of differential abundance in HEK293 and IEC6 doxycycline-inducible ferroportin overexpressing cell lines treated with doxycycline (D) as compared to vehicle (V) for 16 hours. Only changes at $p < 0.05$ compared to V are shown. (B) Pie chart showing the proportion of metabolites of differential abundance in both HEK293 and IEC6 ferroportin overexpressing cells that are involved in nucleotide metabolism. (C) Pathway of de novo pyrimidine biosynthesis, depicting metabolites that were significantly changed in both HEK293 and IEC6 ferroportin overexpressing cells treated with vehicle (V), doxycycline, (D), or doxycycline and recombinant hepcidin for 16 hours. Representative data from IEC6 cells are shown. Data represent the mean ± SEM. Significance was determined by one-way ANOVA followed by Tukey's post hoc. *$P < 0.05$, **$P < 0.01$, ****$P < 0.0001$ compared to V.

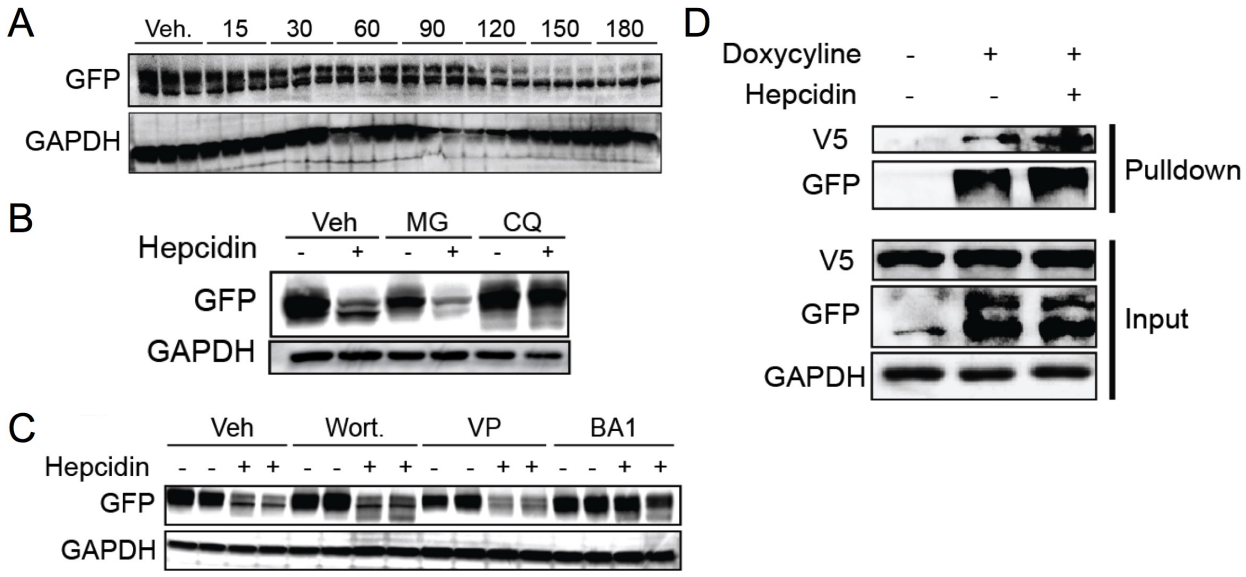

Figure 5.4. Hepcidin interaction with ferroportin leads to binding with HSC70 and lysosomal degradation, independent of canonical macroautophagic machinery. Stable, doxycycline-inducible human ferroportin^{GFP} HEK293 cells (FPN^{GFP}) were treated with vehicle or doxycycline for 16 hours, followed by (A) recombinant hepcidin for the indicated time points (minutes), (B) a pre-treatment for 1 hr. with the proteosomal inhibitor, MG-132, the lysosomal inhibitor, chloroquine (CQ), or vehicle before treatment with recombinant hepcidin for 4 hrs, or (C) pre-treatment for 1 hr. with inhibitors of macroautophagy, wortmannin (Wort.) or verteporfin (VP), the lysosomal inhibitor, bafilomycin A1 (BA1), or vehicle before treatment with recombinant hepcidin for 4 hrs. (D) FPN^{GFP} cells were transfected with an HSC70-V5 expression construct, treated with doxycycline, and recombinant hepcidin or vehicle for 2 hrs. before lysis for co-IP with anti-GFP beads.